PORT DOCUMENTATION PAGE

Form Approved
OMB No. 0704-0188

1. AGENCY USE ONLY (Leave blank)	2. REPORT DATE	3. REPORT TYPE AND DATES COVERED
	4.20.96	Final, 01.01.93-12.31.95

4. TITLE AND SUBTITLE

Cemented Particulate Materials:
From Grain-to-Grain Contact to Macro-Behavior

5. FUNDING NUMBERS

US Air Force Office of
Scientific Research
Contract
F49620-93-1-0052

6. AUTHOR(S)

Jack Dvorkin

7. PERFORMING ORGANIZATION NAME(S) AND ADDRESS(ES)

Geophysics Department, Stanford University
Stanford, CA 94305-2215

9. SPONSORING / MONITORING AGENCY NAME(S) AND ADDRESS(ES)

Capt. Brian Sanders
Program Manager, Structural Mechanics
AFOSR/NA
110 Duncan Avenue
Bolling AFB, DC 20332-0001

NA

AFOSR-TR-96

0266

11. SUPPLEMENTARY NOTES

12a. DISTRIBUTION / AVAILABILITY STATEMENT

Approved for public release,
distribution unlimited

12b. DISTRIBUTION CODE

13. ABSTRACT (Maximum 200 words)

The overall objective of the proposed research was to provide a quantitative description of the microstructural, as well as macroscopic mechanical behavior of particulate materials with intergranular cementation in a wide range of strain amplitudes and for various types of the cementation material. By cementation, a material is meant which fills the space between two surfaces that are (a) separated or (b) contact directly.

This objective was achieved by deriving microstructural contact laws for the combination of two cemented elastic spherical grains subject to normal, shear, or torsional loading. The cement was treated as an elastic, elastic-plastic, purely plastic, and viscous material. The macroscopic constitutive laws were derived from the above microstructural contact laws by using the formulas which relate the effective moduli of the random packing of identical spheres to the normal and tangential contact stiffnesses. The theoretical solutions were positively supported by experiments performed on artificial cemented aggregates, as well as by other experiments performed of real cemented rocks.

The main relevance to the Air Force mission is through a quantitative description of cemented geomaterials such as asphalt cement. The results have been used at the Wright Laboratory to model asphalt concrete's behavior.

14. SUBJECT TERMS

Particulate materials, cementation, micromechanics, constitutive laws

15. NUMBER OF PAGES 112

16. PRICE CODE

17. SECURITY CLASSIFICATION OF REPORT	18. SECURITY CLASSIFICATION OF THIS PAGE	19. SECURITY CLASSIFICATION OF ABSTRACT	20. LIMITATION OF ABSTRACT
Unclassified	Unclassified	Unclassified	UL

CEMENTED PARTICULATE MATERIALS: FROM GRAIN-TO-GRAIN CONTACT TO MACRO-BEHAVIOR

US AIR FORCE OFFICE OF SCIENTIFIC RESEARCH
CONTRACT F49620-93-1-0052

FINAL REPORT

PI DR. JACK DVORKIN

Geophysics Department, Stanford University
Stanford, CA 94305-215
Tel. (415) 725-9296
Fax. (415) 725-7344
E-mail jack@pangea.stanford.edu

Stanford, April 1996

1. SUMMARY

1.1. OBJECTIVE

The overall objective of the proposed research was to provide a quantitative description of the microstructural, as well as macroscopic mechanical behavior of particulate materials with intergranular cementation in a wide range of strain amplitudes and for various types of the cementation material. By cementation, a material is meant which fills the space between two surfaces that are (a) separated or (b) contact directly (Figure 1.1).

This objective was achieved by deriving microstructural contact laws for the combination of two cemented elastic spherical grains subject to normal, shear, or torsional loading. The cement was treated as an elastic, elastic-plastic, purely plastic, and viscous material. The macroscopic constitutive laws were derived from the above microstructural contact laws by using the formulas which relate the effective moduli of the random packing of identical spheres to the normal and tangential contact stiffnesses.

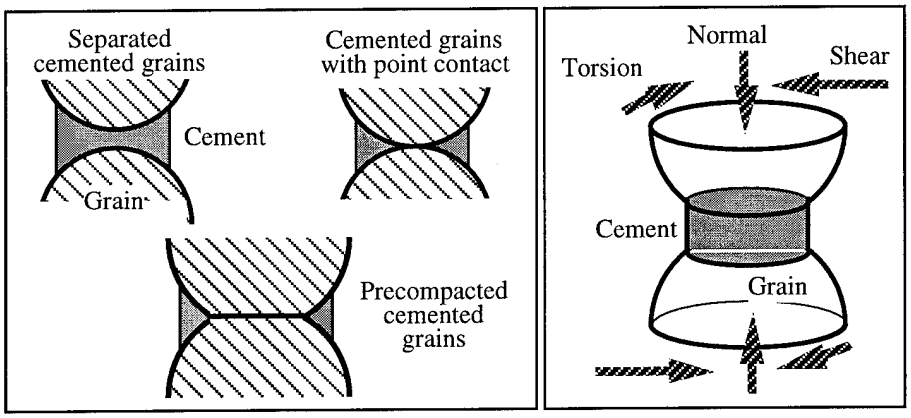

Figure 1.1. Left: Separated grains, grains with a point contact, and precompacted grains. Right: Normal, shear, and torsional deformation of two cemented grains.

The major thrusts of the research were in the theoretical solutions to the problems of deformation of two cemented elastic spherical particles subject to loadings of various types and amplitudes, as well as for various mechanical models of the cement material.

1.2. ACCOMPLISHMENTS

Micromechanics. The micromechanical solutions deal with the interaction of two elastic particles which are cemented at their contact. Typically, the contacting surfaces are assumed to be spherical. However, the solutions obtained are general, and can be used for any non-conforming surfaces. The main assumption is that the contact area is small, as compared to the particle size, so that the particle can be treated as an elastic half-space (in the three-dimensional case) or as a half-plane (in the two-dimensional case). As a result of the solutions were obtained: stress distributions at the contact, and normal, shear, and torsional stiffnesses of a two-grain combination. In all cases the solution was reduced to an ordinary integral equation which had to be solved numerically. The following problems were solved:

- Normal, shear, and torsional deformation of two initially undeformed elastic cemented grains (3-D and 2-D) with elastic cement.
- Easy-to-use formulas for the normal and shear stiffnesses of two initially undeformed elastic cemented grains (3-D) with elastic cement. These formulas have a closed analytical form.
- Normal, shear, and torsional deformation of two precompacted elastic cemented grains (3-D and 2-D) with elastic cement. In this case, the grains were first normally pressed together, and the cement was deposited afterwards.

- Normal and shear deformation of two initially undeformed elastic grains with elastic-plastic cement.
- Normal deformation of two initially undeformed elastic grains with perfectly plastic cement (cement squeezing).
- Normal deformation of two initially undeformed elastic grains with viscous cement (a hydroelasticity problem).
- Normal deformation of two initially undeformed elastic grains where cement is elastic and evenly covers the surface of spherical grains. When a load is applied, a new contact surface develops between the shells of cement. This solution allows for introducing pressure-dependence in the elastic properties of cemented aggregates.

Macroscopic Laws. The micromechanical solutions were used to obtain constitutive macroscopic laws for the deformation of cemented particulate materials. It was assumed that the particulate aggregate is a random dense pack of identical elastic spheres with porosity 0.36 and coordination number 9. The following constitutive laws were derived:

- Small-strain effective elastic moduli for the initially undeformed aggregate with elastic cement.
- Small-strain effective elastic moduli for the precompacted aggregate with elastic cement.
- Small-strain effective elastic moduli for the initially undeformed aggregate with elastic cement where pressure dependence is taken into account.
- Small-strain effective elastic (complex) moduli for the initially undeformed aggregate with viscous cement. The solution provides for calculating velocity-frequency dispersion and attenuation of acoustic waves.
- Large-strain stress-strain laws for the aggregate with elastic-plastic cement for various types of loading (e.g., hydrostatic, uniaxial).
- Large-strain stress-strain law for the hydrostatic compaction of the aggregate with perfectly plastic cement.

Experiments. Elastic wave velocities were measured on:

- epoxy-cemented glass-bead samples;
- ice-cemented glass-bead and sand samples;
- glass-bead samples with viscous cement (uncured epoxy).

Large-strain and failure experiments were performed on epoxy-cemented glass samples. The strength was monitored, and the large-strain bulk modulus was calculated.

Verification. The theoretical solutions were positively supported by the above-mentioned experiments performed on artificial cemented aggregates, as well as by other experiments performed of real cemented rocks. Experiments on visualizing stress distribution in contacting cemented elastic cylinders were performed at the University of Rhode Island. These experiment supported the theoretical predictions as well.

Relevance and Application. The main relevance to the Air Force mission is through a quantitative description of cemented geomaterials such as asphalt cement. Our colleagues at Wright Laboratory used our solutions to model asphalt concrete's behavior.

1.3. PERSONNEL SUPPORTED

Senior Personnel: Dvorkin, Jack, PI; Nur, Amos, Co-PI; Mavko, Gary (all US).
Postdocs: Yin, Hezhu (non-US), Ph.D. in Geophysics, Stanford, 1992.
Students: Frank Liu (non-US), Ph.D. in Geophysics, Stanford, 1994; Maureen Jacoby (US), M.S. in Geophysics, Stanford, 1994; Packwood, James (US), Ph.D. candidate.

1.4. PUBLICATIONS

1. Dvorkin, J., and Nur, A., 1993, Rock Physics for Characterization of Gas Hydrates, in The Future of Energy Gases, USGS Publications, 293-298.
2. Dvorkin, J., Nur, A., and Yin, H., 1994, Effective Properties of Cemented Granular Materials, Mechanics of Materials, 18, 351-366.

3. Yin, H., and Dvorkin, J., 1994, Strength of Cemented Grains, Geophysical Research Letters, 21, 903-906.
4. Dvorkin, J., Yin, H., and Knight, R., 1994, Seismic Detection of Residual Contaminants, 64 Annual Meeting of the Society of Explorational Geophysicists, Expanded Abstracts, Los Angeles, 584-586.
5. Dvorkin, J., and Yin, H., 1995, Contact Laws for Cemented Grains: Implications for Grain and cement Failure, Int. J. Sol. Struct., 32, 2497-2510.
6. Jacoby, M., Dvorkin, J., and Liu, F., 1996, Elasticity of Partially Saturated Frozen Sand, Geophysics, 61, 288-293.
7. Dvorkin, J., and Nur, A., 1996, Elasticity of High-Porosity Sandstones: Theory for Two North Sea Datasets, Geophysics, in press.
8. Elata, D., and Dvorkin, J., 1996, Pressure Sensitivity of Cemented Granular Materials, Mechanics of Materials, in press.
9. Dvorkin, J., 1996, Large Strains in Cemented Granular Aggregates: Elastic-Plastic Cement, Mechanics of Materials, in press.
10. Sienkiewicz, F., Shukla, A., Sadd, M., Zhang, Z., and Dvorkin, J., 1996, A Combined Experimental and Numerical Scheme for the Determination of Contact Loads Between Cemented Particles, Mechanics of Materials, 22, 43-50.
11. Dvorkin, J., and Yale, D., 1996, Plastic Compaction of Cemented Granular Materials, Computers and Geotechnics, in press.

1.5. Interactions and Transitions

Workshops and Conferences:

- Society of Explorational Geophysicists Development and Production Forum, Missouri, June 1993: Role of Cement in Rocks
- American Geophysical Union 1993 Annual Meeting, San Francisco, December 1993: Strength of Cemented Grains
- Caltech, Symposium on the Dynamic Failure Mechanics of Modern Materials, February 1994: Failure and Strength of Cemented Grains
- UC San Diego, Mechanics and Statistical Physics of Particulate Materials, June 1994: Cement among Grains
- SEG 1994 Annual Conference, Los Angeles, October 1994: Seismic Detection of Residual Contaminants
- Phillips Oil Company, and Conoco Oil Company, Oklahoma, January 1995: Effect of Cementation and Diagenesis on Physical Properties of Rocks
- Symposium on Mechanics of Effective Media, University of Karlsruhe, January 1995: Cemented Geomaterials
- The Bay Area Geophysical Society, Invited Lecture, San Ramon, CA, March 1996: Elasticity of High-Porosity Sands

Transitions:

- USAF Laboratories: Wright Laboratory, Tyndall AFB, Dr. Jeff Rish and Dr. Han Zhu -- used the cementation theory (viscoelastic cement) to describe the deformation of asphalt concrete.
- Universities: The University of Rhode Island, Dr. Arun Shukla: Theoretical and experimental (photoelasticity) investigation of the dynamic interaction of cemented disks.

1.6. Patents and Inventions

No patents or inventions resulted form this effort.

2. TECHNICAL PART

IN THIS PART THE TECHNICAL RESULTS ARE PRESENTED IN THE FORM OF JOURNAL ARTICLES. THE NUMERATION OF FORMULAS AND FIGURES IS INTERNAL FOR EVERY SECTION.

2.1. EFFECTIVE PROPERTIES OF CEMENTED GRANULAR MATERIALS

ABSTRACT

An analytical model is developed to describe the effective elastic properties of a cemented granular material that is modeled as a random packing of identical spheres. The elastic moduli of grains may differ from those of cement. The effective bulk and shear moduli of the packing are calculated from geometrical parameters (the average number of contacts per sphere and porosity), and from the normal and tangential stiffnesses of a two-grain combination. The latter are found by solving the problems of normal and tangential deformation of two elastic spherical grains cemented at their contact. A thin cement layer is approximated by an elastic foundation, and the grain-cement interaction problems are reduced to linear integral equations. The solution reveals a peculiar distribution pattern of normal and shear stresses at the cemented grain contacts: the stresses are maximum at the center of the contact region when the cement is soft relative to the grain, and are maximum at the periphery of the contact region when the cement is stiff. Stress distribution shape gradually varies between these two extremes as the cement's stiffness increases. The solution shows that it is mainly the amount of cement that influences the effective elastic properties of cemented granular materials. The radius of the cement layer affects the stiffness of a granular assembly much more strongly than the stiffness of the cement does. This theoretical model is supported by experimental results.

INTRODUCTION

The mechanical characteristics of geologically-derived granular materials such as rock, soil, and concrete can be strongly affected by the properties and position of intergranular bond material. Microstructural contact laws of grain-to-grain interaction provide an indispensable basis to theoretical, as well as to numerical models of deformation of granular media.

In spite of significant progress achieved in modeling macroscopic deformation of granular media (e.g., Cundall and Strack, 1979; Nemat-Nasser, 1983; Nelson et al., 1988; Cundall et al., 1989), the models of microscopic intergranular interaction require further development. The main challenge is in predicting contact stiffness and strength from the geometry of a contact region and from the mechanical properties of grains and intergranular cement. All rigorous theoretical investigations of deformation of aggregates of elastic grains are based on the classical solutions to the problems of normal (Hertz, 1882) or oblique (Mindlin, 1949; Walton, 1978) interaction of elastic spheres. Digby (1981) solved the problem of interaction of spherical particles that are initially bonded together across small areas. These solutions resulted in a number of theoretical and numerical works that examine low-strain, as well as high-strain deformation of granular media (the latter models include relative sliding of grains). Many of these works are discussed in Stoll (1989) in relation to the acoustic properties of sediments.

Only recently, the effect of intergranular cementation on the elastic as well as inelastic behavior of particulate materials started to attract the attention of researchers. Bruno and Nelson (1991) used a two-dimensional discrete element procedure to investigate rock

failure under tensile, uniaxial compression, and biaxial loading. In the elastic domain, contact stiffnesses were assumed to be linear functions of the Young's and shear moduli of the cement, and the thickness and width of cementation bonds. An experimental study by Bernabe et al. (1992), conducted on synthetic cemented granular materials (precompacted Ottawa sand with halite and silica glass as the cement), included triaxial compression tests. It has been found that a small amount of cement can significantly increase the strength of a granular material if it is precisely deposited at previously formed grain-to-grain contacts.

Trent (1989), and Trent and Margolin (1992) numerically investigated the behavior of cemented granular materials under both low-strain and high-strain loads. The materials are composed of circular particles which are glued together with elastic bonds. They show that the effective properties of samples are governed by the properties and distribution of individual intergranular bonds.

The impressive progress of numerical methods combined with the increasing power of computers and computer visualization (Williams and Mustoe, 1993) challenges us to fundamentally understand and theoretically describe interparticle contact laws. Indeed, it is important to know how stresses are transmitted among deformable particles through deformable interparticle bonds. Two cemented grains have to be necessarily considered deformable when, for example, they have a point contact with cement deposited around it. If these grains are absolutely rigid, the two-particle combination will not deform at all. In this case there is no way of finding the contact stiffnesses by examining the deformation of the cement alone.

Dvorkin et al. (1991), examined the normal interaction of two spherical elastic grains and an elastic cementation layer between them. Their results indicate that a thin cement layer subject to normal and shear load can be approximately treated as an elastic foundation. By using this approximation and if the width of the cemented zone is small compared to the grain radius, Dvorkin et al. (1991) were able to reduce the problem of grain-cement deformation (where the grains are deformable) to an ordinary integral equation for the normal stresses at the cemented interface. The stiffness of a cemented system increases with the radius of the cement layer and with its stiffness. The former factor is the most important: the small increase of the cementation content results in significant growth of a contact zone between two contacting grains and, therefore, dramatically increases the stiffness of a two-grain system as well as the macroscopic stiffness of a cemented particulate material (even if the cement is relatively soft).

These theoretical predictions were supported by the experiments of Liu et al. (1991) where a granular material was represented by identical glass beads, and the process of cementation was simulated by freezing the capillary water accumulated at the bead contacts. The measured compressional velocity in the material had small constant values before freezing and increased sharply at the freezing point. This effect is apparently due to the solidification of the pendular rings which form ice intergranular cementation. Qualitatively similar to these are our measurements of velocities in epoxy-cemented glass beads (discussed below). The important message of the experiments is that the velocity increase with cementation is very large between 0% and 10% saturation and small between 10% and 50% saturation (Figure 1). Therefore, cementation can dramatically increase the stiffness of a granular material only if it is placed around grain-to-grain contacts.

In this paper we concentrate on the theoretical modeling of effective elastic properties of random packing of identical elastic spheres with elastic cement at their contacts. The effective bulk and shear moduli of a packing are calculated from the average number of contacts per sphere and porosity of the aggregate, and from the normal and tangential stiffnesses of a two-grain combination (Digby, 1981). These stiffnesses are found by solving the problems of normal and tangential deformation of two elastic spherical grains cemented at their contact. The approach used in obtaining this solution is similar to that of Dvorkin et al. (1991): a thin cement layer is approximated by an elastic foundation, and the grain-cement interaction problems are reduced to linear integral equations.

Our mathematical approach to solving these elastic contact problems is similar to those used in many contact-dominated theories. Among them are solutions that describe the effective viscosity of concentrated suspensions (e.g., Frankel and Acrivos, 1967; Goddard, 1977; Nunan and Keller, 1984); adhesive-contact interaction (e.g., Johnson, et al., 1971); and thermal and electrical conduction through a granular material (e.g., Batchelor and O'Brien, 1976).

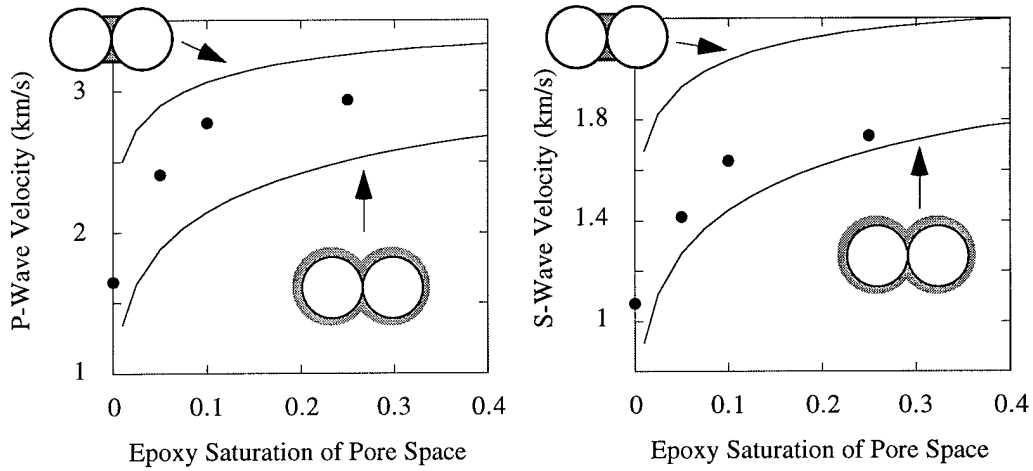

Figure 1. P-wave and S-wave velocities measured in epoxy-cemented glass beads at varying cement saturation at hydrostatic confining pressure 30 MPa. The circles indicate the measurement points. The experiments have been conducted using the ultrasonic pulse transmission method. The experimental data is compared to our upper and lower bound theoretical predictions -- solid lines obtained under two different assumptions of cement placement around the grains.

The solution reveals a peculiar pattern of normal and shear stresses distribution at the cemented grain contacts: the stresses are maximum at the center of the contact region when the cement is soft relative to the grain, and are maximum at the periphery of the contact region when the cement is stiff. Stress distribution shape gradually varies between these two extremes. This result provides an important insight into possible modes of intergranular cement failure: relatively stiff cement will yield at the periphery of a cement layer. Our theoretical solution shows that it is mainly the amount of cement that influences the effective elastic properties of cemented granular materials. The radius of the cement layer affects the stiffness of a granular assembly much more strongly than the stiffness of the cement does.

Our theoretical prediction of the effective properties of cemented granular materials is applicable to a random packing of identical spheres. The solutions to the problems of normal and shear deformation of a two-grain combination are more general and thus can be used as constitutive contact laws in rigorous numerical simulations. Still, caution should be exercised when substituting these contact laws into mean-field approximations, such as the above-mentioned Digby's solution. Such approximations may become invalid in highly-disordered or contact-depleted systems (e.g., Goddard, 1990).

Finally, the problems of normal and tangential deformation of two cemented elastic cylinders (the plane case) are considered in the Appendix.

Effective Properties of Identical Sphere Packings

The effective elastic properties of a random packing of identical spherical particles can be expressed through its porosity ϕ, coordination number C (the average number of contacts per sphere), the radius of a particle R, and the normal (S_n) and tangential (S_τ)

stiffnesses of a two-sphere combination (Digby, 1982; and Winkler, 1983). The normal and shear stiffnesses are defined as the ratios of a corresponding force increment to the displacement of the sphere center relative to the contact region (Figure 2):

$$S_n=\frac{\partial F}{\partial \delta},\ S_\tau=\frac{\partial T}{\partial \tau}. \tag{1}$$

Effective bulk (K_{eff})and shear (G_{eff}) moduli are:

$$K_{eff}=\frac{C(1-\phi)}{12\pi R}S_n,\ G_{eff}=\frac{C(1-\phi)}{20\pi R}(S_n+\frac{3}{2}S_\tau). \tag{2}$$

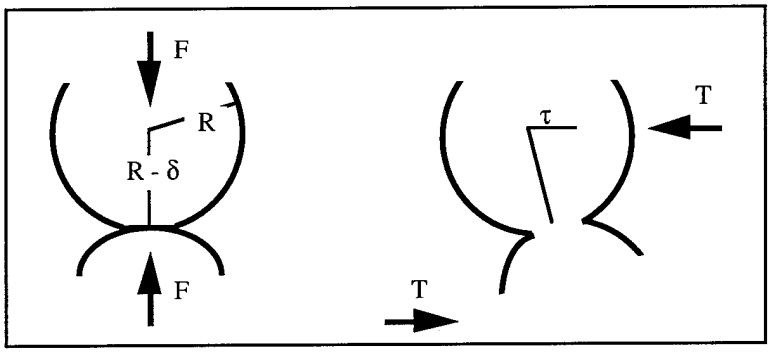

Figure 2. Normal and shear deformation of a two-grain combination.

Therefore, the effective compressional and shear velocities can be found as

$$V_p^2=\frac{3C}{20\pi R\rho}(S_n+\frac{2}{3}S_\tau),\ V_s^2=\frac{C}{20\pi R\rho}(S_n+\frac{3}{2}S_\tau),$$

where ρ is the density of the grain material.

NORMAL DEFORMATION OF TWO CEMENTED SPHERES

Normal Stiffness and Effective Bulk Modulus

The solution to the problem of the normal deformation of two cemented grains (Dvorkin et al., 1991) is based on the assumption that a contact region is small as compared to the grain. Therefore, normal displacements v of the surface of an elastic grain due to a concentrated force P can be expressed in the (x,y,z) coordinate system (Figure 3) as those of the surface of an elastic half-space (Johnson, 1985):

$$v(x,y)=\frac{(1-\nu)}{2\pi G}\frac{P}{r},\ r=\sqrt{x^2+y^2}, \tag{3}$$

where G and ν are the shear modulus and Poisson's ratio of the grain, respectively.

We assume that the cemented region is symmetrical with respect to the line that connects the centers of the two contacting spheres (Figure 4a). Therefore, the contact region on the surface of the sphere is a circle of radius a (Figure 4b), and contact stresses

and displacements are axisymmetrical, and depend on the radius r only. Normal stresses $p(r)$ are related to normal displacements $v(r)$ as (Timoshenko and Goodier, 1970)

$$v(r)=\frac{(1-\nu)}{\pi G}\int_0^{\pi} d\varphi \int_0^{r\cos\varphi+\sqrt{a^2-r^2\sin^2\varphi}} p(\sqrt{r^2+s^2-2rs\cos\varphi})\,ds, \tag{4}$$

where integration is conducted inside the circle $|r|< a$ (Figure 5).

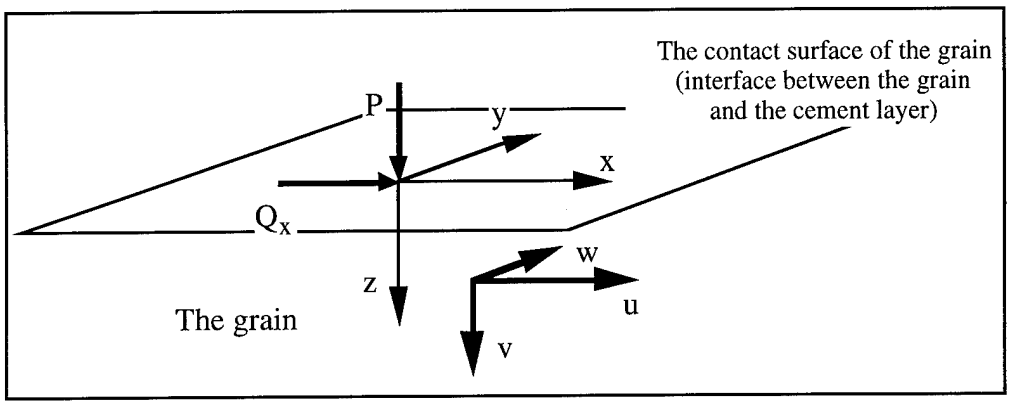

Figure 3. Concentrated forces acting upon the surface of an elastic half-space. A cemented contact region between two grains is assumed to be small as compared to the grain. On the basis of this assumption, displacements of the surface of the grain are related to stresses through the formulas for an elastic half-space.

The displacement of the center of the spherical grain relative to the median plane of the cement layer δ can be related to the displacements $V(r)$ of the surface of the cement layer and $v(r)$ of the surface of the grain (Figures 4b, c, and d) as

$$\delta=v(r)-V(r). \tag{5}$$

The results of Dvorkin et al. (1991) show that a thin cement layer subject to normal and shear load can be approximately treated as an elastic foundation. Therefore, normal stresses p acting upon the surface of the grain are related to the displacements V of the surface of the cement layer as

$$p(r)=-\frac{2G_c(1-\nu_c)}{1-2\nu_c}\frac{V(r)}{h(r)}, \tag{6}$$

where G_c and ν_c are the shear modulus and Poisson's ratio of the cement, and $h(r)$ is half-thickness of the cement layer. For the case under consideration we have

$$h(r)=R[\varepsilon+\frac{1}{2}(\frac{r}{R})^2],\ \varepsilon=\frac{h(0)}{R}. \tag{7}$$

By assuming in addition that shear stresses at the grain surface do not significantly influence its normal deformation (Johnson, 1985), we can combine equations (4) - (7) into the following integral equation:

$$\delta + V(r) = -\Lambda \int_0^{\pi} d\varphi \int_0^{r\cos\varphi + \sqrt{a^2 - r^2\sin^2\varphi}} \frac{V(\sqrt{r^2 + s^2 - 2rs\cos\varphi})}{R[\varepsilon + \frac{1}{2}(\frac{r^2}{R^2} + \frac{s^2}{R^2} - 2\frac{rs}{R^2}\cos\varphi)]}\, ds,$$

$$\Lambda = \frac{2G_c}{\pi G}\frac{(1-\nu)(1-\nu_c)}{1-2\nu_c}.$$

The constant δ here can be determined from the resulting compressional force F:

$$F = \int_0^a p(r) 2\pi r\, dr = -\frac{4\pi G_c(1-\nu_c)}{1-2\nu_c}\int_0^a \frac{V(r) r}{h(r)} dr.$$

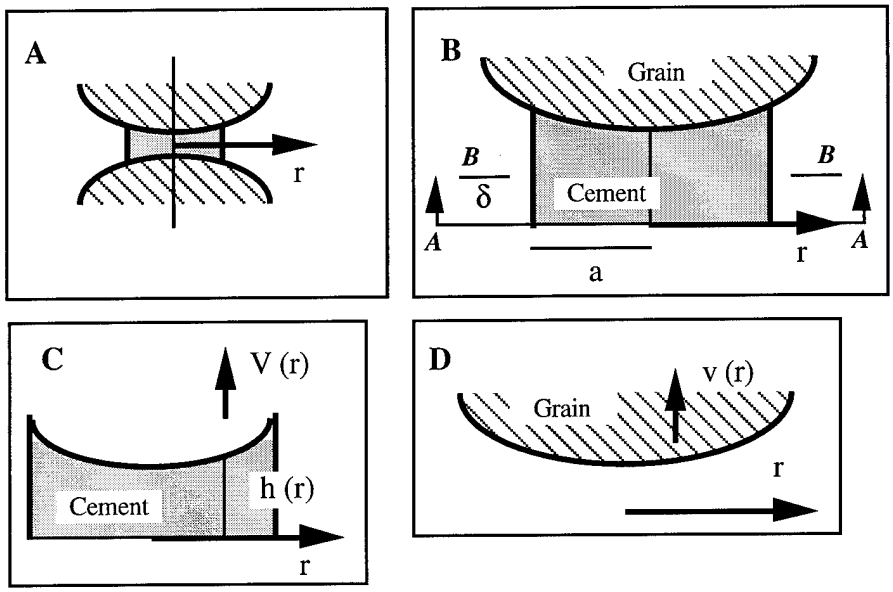

Figure 4. A cemented contact region between two spherical grains: a) The cement forms an axisymmetrical thin layer. b) Normal deformation of the grain and the cement -- δ is the displacement of the center of the sphere relative to the median plane of the cement layer AA (this plane moves into position BB). c) Normal axisymmetrical displacement of the cement layer. d) Normal axisymmetrical displacement of the surface of the grain.

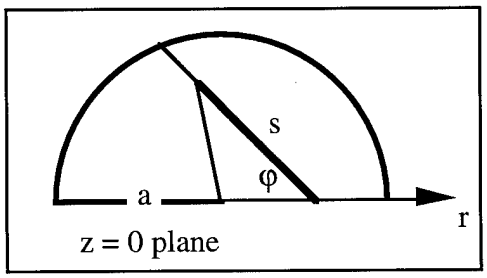

Figure 5. The region of contact on the grain surface $|r| < a$ in the plane $z = 0$.

After normalizing the above equations, and using (1), we arrive at the following scheme of determining normal stiffness S_n:

1. Find an as yet unknown function $H(t)$ from the integral equation

$$\Delta_0 + H(t) = -\Lambda \int_0^{\pi} d\varphi \int_0^{t\cos\varphi + \sqrt{\alpha^2 - t^2\sin^2\varphi}} \frac{H(\sqrt{t^2+s^2-2ts\cos\varphi})}{\varepsilon + \frac{1}{2}(t^2+s^2-2ts\cos\varphi)}\, ds,$$

where $\alpha = a / R$, and Δ_0 is an arbitrarily chosen non-zero constant.

2. Calculate integral

$$\int_0^{\alpha} \frac{H(t)\, t\, dt}{\varepsilon + t^2/2} = k.$$

3. Find normal stiffness S_n as

$$S_n = -\frac{4\pi R G_c (1-\nu_c)}{1-2\nu_c} \frac{k}{\Delta_0}.$$

Formula (2) now yields the following final expression for the effective bulk modulus of a random sphere packing of porosity ϕ and coordination number C:

$$K_{eff} = \frac{G_c(1-\nu_c)}{1-2\nu_c} \frac{C(1-\phi)}{3(1+\varepsilon)} \left(-\frac{k}{\Delta_0}\right),$$

where ε is proportional to the minimal thickness of the cement layer (at $r = 0$), and $\varepsilon = 0$ for the case where grains have direct point contacts.

The above integral equations allow for a straightforward numerical solution using the quadrature method (e.g., Delves and Mohamed, 1985).

Normal Stress Distribution at the Contact

We used the above equations to calculate normal stress distribution at the contact of two cemented elastic spheres. In the following example, the Poisson's ratios of both the grain and the cement materials were constant: $\nu = \nu_c = 0.28$, the densities were also constant and equal 2480 kg/m^3. The minimal separation between grains was zero ($\varepsilon = 0$), the ratio of the radius of the cement layer to the grain radius was 0.33. We considered six cases where the rigidity of the cement material relative to that of the grains varied from very soft cement ($V_{p\,\text{cement}} / V_{p\,grain} = 0.2$) to relatively stiff cement ($V_{p\,\text{cement}} / V_{p\,grain} = 1.4$), where V_p is the compressional velocity in a material.

The results reveal a peculiar picture of normal stress distribution at the cemented grain contacts: the stresses are maximum at the center of the contact region when the cement is soft relative to the grain, and are maximum at the periphery of the contact region when the cement is stiff. Stress distribution shape gradually varies between these two extremes as the cement's stiffness increases. These results allow for a simple physical interpretation: When a soft cement layer is confined between two rigid grains, its maximum compression occurs at its thinnest part -- near the point of direct grain-to-grain contact. If the cement is stiff, the problem approaches that of a rigid punch (the cement) penetrating an elastic half-space (the grain). In the latter case, normal stress becomes infinite at the edge of the punch

(Johnson, 1985) which explains the observed maximum of the normal stresses at the periphery of the contact region. One practical implication of the observed normal stress distribution is that a relatively stiff intergranular cement layer will tend to yield at its edges.

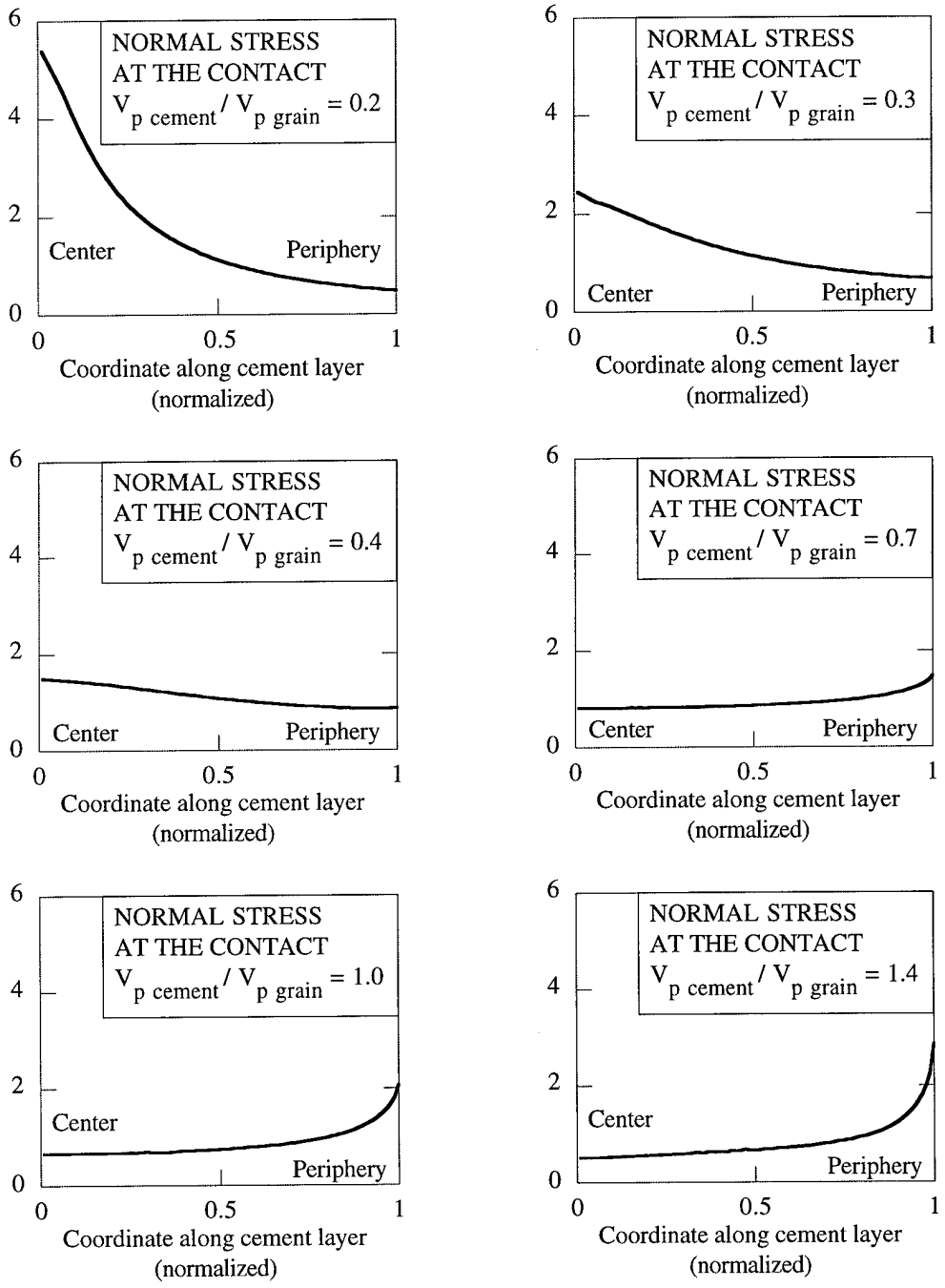

Figure 6. Normal stress distribution along the radii of cement layers for varying relative rigidity of the cement and the grain materials -- from very soft to very stiff cement. Stresses are normalized by the average stress. The horizontal axis is the normalized distance along the radius of the cement layer.

TANGENTIAL DEFORMATION OF TWO CEMENTED SPHERES

Tangential Stiffness of a Two-Grain Combination

Our approach to solving the problem of tangential deformation of two cemented grains with the relative displacement 2τ in the x direction (the coordinate system on the surface of a grain is shown in Figure 3) is similar to the one used for the problem of normal deformation. Again, we assume that the contact region is small compared to the grain and, therefore, the formulas for an elastic half-space can be used to relate stresses on the grain surface to its displacements.

A concentrated tangential force Q_x when applied to an elastic half-space (Figure 3), produces the following displacements of the surface (Johnson, 1985):

$$u=\frac{Q_x}{4\pi G}\frac{1}{r}[(1+\frac{x^2}{r^2})+(1-2\nu)(1-\frac{x^2}{r^2})],$$
$$w=\frac{Q_x\nu}{2\pi G}\frac{xy}{r^3},\quad v=\frac{Q_x(1-2\nu)}{4\pi G}\frac{x}{r^2},\quad r^2=x^2+y^2 \tag{8}$$

at $z=0$.

It follows from the above equations that the problem under consideration is not axisymmetrical as in the case of normal compression. Indeed, a tangential deformation of a two-grain combination in the x direction will produce displacements in the cement layer not only in the x but also in the y direction. The latter are symmetrical with respect to the x axis and thus are zero at $y=0$ and, generally, non-zero elsewhere.

Similar to (4), the following integral equations can be obtained to relate tangential stresses q_x and q_y distributed in the circle of radius a, to the corresponding displacements u and w:

$$u(r,\theta)=\frac{1}{2\pi G}\int_0^{2\pi}d\varphi\int_0^{L(r,\theta,\varphi)}[q_x(r_c,\theta_c)(1-\nu\sin^2\varphi)-q_y(r_c,\theta_c)\,\nu\sin\varphi\cos\varphi]ds,$$
$$w(r,\theta)=\frac{1}{2\pi G}\int_0^{2\pi}d\varphi\int_0^{L(r,\theta,\varphi)}[q_y(r_c,\theta_c)(1-\nu\cos^2\varphi)-q_x(r_c,\theta_c)\,\nu\sin\varphi\cos\varphi]ds, \tag{9}$$

where

$$L(r,\theta,\varphi)=a[\sqrt{1-(\frac{r}{a})^2\sin^2(\theta+\varphi)}+\frac{r}{a}\cos(\theta+\varphi)],$$
$$r_c=\sqrt{r^2+s^2-2rs\cos(\theta+\varphi)},\ \theta_c=\arctan(\frac{r\sin\theta+s\sin\varphi}{r\cos\theta-s\cos\varphi}),$$
$$r=\sqrt{x^2+y^2},\ \theta=\arctan(\frac{y}{x}).$$

The domain of integration in the $z=0$ plane is shown in Figure 7.

Similar to the above case of normal deformation, the following compatibility equations can be written for the tangential displacements of the cement and the grain:

$$\tau = u(r,\theta) - U(r,\theta),\ w(r,\theta) = W(r,\theta),$$

where U and W are the tangential displacements of the surface of the cement layer in the x and y directions, respectively, and τ is the tangential displacement of the center of the grain along the x direction.

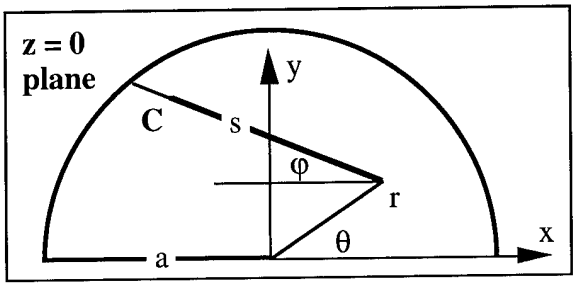

Figure 7. The domain of integration used in equations (9).

Employing in addition the assumption that a cement layer, when deforming in shear, can be treated as an elastic foundation:

$$q_x(r,\theta) = -G_c \frac{U(r,\theta)}{h(r,\theta)},\ q_y(r,\theta) = -G_c \frac{W(r,\theta)}{h(r,\theta)},$$

we can transform (9) into the following system of two integral equations:

$$\begin{aligned}
&\tau + U(r,\theta) = \\
&-\frac{G_c}{2\pi G}\int_0^{2\pi} d\varphi \int_0^{L(r,\theta,\varphi)} \left[\frac{U(r_c,\theta_c)}{h(r_c)}(1-\nu\sin^2\varphi) - \frac{W(r_c,\theta_c)}{h(r_c)}\nu\sin\varphi\cos\varphi \right] ds, \\
&W(r,\theta) = \\
&-\frac{G_c}{2\pi G}\int_0^{2\pi} d\varphi \int_0^{L(r,\theta,\varphi)} \left[\frac{W(r_c,\theta_c)}{h(r_c)}(1-\nu\cos^2\varphi) - \frac{U(r_c,\theta_c)}{h(r_c)}\nu\sin\varphi\cos\varphi \right] ds.
\end{aligned} \tag{10}$$

For the case of two spherical grains in contact, h is given by (7).

In these equations, τ can be determined from the resulting tangential force T:

$$T = \int_0^a \int_0^{2\pi} q_x(r,\theta)\, r\, d\theta\, dr = -G_c \int_0^a \int_0^{2\pi} \frac{U(r,\theta) r}{h(r)}\, d\theta\, dr.$$

The resulting tangential stiffness can be found from (1).

Approximate Simplified Solution for Tangential Stiffness

The above system of two integral equations for determining the tangential stiffness of a two-grain combination can be simplified and reduced to one integral equation. It follows from (8) that a force acting in the x ($\theta = 0$) direction produces tangential displacements u and w with the ratio

$$\frac{w(r,\theta)}{u(r,\theta)}=\frac{\nu\sin\theta\cos\theta}{1-\nu\sin^2\theta}.$$

This ratio monotonously increases with the increasing ν. Its maximum value for $\nu = 0.4$ is about 0.25. Therefore, a tangential force acting on an elastic half-space produces lateral displacements that do not exceed 25% of the displacements in the parallel direction. By rewriting the first integral equation in (10) as

$$u(r,\theta)=-\frac{G_c}{2\pi G}\int_0^{2\pi}d\varphi\int_0^{L(r,\theta,\varphi)}[\frac{u(r_c,\theta_c)-\tau}{h(r_c)}(1-\nu\sin^2\varphi)-\frac{w(r_c,\theta_c)}{h(r_c)}\nu\sin\varphi\cos\varphi]ds,$$

we conclude that the contribution of these lateral displacements is no more that 25% of that of the displacements in the parallel direction. Therefore, the total error of neglecting displacement w does not exceed 6.25%.

Based on this approximation, we can reduce (10) to a single integral equation

$$\tau+U(r)=-\Lambda_\tau\int_0^{\pi}d\varphi\int_0^{r\cos\varphi+\sqrt{a^2-r^2\sin^2\varphi}}\frac{U(\sqrt{r^2+s^2-2rs\cos\varphi})(1-\nu\sin^2\varphi)}{R[\varepsilon+\frac{1}{2}(\frac{r^2}{R^2}+\frac{s^2}{R^2}-2\frac{rs}{R^2}\cos\varphi)]}ds,\quad \Lambda_\tau=\frac{G_c}{\pi G}.$$

The constant τ can be determined from the resulting tangential force T:

$$T=\int_0^a q_x(r)2\pi r\,dr=-2\pi G_c\int_0^a\frac{U(r)r}{R[\varepsilon+\frac{1}{2}(\frac{r}{R})^2]}dr.$$

After normalizing the above equations for tangential deformation, we arrive at the following scheme of determining tangential stiffness S_τ of a two-grain combination:

1. Find an as yet unknown function $H(t)$ from the integral equation

$$\Delta_0+H(t)=-\Lambda_s\int_0^{\pi}d\varphi\int_0^{t\cos\varphi+\sqrt{\alpha^2-t^2\sin^2\varphi}}\frac{H(\sqrt{t^2+s^2-2ts\cos\varphi})(1-\nu\sin^2\varphi)}{\varepsilon+\frac{1}{2}(t^2+s^2-2ts\cos\varphi)}ds,$$

where $\alpha = a / R$, and Δ_0 is an arbitrarily chosen non-zero constant.

2. Calculate integral

$$\int_0^{\alpha}\frac{H(t)t\,dt}{\varepsilon+t^2/2}=k.$$

3. Find tangential stiffness S_τ as

$$S_\tau=-2\pi RG_c\frac{k}{\Delta_0}.$$

Formula (2) now yields the following final expression for the effective shear modulus of a random sphere packing of porosity ϕ and coordination number C:

$$G_{eff} = \frac{3}{5} K_{eff} + G_c \frac{3C(1-\phi)}{20(1+\varepsilon)} (-\frac{k}{\Delta_0}),$$

where K_{eff} can be found from the above solution for the normal deformation of two cemented grains.

Shear Stress Distribution at the Contact

We used the above equations to calculate shear stress distribution at the contact of two cemented elastic spheres. All parameters in the following example are identical to those in the above example for normal stresses.

The results (Figure 8) are similar to those for normal stresses: shear stresses are maximum at the center of the contact region when the cement is soft relative to the grain, and are maximum at the periphery of the contact region when the cement is stiff. The shape of the stress distribution curve gradually varies between these two extremes with the increasing stiffness of the cement.

EXAMPLES - EFFECTIVE PROPERTIES OF CEMENTED SPHERICAL GRAINS

Effect of the Amount of Cement

In the following example we explore the influence of the amount of cementation on the effective properties (compressional and shear velocities) of a random packing of identical spheres. The porosity of the packing (without cementation) was 0.36, the coordination number was assumed 9. The properties of the grain material were: density 2480 kg/m^3, bulk modulus 49.9 GPa, and shear modulus 26.2 GPa -- parameters typical for glass. The density of the cement material was 1160 kg/m^3. We explored four cases of the increasing stiffness of the cement: a. K_c = 3.4 GPa, G_c = 1.0 GPa; b. K_c = 6.8 GPa, G_c = 2.0 GPa; c. K_c = 13.6 GPa, G_c = 4.0 GPa; and d. K_c = 27.2 GPa, G_c = 8.0 GPa. The second case here corresponds to typical epoxy parameters. The ratio of the cement layer radius a to the grain radius varied from 0.01 to 0.5.

Plots in Figure 9 show that both compressional and shear velocities dramatically increase with the increasing radius of the cement layer. The influence of this parameter is clearly much stronger than that of the cement stiffness: even a small increase in the amount of relatively soft cement gives a significant rise to both V_p and V_s. These theoretical predictions are well supported by the earlier experiments of Liu et al. (1991) which are discussed in the Introduction, and by our experiments on epoxy-cemented glass beads.

The effective Poisson's ratio of the cemented sphere packings increases with the increasing amount of cementation (Figure 10). The effect of cement stiffness is opposite to that in the case of compressional and shear velocities: the Poisson's ratio decreases with the increasing stiffness.

Effect of Cement Stiffness

We explored the effect of cement stiffness on compressional and shear velocities (Figure 11) in the above-described random packings of identical spheres for constant amount of cement (a / R = 0.1). The parameters of the grain material were kept constant

with bulk and shear moduli 49.9 and 26.2 GPa, respectively, whereas the stiffness of the cement varied from K_c = 3.4 GPa and G_c = 1.0 GPa to K_c = 68 GPa and G_c = 20 GPa. This dramatic increase of cement stiffness results in only about a 15% increase in compressional and a 20% increase in shear velocity -- an effect much smaller than that of increasing cement content.

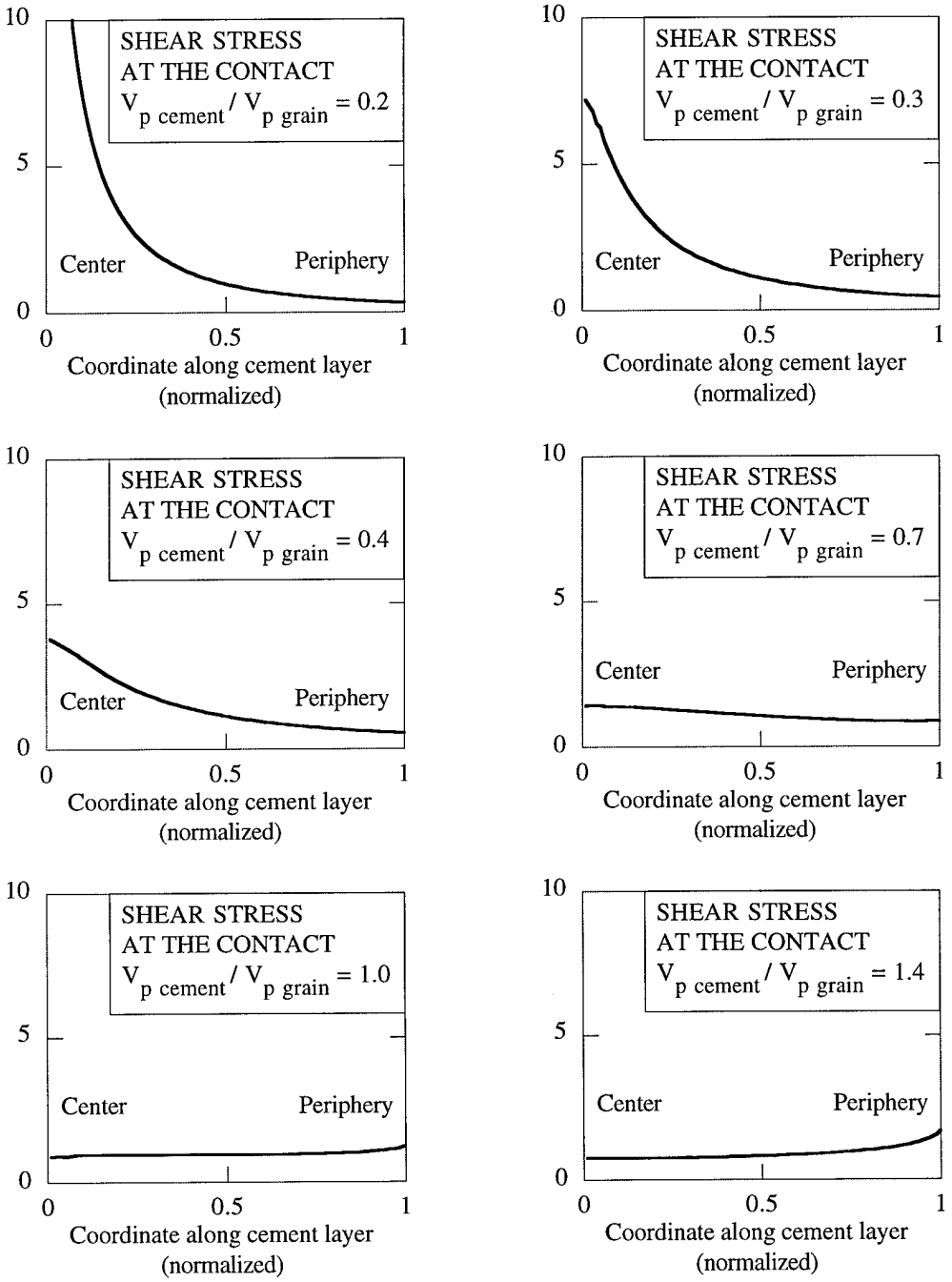

Figure 8. Shear stress distribution along the radii of cement layers for varying relative rigidity of the cement and the grain materials -- from very soft to very stiff cement. Stresses are normalized by the average stress. The horizontal axis is the normalized distance along the radius of the cement layer.

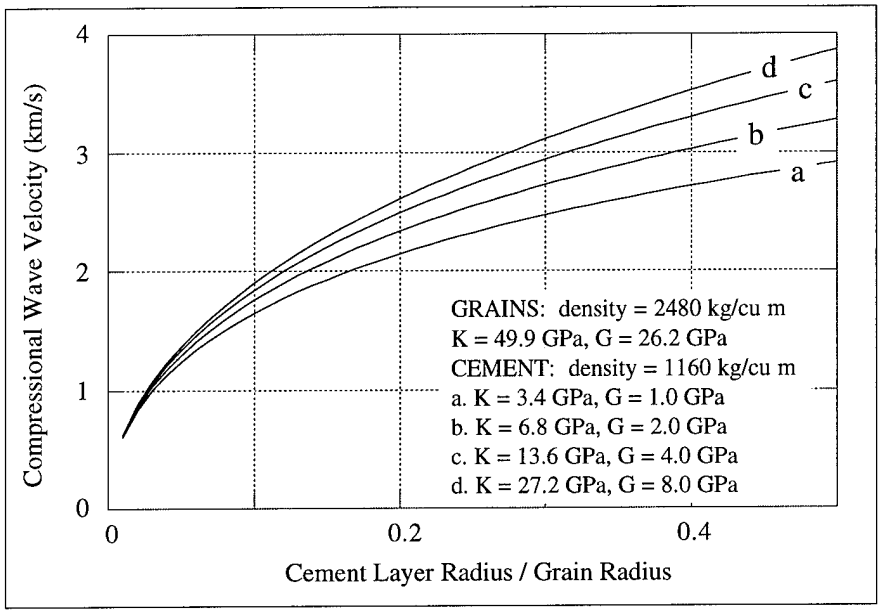

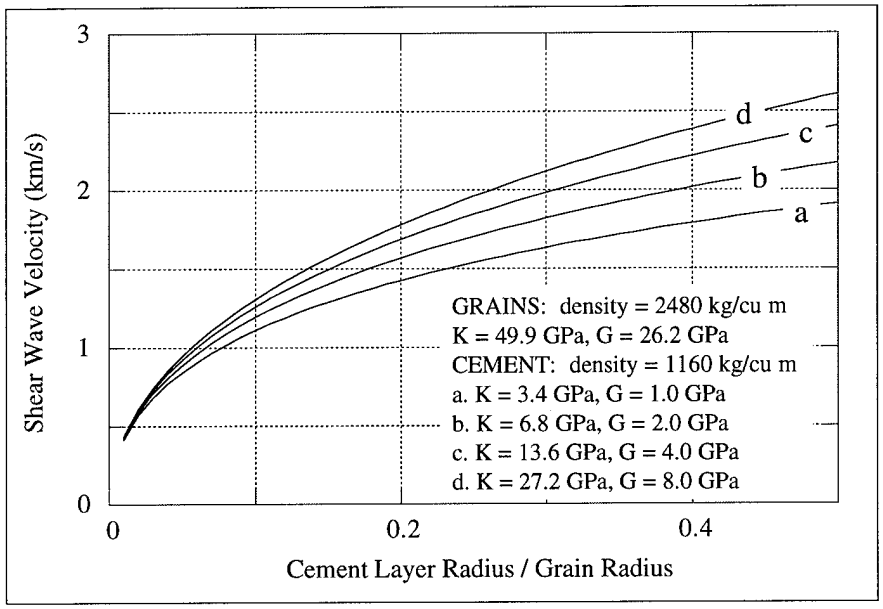

Figure 9. Compressional and shear velocities in random packings of identical cemented spherical particles as functions of the amount of cementation. The parameters of the grain material are constant; the parameters of the cement vary from soft ("a") to stiff ("d") cement.

EXPERIMENTAL RESULTS

In order to check the validity of our theoretical model, we have conducted ultrasonic (0.42 MHz) pulse transmission experiments on epoxy-cemented glass beads. We used spherical glass beads of 0.42 - 0.5 mm diameter. The material contains no more than two percent of irregularly-shaped grains, and is reasonably free of sharp angular particles, or particles showing milkiness, surface scoring, and foreign matter. The porosity of the uncemented glass bead sample was about 36 percent -- close to the porosity of a dense

random pack of identical spheres. The cemented sample was prepared by mixing glass beads with a given volume of epoxy. The mixture was placed into a holder where the epoxy solidified.

The measured compressional- and shear-wave velocity is compared to the theoretical predictions in Figure 1. The upper theoretical curve (upper bound estimate) corresponds to the case where all cement is deposited precisely at grain contacts, the coordination number here was chosen as 9. The lower theoretical curve (lower bound estimate) was calculated for the case where a contact cement region is formed as the intersection of cement shells that are uniformly deposited on grain surfaces. For a random pack of identical spheres, the average number of contacts per grain is between 8 and 9. Therefore, we choose 8 as the coordination number for this lower bound estimate. The measurements are within the predicted bounds.

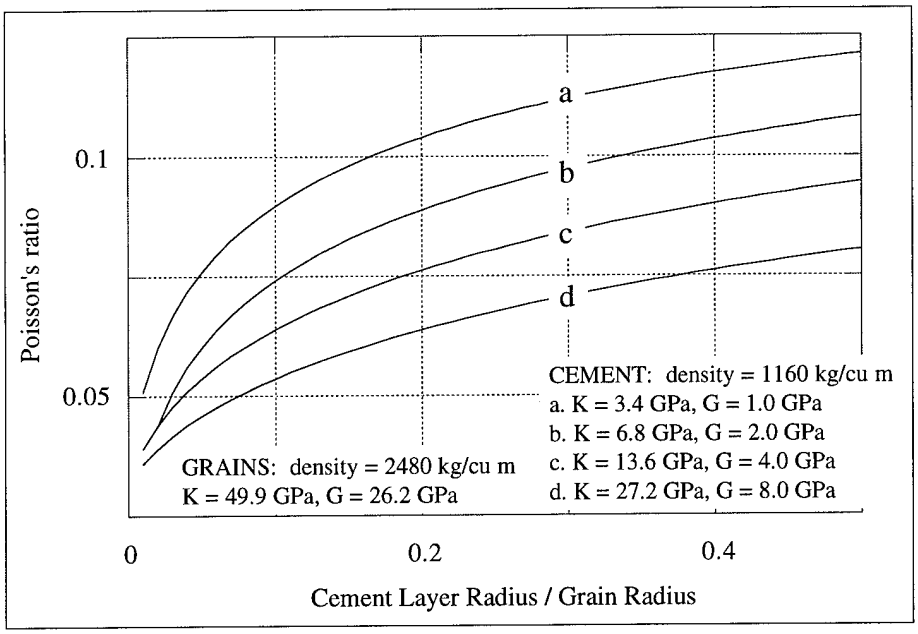

Figure 10. Poisson's ratio of random packings of identical cemented spherical particles as a function of the amount of cementation. The parameters of the grain material are constant; the parameters of the cement vary from soft ("a") to stiff ("d") cement.

CEMENT DEPOSITION, POROSITY AND EFFECTIVE PROPERTIES

The following example illustrates how two possible schemes of cement deposition may affect the porosity and the elastic moduli of a granular material. Both grain and cement materials were identical (glass), which is relevant to the process of quartz cementation of unconsolidated well-sorted sands. The process of cementation starts at the critical porosity point (about 36% for a random identical sphere packing) at which both bulk and shear moduli are zero in an unconsolidated granular material. The first model (Arrangement 1) is where all added cement is accumulated at the intergranular contacts. In the second model, (Arrangement 2) the cement evenly covers the grains and the contact cement layer is formed as an intersection of these cement shells. It is clear that in the first arrangement, the size of a contact cement layer is larger (for given porosity) than in the second arrangement. This effect results in a steeper increase of the effective moduli with decreasing porosity in the first model as compared to the second one (Figure 12). Both bulk and shear moduli steeply increase at the very beginning of cement deposition because even a small addition of cement at intergranular contact points leads to the fast growth of the radius of the cement layer. It

is important to note that our theoretical model is applicable only for small amounts of cement at intergranular contacts.

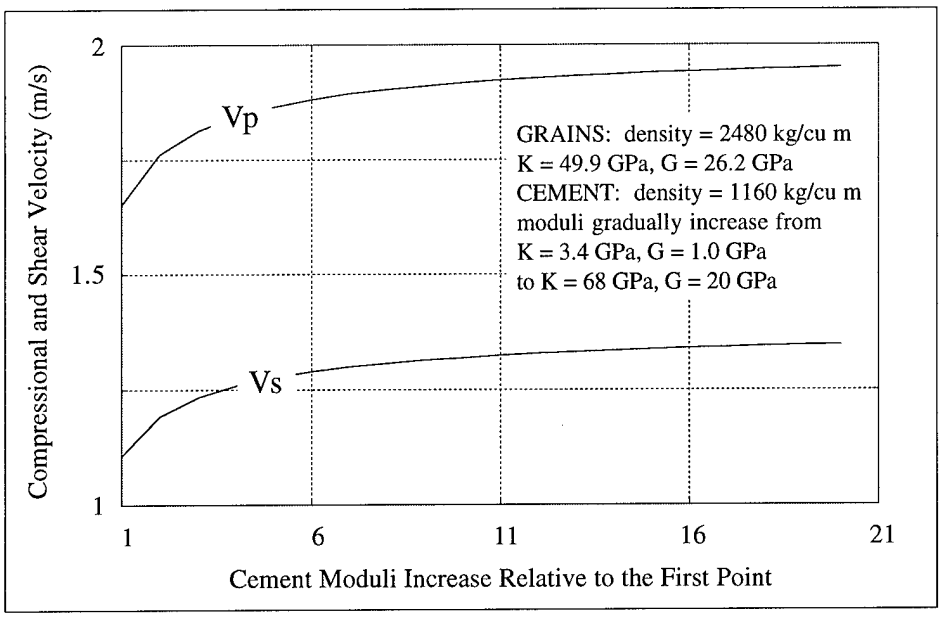

Figure 11. Compressional and shear velocities in a random packing of identical cemented spherical particles as a function of cement stiffness. The ratio of the radius of the cement layer to grain radius is constant and equals 0.1.

CONCLUSIONS

A theoretical solution is given to the problems of normal and tangential deformation of two cemented elastic grains. The elastic moduli of grains may differ from those of cement. This solution is used to describe the effective elastic properties of a cemented granular material that is modeled as a random packing of identical spheres. The effective bulk and shear moduli of the packing are calculated from porosity and coordination number, and from the normal and tangential stiffnesses of a two-grain combination. A thin elastic cement layer is approximated by an elastic foundation, and the grain-cement interaction problems are reduced to linear integral equations. The theoretical solution shows a peculiar pattern of normal and shear stresses distribution at the cemented grain contacts: the stresses are maximum at the center of the contact region when the cement is soft relative to the grain, and are maximum at the periphery of the contact region when the cement is stiff. Stress distribution shape gradually varies between these two extremes as the cement's stiffness increases. The solution reveals that the radius of the cement layer has a much stronger effect on the stiffness of a granular assembly than does the stiffness of the cement. This result provides an important insight into possible modes of intergranular cement failure: relatively stiff cement will fail at the periphery of a cement layer. The results of our theoretical solution to the problem of deformation of a two-grain combination provide constitutive contact laws that can be used in rigorous numerical simulations. It is important to keep in mind that in this paper we present the effective elastic constants of a composite material that have been obtained from the static analysis. These constants cannot be used in predicting wave velocities if frequencies are so high that wavelengths are comparable to the individual grain size. However, static elastic constants can be used with confidence if the wavelength is significantly larger that the individual grain size. In our experiments, the wavelengths were about twelve times the average grain diameter.

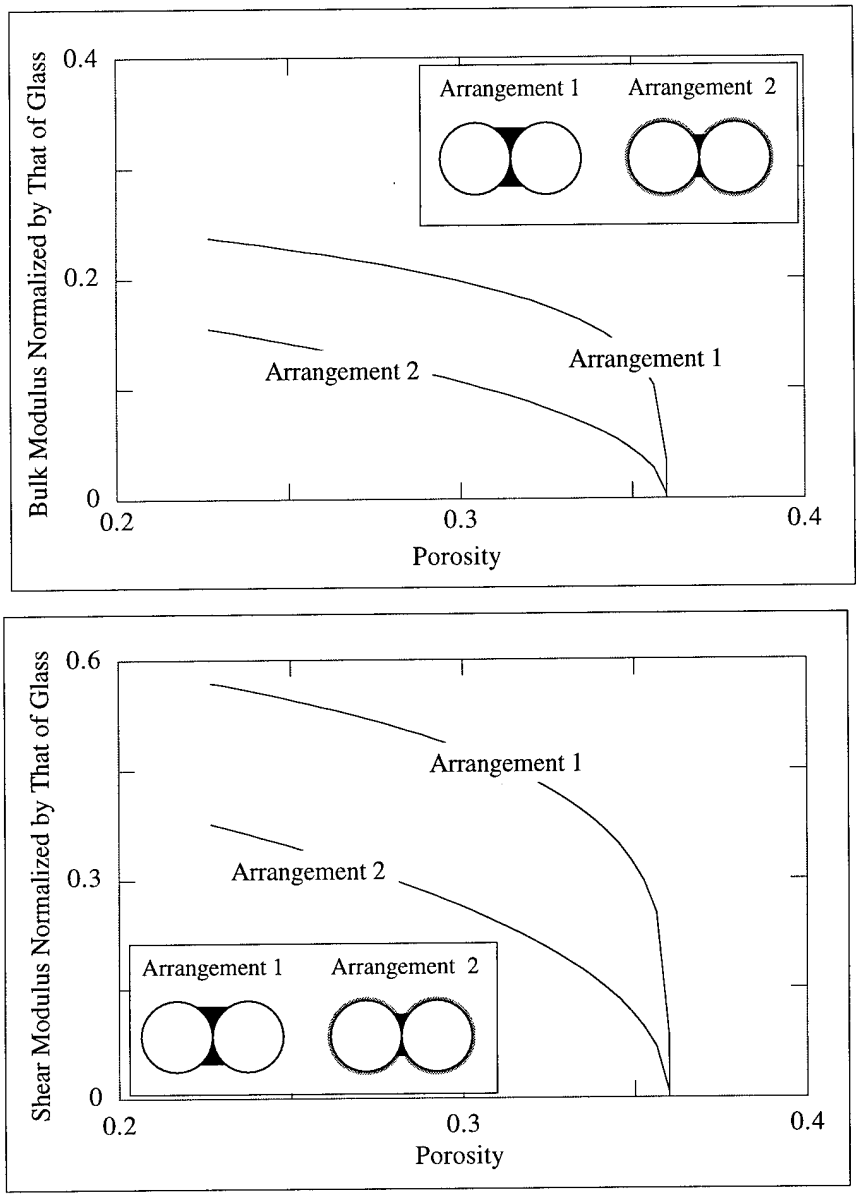

Figure 12. Bulk and shear moduli of a random packing of identical glass-cemented glass beads for two models of cement deposition. The moduli are normalized by those of glass. The porosity of the aggregate reduces with the increasing amount of the cement.

REFERENCES

Batchelor, G.K. and O'Brien, R.W., 1977, Thermal or electrical conduction through a granular material, Proc. R. Soc. Lond., A. **355**, 313 - 333.

Bernabe, Y., Fryer, D.T. and Hayes, J.A., 1992, The effect of cement on the strength of granular rocks, Geophys. Res. Let., **19**, 1511 - 1514.

Bruno, M.S. and Nelson, R.B., 1991, Microstructural analysis of the inelastic behavior of sedimentary rock, Mechanics of Materials, **12**, 95 - 118.

Cundall, P.A., Jenkins, J.T. and Ishibashi, I., 1989, Evolution of elastic moduli in a deforming granular assembly, Int. Conf. on Micromechanics of Granular Media, Clermont-Ferrand, France.

Cundall, P.A. and Strack, O.D.L., 1979, A discrete numerical model for granular assemblies, Geotechnique, **29**, 47 - 65.

Delves, L.M. and Mohamed, J.L., 1985, Computational Methods for Integral equations, Cambridge University Press, Cambridge.
Digby, P.J., 1981, The effective elastic moduli of porous granular rocks, J. Appl. Mech., **48**, 803 - 808.
Dvorkin, J., Mavko, G. and Nur, A., 1991, The effect of cementation on the elastic properties of granular material, Mechanics of Materials, **12**, 207 - 217.
Frankel, N.A. and Acrivos, A., 1967, On the viscosity of a concentrated suspension of solid spheres, Chemical Eng. Science, **22**, 847 - 853.
Goddard, J.D., 1977, An elastohydrodynamic theory for the rheology of concentrated suspensions of deformable particles, Proc. R. Soc. Lond., A. **430**, 105 - 131.
Goddard, J.D., 1990, Nonlinear elasticity and pressure-dependent wave speeds in granular media, J. Non-Newtonian Fluid Mechanics, **2**, 169 - 189.
Hertz, H., 1882, Uber die Beruhrung fester elastisher Korper (On the contact of elastic solids), J. reine und angewandte Mathematik, **92**, 156 - 171.
Johnson, K.L., 1985, Contact Mechanics, Cambridge University Press, Cambridge.
Johnson, K.L, Kendall, K. and Roberts, A.D., 1971, Surface energy and the contact of elastic solids, Proc. R. Soc. Lond., A. **324**, 301 - 313.
Nunan, K.C. and Keller, J.B., 1984, Effective viscosity of a periodic suspension, J. Fluid Mech., **142**, 269 - 287.
Liu, X., Dvorkin, J. and Nur, A., 1991, The effect of intergranular cementation on rock properties: Experimental study, abstract, AGU Annual Meeting, San Francisco, December 1991.
Mindlin, R.D., 1949, Compliance of elastic bodies in contact, Trans. ASME, **71**, A-259.
Nemat-Nasser, S., 1983, On finite plastic flow of crystalline solids and geomaterials, J. Appl. Mech., **50**, 1114 - 1126.
Nelson, R.B., Lade, T.V., Issa, J., Chamieh, N. and Yamamuro, J., 1988, Micromechanical behavior of frictional geologic materials, Final Report AFOSR Grant 86-0290, Bolling AFB, Washington D.C.
Stoll, R.D., 1989, Sediment Acoustics, Springer, Berlin.
Timoshenko, S.P. and Goodier, J.N., 1970, Theory of Elasticity, McGraw-Hill, New York.
Trent, B.C., 1989, Numerical simulation of wave propagation through cemented granular material, in AMD -- **101**, Wave Propagation in Granular Media, eds. D. Karamanlidis and R.B. Stout, 9 - 15.
Trent, B.C. and Margolin, L.G., 1992, A numerical laboratory for granular solids, Eng. Comp., 9, 191 - 197.
Walton, K., 1978, The oblique compression of two elastic spheres, J. Mech. Phys. Solids, **26**, 139 - 150.
Williams, J.R. and Mustoe, G.W. (eds.), 1993, Proc. 2nd Int. Conf. Discrete Element Methods, MIT.
Winkler, K.W., 1983, Contact stiffness in granular porous materials: comparison between theory and experiment, Geophys. Res. Let., **10**, 1073 - 1076.

APPENDIX: DEFORMATION OF TWO CEMENTED CYLINDERS -- PLANE CASE

The problem of normal deformation of two cemented elastic cylinders was considered by Dvorkin et al. (1991). The assumptions in this solution are similar to those in the above case of two spherical grains: a thin elastic cement layer between two elastic grains is approximated by an elastic foundation, and a contact region is assumed to be small as compared to a grain, so that stress distribution in the grain is close to one in a half-plane with identical surface deformation.

In the plane case, normal displacements of the grain surface $v(x)$ are related to normal stress $p(x)$ as (Johnson, 1985)

$$v(x)=-\frac{1-\nu}{\pi G}\int_{-a}^{a} p(s)\ln|x-s|ds+\text{const}, \qquad \text{(A1)}$$

where x is a coordinate along the contact interface (consider Figure 4 with x instead of r). By using equations (5) and (6) with x instead of r, we arrive at the following integral equation for $V(x)$:

$$V(x)=\Lambda\int_{-a}^{a}\frac{V(s)}{h(s)}\ln|x-s|ds+\text{const}, \tag{A2}$$

where V is the normal displacement of the surface of the cement layer (Figure 4), and h is given by (7). The constant in the right-hand side of (A2) can be found using the condition of a given integral compressional force F per unit length of an elastic cylinder:

$$F=-\frac{2G_c(1-\nu_c)}{(1-2\nu_c)}\int_{-a}^{a}\frac{V(s)}{h(s)}ds. \tag{A3}$$

Equation (A2) with condition (A3) can be easily solved by the quadrature method. The solution results in normal stress distributions similar to those given in Figure 6 (Dvorkin et al., 1991).

The problem of tangential deformation of two cemented cylinders is identical to that of normal deformation. Indeed, equation (A2) will hold if we substitute tangential displacement u instead of v and shear traction q instead of p (Johnson, 1985). The final set of equations for the tangential displacement of the surface of the cement layer U is:

$$U(x)=\frac{G_c(1-\nu)}{\pi G}\int_{-a}^{a}\frac{U(s)}{h(s)}\ln|x-s|ds+\text{const},$$

$$T=-G_c\int_{-a}^{a}\frac{U(s)}{h(s)}ds,$$

where T is an integral tangential force per unit length of an elastic cylinder.

2.2. CONTACT LAWS FOR CEMENTED GRAINS: IMPLICATIONS FOR GRAIN AND CEMENT FAILURE

ABSTRACT

Analytical solutions are presented to predict the intergranular contact load transfer in cemented granular media where both grain material and cement are elastic. The grains can be separated, have a direct point contact, or be compacted prior to cement deposition. For all these cases contact stress distributions are obtained for normal, tangential, and torsional deformation of two cemented deformable grains. An important result is that intergranular cement, even if very soft, is load-bearing. Thus cementation reduces contact stress concentration (as compared to direct Hertzian interaction). Contact stresses are maximum near the center of the contact region when the cement is soft relative to the grains, and are maximum at the periphery of the contact region when the cement is stiff. These results allow us to predict the following modes of static and dynamic failure of the grains and intergranular bonds in a particulate material: (1) Uncemented grains will tend to shatter whereas cemented grains will stay intact, and the cement will fail. (This conclusion is supported by hydrostatic loading experiments where intensive crushing of uncemented glass beads was observed at about 50 MPa, whereas grains cemented at their contacts with small amounts of epoxy stayed intact.) (2) Where intergranular cementation is present, grain failure may still be expected if the cement is strong and stiff. In this case, grain damage will be initiated at the periphery of the cement layer. (3) Yielding of a cement material that is soft (as compared to the grain material) will initiate at the center of the contact region, whereas stiff cement will yield at the periphery.

INTRODUCTION

The study of dynamic and static load transmission in granular media is important in different branches of engineering and geophysics. Artificial and natural granular materials behave as good shock attenuators and as such are used to isolate shock-sensitive instruments. Such materials can be used to protect underground facilities from explosion-associated damage. Many rocks can be treated as granular media. Understanding and quantifying shock wave propagation in rocks helps in detecting and locating nuclear explosions.

The mechanical static and dynamic characteristics of granular materials can be significantly affected by intergranular cementation. One way to understand and quantify this dependence is by studying grain-to-grain microscale interaction because in a dry granular material load is transferred mainly through contact mechanisms between neighboring particles (e.g., Oda et al., 1982; Shukla et al., 1988; Sadd et al., 1989).

Recent advancements in studying the effect of intergranular cementation on the elastic and inelastic behavior of particulate materials include a numerical and experimental investigation by Bruno and Nelson (1991), an experimental study by Bernabe et al. (1992), and numerical (distinct element method) works by Trent (1989), and Trent and Margolin (1992). One important detail that has been missing in all these cementation-related works is a theoretical description of interparticle contact laws. Dvorkin et al. (1991 and 1994) have examined normal and shear stress transmission between deformable particles through deformable interparticle cement bonds. Two cemented particles could be separated or have a point direct contact (Figure 1). Three main assumptions were: (1) a thin cement layer subject to normal and shear load can be approximately treated as an elastic foundation, (2) the width of the cemented zone is small as compared to the grain radius so that a grain can be treated as an elastic half-space, and (3) there is no slip between grains and at grain/cement interfaces. The first assumption has been justified by an approximate analytical solution for the normal and shear deformation of a thin smooth cement layer

(Dvorkin et al., 1991). Based on these assumptions the problem of grain-cement deformation has been reduced to an ordinary integral equation for the normal and shear stresses at the cemented interface.

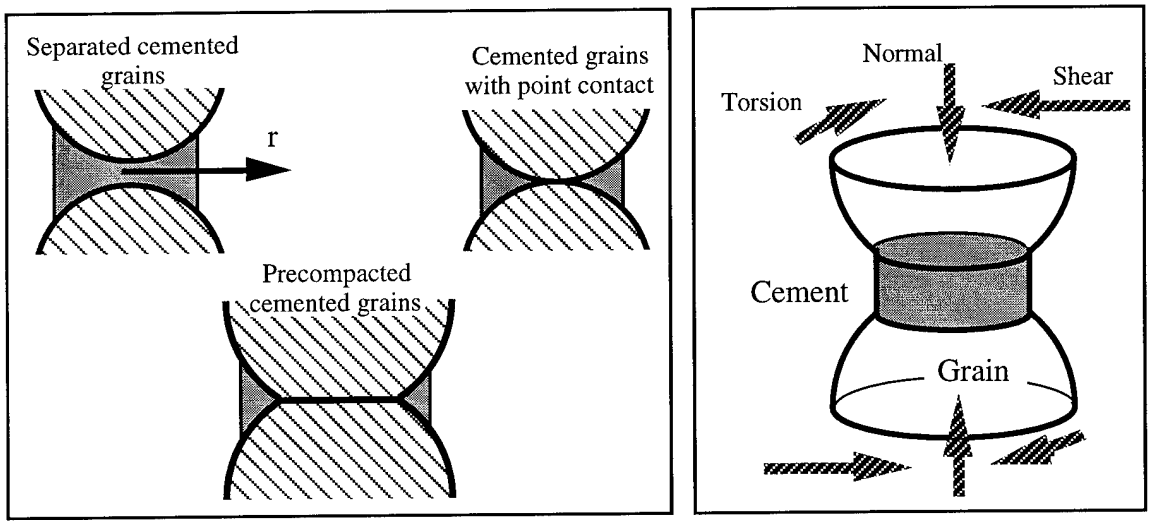

Figure 1. Left: Separated grains, grains with a point contact, and precompacted grains. Right: Normal, shear, and torsional deformation of two cemented grains.

The solution has revealed a peculiar pattern of normal and shear stresses distribution at the cemented grain contacts: the stresses are maximum at the center of the contact region when the cement is soft relative to the grain, and are maximum at the periphery of the contact region when the cement is stiff (Figure 2). The physical explanation of this pattern is as follows: When a soft cement layer is confined between two rigid grains, strain and stress in it are maximum at its thinnest part -- near the center of contact. When the cement is stiff relative to the grain material, its action on the grain is close to that of a rigid punch penetrating an elastic half-space (e.g., Johnson, 1992). In this case stress concentration is expected at the periphery of the punch.

The macroscopic stiffness of a cemented system increases with the increasing radius of the cement layer and with its increasing stiffness. The former factor is the most important: the small increase of the cementation content results in significant growth of a contact zone between two contacting grains and, because the cement is load-bearing, dramatically increases the stiffness of a two-grain system and thus the macroscopic stiffness of a cemented particulate material. This conclusion holds even if the cement is relatively soft.

In this paper we concentrate on the description of normal, shear, and torsional stress transmission between two elastic grains that were initially precompacted by a normal force to develop a finite (Hertzian) direct contact area. Afterwards cement was deposited around the initial contact zone (Figure 1). Our analytical solutions have been obtained under the same assumptions as in the uncompacted case. The results show that in soft cement, normal and shear stresses developed due to the continuing deformation of two grains are maximum at the periphery of the initial contact zone between two grains. These stresses reduce towards the periphery of the cement layer. However, in stiff cement, contact stresses are maximum at the periphery of the cement layer.

Below, we give solutions to the problems of normal and shear deformation of two precompacted cemented spherical grains. Similar solutions for two-dimensional grains (cylinders) are given in Appendix 1. Torsional deformation of two spherical cemented grains (both uncompacted and precompacted cases) is explored in Appendix 2. The theoretical results are compared to our experimental data.

We also discuss the implications of the obtained solutions for the failure of cemented granular materials.

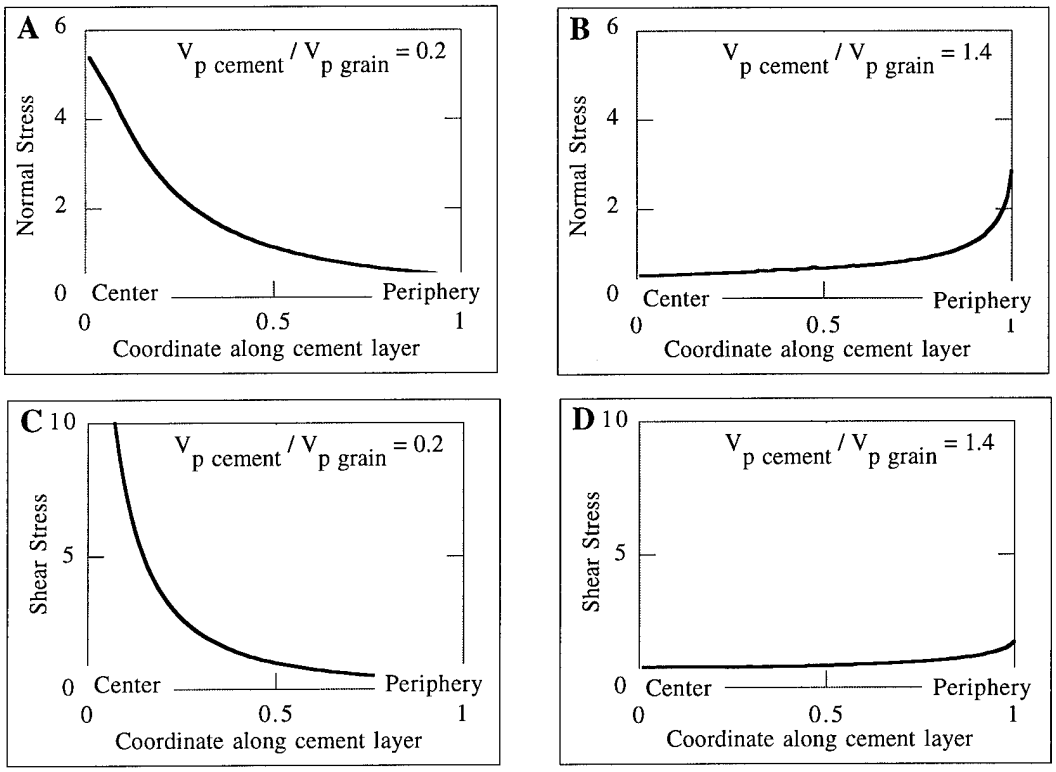

Figure 2. Normal (A and B) and shear (C and D) stresses in the cement along the radii of the cement layers between two spherical grains with a point contact. The Poisson's ratios of both grain and cement materials are constant and equal 0.28. The stiffness of the cement varies relative to that of the grains: from very soft cement (A and C) to very stiff cement (B and D). V_p is compressional wave velocity in the material. The ratio of the radius of the cement layer to the grain radius is 0.33. Stresses are normalized by the average stress. The radial coordinate r (Figure 1) is normalized by the radius of the cement layer.

NORMAL AND SHEAR DEFORMATION OF TWO PRECOMPACTED GRAINS

Precompacted Grains

Consider two identical elastic spherical grains of radius R that are normally pressed together by force P_H to form a circular contact area of radius a. Then

$$a = \sqrt[3]{\frac{3P_H R(1-\nu)}{8G}}, \qquad (1)$$

where G and ν are the grain shear modulus and Poisson's ratio, respectively (e.g., Johnson, 1992). This intergranular force P_H can be easily calculated from the hydrostatic pressure P_0 acting at a random pack of identical spherical grains:

$$P_H = \frac{4\pi R^2 P_0}{C(1-\phi)}, \tag{2}$$

where C is the average number of contacts per grain (about 9) and ϕ is the porosity of the pack (about 36%).

From Hertz's solution, the initial distribution of normal stresses p_H on the surface of the precompacted grains is:

$$p_H = \frac{4G}{\pi R(1-\nu)}\sqrt{a^2 - r^2}, \; r \le a; \qquad p_H = 0, \; r > a. \tag{3}$$

The corresponding initial displacements v_H of the grain surface are:

$$v_H(r) = \frac{a^2}{R} - \frac{r^2}{2R}, \; 0 \le r \le a; \qquad v_H(r) = \frac{1}{\pi R}\left[\left(2a^2 - r^2\right)\arcsin\left(\frac{a}{r}\right) + ar\sqrt{1 - \frac{a^2}{r^2}}\right], \; a < r \le b. \tag{4}$$

After the initial compaction, elastic cement is uniformly added around the direct grain contact zone to increase the radius of the contact area to b (Figure 3). It follows from equations (4) that the half-thickness of the undeformed cement layer between two precompacted spherical grains is:

$$h_H(r) = \frac{a^2}{\pi R}\left[\left(\frac{r^2}{a^2} - 2\right)\arctan\sqrt{\frac{r^2}{a^2} - 1} + \sqrt{\frac{r^2}{a^2} - 1}\right], \; a \le r \le b. \tag{5}$$

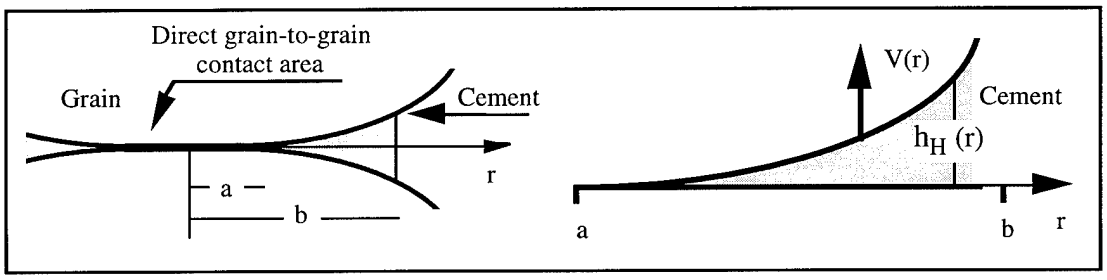

Figure 3. Left: Contact area between two precompacted cemented grains with cement added after compaction. Right: Cement layer, its initial thickness and its displacements.

Normal Deformation

Consider now additional normal loading of the grains with force ΔP that produces additional displacement δ of each grain's center towards their contact zone. The resulting total normal displacements $v(r)$ of the grain surface within the area of the initial direct contact are:

$$v(r) = \delta - \frac{r^2}{2R}, 0 < r \le a. \tag{6}$$

Within the cemented zone, $a < r \le b$, the total normal displacements of the grain surface $v(r)$ are related to the normal displacements of the cement as:

$$V(r) = v(r) - v_H(r) - \delta + \frac{a^2}{R}, \tag{7}$$

where $V(r)$ is the normal displacement of the cement surface (at the cement-grain interface) relative to the median plane of the cement layer (Figure 3).

By treating the cement layer as an elastic foundation, we have the following expression for normal stresses $p(r)$ at the cement-grain interface:

$$p(r) = -\frac{2G_c(1-\nu_c)}{1-2\nu_c}\frac{V(r)}{h_H(r)}, a < r \le b, \tag{8}$$

where G_c and ν_c are the cement's shear modulus and Poisson's ratio, respectively.

Finally, treating the grain as an elastic half-space, we have the following expression that relates normal stresses $p(r)$ to normal displacements $v(r)$ of the grain's surface (Timoshenko and Goodier, 1970):

$$v(r) = \frac{(1-\nu)}{\pi G}\int_0^{\pi} d\varphi \int_0^{r\cos\varphi+\sqrt{b^2-r^2\sin^2\varphi}} p(\sqrt{r^2+s^2-2rs\cos\varphi})\,ds, \tag{9}$$

where the integration is inside the circle $|r| \le b$ (Figure 4).

Now we combine equations (6), (7), (8), and (9) to obtain the following integral equation for normal stress $p(r)$:

$$v(r) = \frac{(1-\nu)}{\pi G}\int_0^{\pi} d\varphi \int_0^{r\cos\varphi+\sqrt{b^2-r^2\sin^2\varphi}} p(\sqrt{r^2+s^2-2rs\cos\varphi})\,ds =$$
$$\begin{cases} \delta - \dfrac{r^2}{2R}, & 0 \le r \le a; \\ v_H(r) + \delta - \dfrac{a^2}{R} - \dfrac{1-2\nu_c}{2G_c(1-\nu_c)} p(r)h_H(r), & a < r \le b. \end{cases} \tag{10}$$

Let us present the normal stress $p(r)$ as the sum of the initial Hertzian stress $p_{\mathrm{H}}(r)$ and the additional normal stress $f(r)$:

$$p(r) = p_{\mathrm{H}}(r) + f(r). \tag{11}$$

It follows then from equations (4), (9), (10), and (11) that

$$\frac{(1-\nu)}{\pi G}\int_0^{\pi} d\varphi \int_0^{r\cos\varphi+\sqrt{b^2-r^2\sin^2\varphi}} f(\sqrt{r^2+s^2-2rs\cos\varphi})\,ds =$$

$$\begin{cases} \delta - \dfrac{a^2}{2R}, & 0 \le r \le a; \\ \delta - \dfrac{a^2}{R} - \dfrac{1-2\nu_c}{2G_c(1-\nu_c)} f(r)h_H(r), & a < r \le b. \end{cases} \tag{12}$$

This last equation can be easily solved using the numerical quadrature method (e.g., Delves and Mohamed, 1985).

The constant δ can be found from the resulting force ΔP:

$$\Delta P = \int_0^b f(r) 2\pi r dr. \tag{13}$$

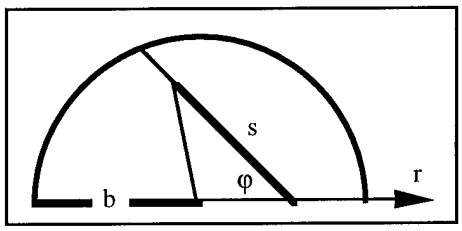

Figure 4. Domain of integration in equation (9).

Shear Deformation

Our treatment of the shear deformation of two cemented grains is analogous to that of the normal deformation: we assume that after cement deposition a tangential force Q is exerted on the system to produce the tangential displacement τ of each grain's center relative to the contact zone. The resulting tangential displacements $u(r)$ of the grain surface within the area of the initial direct contact are:

$$u(r) = \tau, 0 < r \le a. \tag{14}$$

Within the cemented zone, $a < r \le b$, the tangential displacements of the grain surface $u(r)$ are related to the tangential displacements of the cement as:

$$U(r) = u(r) - \tau, \tag{15}$$

where $U(r)$ is the displacement of the cement surface (at the cement-grain interface) relative to the median plane of the cement layer.

By treating the cement layer as an elastic foundation in shear, we have the following expression for tangential stresses $q(r)$ at the cement-grain interface:

$$q(r) = -G_c \frac{U(r)}{h_H(r)}, a < r \le b. \tag{16}$$

Now treating the grain as an elastic half-space, we have the following approximate expression that relates shear stresses $q(r)$ to tangential displacements $u(r)$ of the grain's surface (Dvorkin et al., 1994):

$$u(r)=\frac{1}{\pi G}\int_0^{\pi} d\varphi \int_0^{r\cos\varphi+\sqrt{b^2-r^2\sin^2\varphi}} q(\sqrt{r^2+s^2-2rs\cos\varphi})(1-\nu\sin^2\varphi)ds, \tag{17}$$

where the integration is inside the circle $|r| \le b$ (Figure 4).

Finally, we combine equations (14), (15), (16), and (17) to obtain the following integral equation for shear stress $q(r)$:

$$u(r)=\frac{1}{\pi G}\int_0^{\pi} d\varphi \int_0^{r\cos\varphi+\sqrt{b^2-r^2\sin^2\varphi}} q(\sqrt{r^2+s^2-2rs\cos\varphi})(1-\nu\sin^2\varphi)ds =$$

$$\begin{cases} \tau, & 0 \le r \le a; \\ \tau-\dfrac{1}{G_c}q(r)h_H(r), & a < r \le b. \end{cases} \tag{18}$$

Again, this integral equation can be easily solved using the numerical quadrature method.

The constant τ can be found from the resulting force Q:

$$Q=\int_0^b q(r)2\pi r dr. \tag{19}$$

Contact Stresses

Normal stresses in the contact zone of two precompacted grains are given in Figure 5.

The ratio of the cement radius b to the grain radius R was 0.7, the radius a of the initial zone of direct grain contact was 0.105 of R (0.15 of b). The elastic moduli of the grains were constant and equal to those of glass (bulk modulus 49.9 GPa and shear modulus 26.2 GPa). The bulk and shear moduli of the cement varied from 1.7 GPa and 0.5 GPa, respectively, to 170.0 GPa and 50.0 GPa. In the second example (6.8 GPa and 2.0 GPa) the elastic moduli of the cement are identical to those of epoxy.

When the cement is relatively soft, we observe the concentration of the additional normal contact stresses at the periphery of the direct grain contact zone ($r=a$). The physical meaning of this effect is: In the soft cement layer stresses are maximum at its thinnest part -- near its inner boundary ($r \to a, r > a$). In the direct grain contact region we have the condition of a constant additional displacement δ -- analogous to that on the face of a rigid punch penetrating an elastic half-space. This is the reason for the additional contact stress concentration on the direct contact side ($r \to a, r < a$) of the contact region $0 \le r \le b$.

As the cement becomes stiffer, its action on the grain approaches that of a rigid punch of radius b. Therefore, we observe stress concentration on the periphery of the cement layer at $r=b$.

Shear stresses for the six above cases are given in Figure 6. The patterns of stress distribution and their physical meaning are similar to those observed for normal stresses. It is important to notice that in this case we have used the no-slip condition in the direct grain-to-grain contact zone. Clearly, this condition is not valid if shear stresses are high and slip

does occur. However, we justify this approximation by the fact that for small tangential forces exerted on contacting bodies, stress distributions that are produced from the no-slip solutions are fairly close to those produced from the partial-slip solutions (see examples in Johnson, 1992).

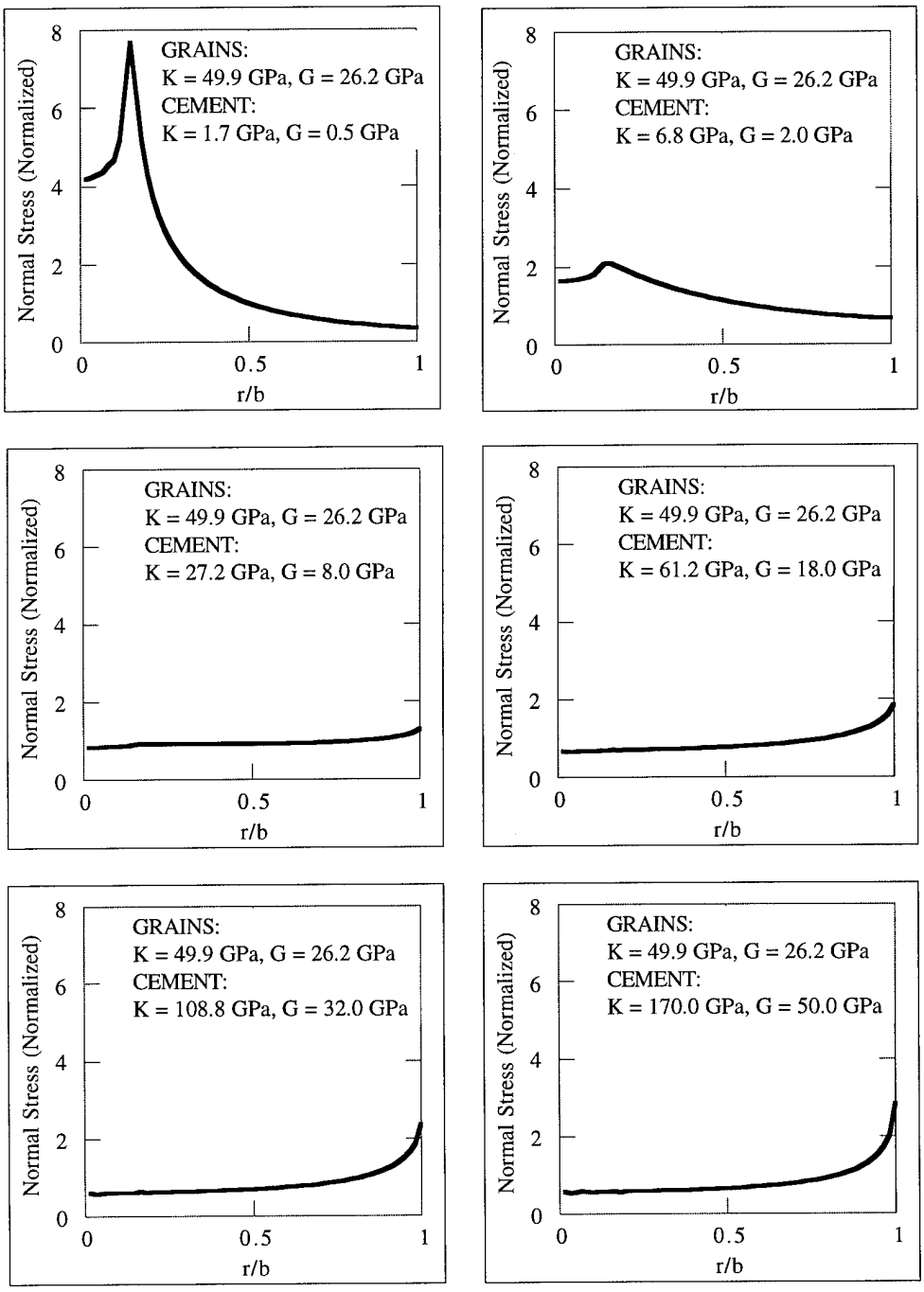

Figure 5. Additional normal stresses $f(r)$ along the radii of cement layers for varying relative rigidity of the cement and grain materials. Stresses are normalized by the average additional stress. The horizontal axis is the normalized distance along the radius of the cement layer.

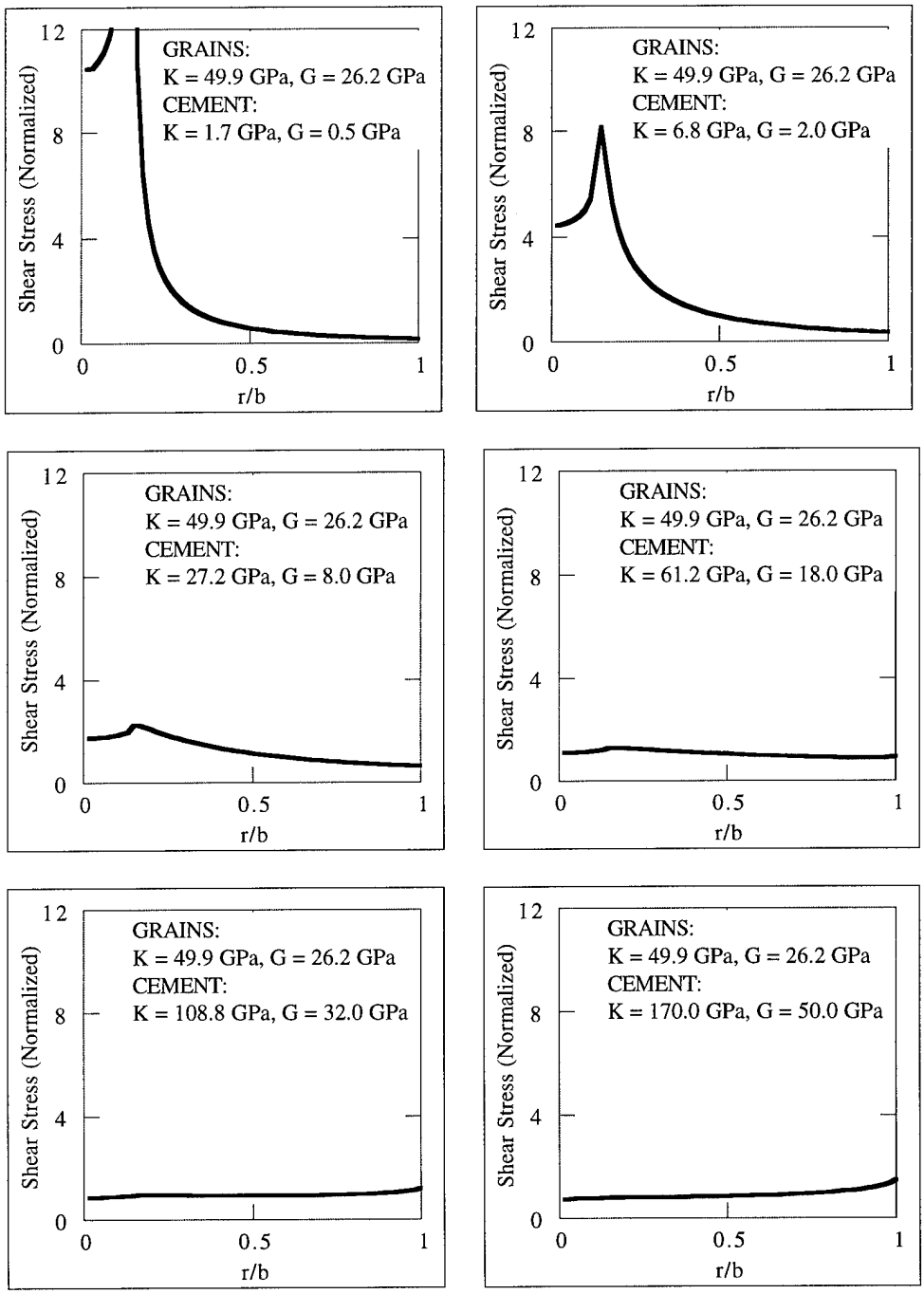

Figure 6. Shear stresses $q(r)$ along the radii of cement layers for varying relative rigidity of the cement and grain materials. Stresses are normalized by the average shear stress. The horizontal axis is the normalized distance along the radius of the cement layer.

EXPERIMENT

Our experiment has been conducted on hydrostatically precompacted glass beads cemented with epoxy. The cemented samples were prepared by mixing glass beads (0.2 - 0.3 mm in diameter) with a given volume of epoxy (10, 25, 50, and 100% of the pore

space volume). They were compacted at 20 MPa prior to epoxy solidification. Compressional (V_p) and shear (V_s) wave velocities have been measured at 1 MHz frequency using the pulse transmission technique.

The above-derived contact laws for the normal and shear deformation of two precompacted cemented grains have been used to calculate the effective bulk and shear moduli of a random packing of identical elastic spheres. These theoretical predictions are compared to the experimental results in Figure 7. The agreement between the theory and the experiments is within 15% accuracy.

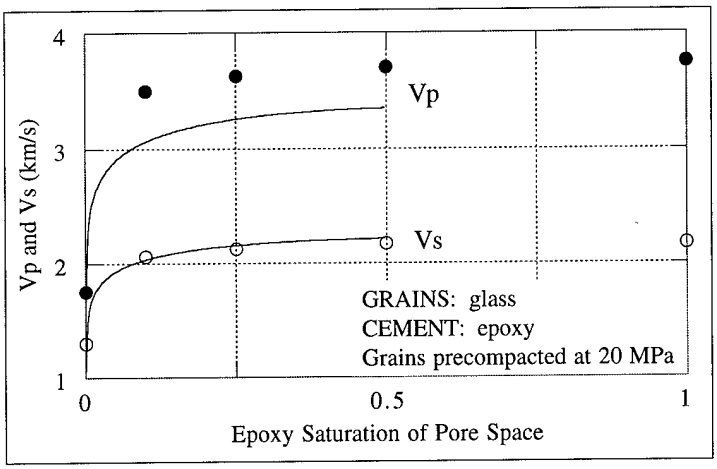

Figure 7. Experimental and theoretical results on precompacted epoxy-cemented glass beads. Circles show experimental points, solid lines are theoretical predictions.

IMPLICATIONS FOR GRAIN AND CEMENT FAILURE

One important result following from the above-derived grain-cement-grain contact laws is that intergranular cement, even if very soft, is load-bearing. Thus cementation reduces contact stress concentration (as compared to direct Hertzian interaction). As a result, even small amounts of relatively soft cement may prevent grain failure: uncemented grains will tend to shatter whereas cemented grains will stay intact, and the cement will fail. This conclusion has been supported by hydrostatic loading experiments where intensive crushing of uncemented glass beads was observed at about 50 MPa, whereas grains cemented at their contacts with small amounts of epoxy (10% of the pore space volume) stayed intact (Figure 8). The observed effect follows from our theory of cemented granular materials: stress concentration is high at the contacts of uncemented grains, whereas even small amounts of relatively soft cement result in a more uniform stress distribution over a larger contact area. The total force transmitted between two grains must, of course, remain the same in the cemented and uncemented cases; however, the stresses at the cemented interface decrease dramatically as compared to the Hertzian contact case.

The contact stress distributions as obtained, imply the following modes of static and dynamic failure of the grains and intergranular bonds in a particulate material: (1) Uncemented grains will tend to fail whereas cemented grains will stay intact, and the cement will fail. (2) Where intergranular cementation is present, grain failure may still be expected if the cement is strong and stiff. In this case, grain damage will be initiated at the periphery of the cement layer. (3) Yielding of a cement material that is soft (as compared to the grain material) will initiate at the center of the contact region, whereas stiff cement will yield at the periphery.

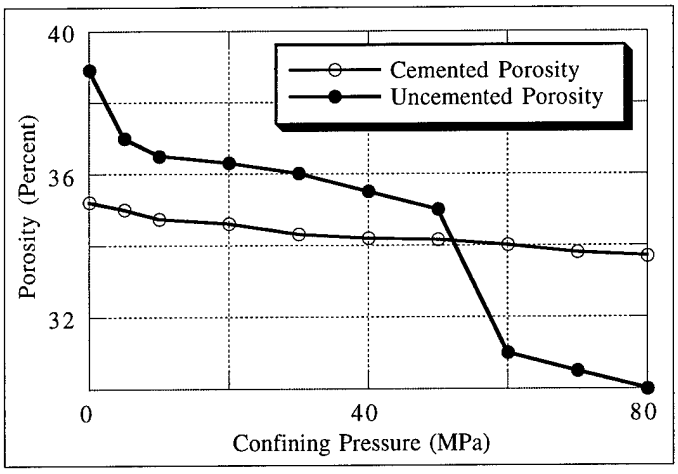

Figure 8. Porosity versus hydrostatic confining pressure in water-saturated randomly packed glass beads that were a) uncemented and b) cemented by epoxy at their contacts (Yin and Dvorkin, 1994). Porosity was measured by the volume of expelled fluid. In the uncemented case, a sharp porosity decrease is observed at about 50 MPa. The decrease is associated with the crushing of grains. The cemented grains (the volume of the epoxy accounted for only 10 percent of the pore space) did not crush. The photos showed that in the latter case, the grains stayed intact with the failure being localized within the epoxy.

CONCLUSIONS

All the solutions presented in this paper have been applied to the interaction of two circular grains. Note that the obtained contact law solutions are more general and can be applied to cemented elastic grains with arbitrarily-shaped contact surfaces as long as the underlying assumptions are valid. Specifically, the cement layer has to be thin and small as compared to a grain, and in addition contacting grain surfaces have to be smooth, so that the elastic foundation approximation is valid. The shape of grain surfaces will affect the thickness of the cement layer, and the initial stress distribution at the direct contact area of precompacted grains.

In the example presented in Figure 7 we have used formulas for the effective bulk and shear moduli of a random packing of identical spherical grains as given in Digby (1981) and Winkler (1983). Again, our contact laws can be used to describe the effective properties of more complicated arrangements of cemented grains. Specifically, these contact laws can be plugged into sophisticated numerical schemes (e.g., Distinct Element Method).

One important assumption that has been used in treating the problems of shear and torsional deformation of precompacted cemented grains is the no-slip condition in the direct grain-to-grain contact zone. This assumption is valid only if stresses are small, so that stress distributions obtained under the no-slip assumption are close to those obtained by considering the relative sliding of contacting grains (see examples in Johnson, 1992). At the same time, the computed shear stress distributions shown in Figure 6 indicate that the sliding will initiate at the periphery of the direct grain-to grain contact area only if the cement is very soft as compared to the grain material. In most cases, we do not expect to encounter high stress concentration and sliding in the mentioned area.

The presented solutions can describe the dynamic interaction of cemented grains only if the quasi-static approximation is valid, i.e. the wavelength is significantly larger than the characteristic microscopic dimension (the grain radius). This was the case in the ultrasonic pulse transmission experiment described above: the wavelength was approximately ten

times the average grain diameter. These solutions can be also applied to describing shock wave propagation in a particulate medium if the length of the pulse is much larger than the grain radius.

REFERENCES

Bernabe, Y., Fryer, D.T. and Hayes, J.A., 1992, The effect of cement on the strength of granular rocks, Geophys. Res. Let., **19**, 1511 - 1514.

Bruno, M.S. and Nelson, R.B., 1991, Microstructural analysis of the inelastic behavior of sedimentary rock, Mechanics of Materials, **12**, 95 - 118.

Delves, L.M. and Mohamed, J.L., 1985, Computational Methods for Integral equations, Cambridge University Press.

Digby, P.J., 1981, The effective elastic moduli of porous granular rocks, J. Appl. Mech., **48**, 803 - 808.

Dvorkin, J., Mavko, G., and Nur, A., 1991, The effect of cementation on the elastic properties of granular material, Mechanics of Materials, **12**, 207-218.

Dvorkin, J., Nur, A., and Yin, H., 1994, Effective Properties of Cemented Granular Materials, Mechanics of Materials, **18**, 351-366.

Johnson, K.L., 1992, Contact Mechanics, Cambridge University Press.

Oda, M., Nemat-Nasser, S., and Mehrabadi, M.M. , 1982, A statistical study of fabric in a random assembly of spherical granules, Int. J. Numer. Analyt. Methods Geomech., **6**, 77-94.

Sadd, M.H., Shukla, A., and Mei, H., 1989, Computational and experimental modeling of wave propagation in granular materials, in Proc. 4th Int. Conf. Computational Methods and Experimental Measurements, Capri, Italy, 325-334.

Shukla, A., Zhu, C.Y., and Sadd, M.H., 1988, Angular dependence of dynamic load due to explosive loading in two dimensional granular aggregates, J. Strain Anal., **23**, 121-127.

Timoshenko, S.P. and Goodier, J.N., 1970, Theory of Elasticity, McGraw-Hill, New York.

Trent, B.C., 1989, Numerical simulation of wave propagation through cemented granular material, in AMD -- 101, Wave Propagation in Granular Media, eds. D. Karamanlidis and R.B. Stout, 9 - 15.

Trent, B.C. and Margolin, L.G., 1992, A numerical laboratory for granular solids, Eng. Comp., **9**, 191 - 197.

Yin, H. and Dvorkin, J., 1994, Strength of cemented grains, Geophysical Research Letters, **21**, 903-906.

Winkler, K.W., 1983, Contact stiffness in granular porous materials: comparison between theory and experiment, Geophys. Res. Let., **10**, 1073 - 1076.

APPENDIX 1: TWO PRECOMPACTED CYLINDERS

Precompaction

Consider two identical elastic circular cylinders (plane strain) of radius R that are normally pressed together by force P_H to form a contact area of half-width a. Then

$$a=\sqrt{\frac{2P_H R(1-\nu)}{\pi G}} \tag{A1.1}$$

(Johnson, 1992). The initial distribution of normal stresses p_H on the surface of the precompacted cylinders is:

$$p_H = \frac{G}{R(1-\nu)}\sqrt{a^2-r^2}, |x| \le a; \tag{A1.2}$$

$$p_H = 0, |x| > a.$$

Here x is the coordinate along the median line of the cement layer in the plane perpendicular to the cylinder's axis, analogous to the r coordinate in the three-dimensional case.

By treating the cylinder as an elastic half-plane, we have the following expression for the initial normal displacements $v_H(r)$ of the cylinder's surface from normal stresses $p_H(r)$ (Johnson, 1992):

$$v_H(x) = -\frac{1-\nu}{\pi G}\int_{-b}^{b} p_H(s)\ln|x-s|ds + \text{const}. \qquad \text{(A1.3)}$$

After the initial compaction, cement is uniformly added around the direct contact zone to increase the half-width of the contact area to b. It follows from equation (A1.3) that the half-thickness of the undeformed cement layer between two precompacted circular cylinders is:

$$h_H(x) = \frac{x^2-a^2}{2R} - \frac{1}{\pi R}\int_{-a}^{a}\sqrt{a^2-s^2}\ln\left|\frac{x-s}{a-s}\right|ds + \text{const},\ a<|x|\le b. \qquad \text{(A1.4)}$$

Normal Deformation

Consider now additional normal loading of the cylinders with force ΔP. The resulting total normal displacements $v(x)$ of the cylinder surface within the area of the initial direct contact are:

$$v(x) - v(a) = \frac{a^2-x^2}{2R},\ |x|\le a. \qquad \text{(A1.5)}$$

Within the cemented zone, $a<|x|\le b$, the total normal displacements of the grain surface $v(x)$ are related to the normal displacements of the cement as:

$$V(x) = v(x) - v(a) - [v_H(x) - v_H(a)],\ a<|x|\le b, \qquad \text{(A1.6)}$$

where $V(r)$ is the normal displacement of the cement surface (at the cement-cylinder interface) relative to the median line of the cement layer.

By treating the cement layer as an elastic foundation, we have the following expression for normal stresses $p(x)$ at the cement-grain interface:

$$p(x) = -\frac{2G_c(1-\nu_c)}{1-2\nu_c}\frac{V(x)}{h_H(x)},\ a<|x|\le b. \qquad \text{(A1.7)}$$

Equation (A1.3) now takes the following form:

$$v(x) = -\frac{1-\nu}{\pi G}\int_{-b}^{b} p(s)\ln|x-s|ds + \text{const}. \qquad \text{(A1.8)}$$

Now we combine equations (A1.5), (A1.6), (A1.7), and (A1.8) to obtain the following integral equation for normal stress $p(x)$:

$$v(x)-v(a)=-\frac{1-\nu}{\pi G}\left[\int_{-b}^{b} p(s)\ln|x-s|ds-\int_{-b}^{b} p(s)\ln|x-s|ds\right]=$$

$$\begin{cases}\dfrac{a^2-x^2}{2R}, & |x|\le a; \\ v_H(x)-v_H(a)-\dfrac{1-2\nu_c}{2G_c(1-\nu_c)}p(x)h_H(x), & a<|x|\le b.\end{cases} \tag{A1.9}$$

Let us now present the normal stress $p(x)$ as the sum of the initial Hertzian stress $p_H(x)$ and the additional normal stress $f(x)$:

$$p(x)=p_{\mathrm{H}}(x)+f(x). \tag{A1.10}$$

It follows then from equations (A1.2), (A1.3), (A1.9), and (A1.10) that

$$\int_{-b}^{b} f(s)\ln|x-s|ds+\text{const}=$$

$$\begin{cases}0, & |x|\le a; \\ \dfrac{\pi G}{1-\nu}\dfrac{1-2\nu_c}{2G_c(1-\nu_c)}f(x)h_H(x), & a<|x|\le b.\end{cases} \tag{A1.11}$$

This last equation can be solved using the numerical quadrature method.

The constant in the left-hand part of equation (A1.11) can be found from the resulting force ΔP:

$$\Delta P=\int_{-b}^{b} f(x)dx. \tag{A1.12}$$

Shear Deformation

In the two-dimensional case under consideration, the treatment of the shear deformation of two cemented grains is identical to that of the normal deformation: Equation (A1.8) is replaced by:

$$u(x)=-\frac{1-\nu}{\pi G}\int_{-b}^{b} q(s)\ln|x-s|ds+\text{const}; \tag{A1.13}$$

equation (A1.5) is replaced by

$$u(x)-u(a)=0,|x|\le a; \tag{A1.14}$$

equation (A1.6) is replaced by

$$U(x)=u(x)-u(a), a<|x|\le b; \tag{A1.15}$$

and equation (A1.7) is replaced by

$$q(x) = -G_c \frac{U(x)}{h_H(x)}, \; a < |x| \le b. \tag{A1.16}$$

The definitions of the tangential displacements $u(x)$ of the cylinder's surface, tangential displacements $U(x)$ of the cement, and shear stresses $q(x)$ in contact zone are the same as in the spherical case. Again, as in the spherical case, we assume the no-slip condition in the direct contact zone. This assumption is valid if shear stresses are small.

Similar to the case of normal deformation, we arrive at the following integral equation for stresses $q(x)$:

$$\int_{-b}^{b} q(s) \ln|x-s| ds + \text{const} =$$
$$\begin{cases} 0, & |x| \le a; \\ \dfrac{\pi G}{(1-\nu)G_c} q(x) h_H(x), & a < |x| \le b, \end{cases} \tag{A1.17}$$

where the constant in the left-hand part of equation can be found from the resulting shear force Q:

$$Q = \int_{-b}^{b} q(x) dx. \tag{A1.18}$$

Normal and shear stress distributions in this two-dimensional case are qualitatively similar to those obtained for two precompacted spheres.

APPENDIX 2: TORSIONAL DEFORMATION OF TWO SPHERICAL GRAINS

Uncompacted Grains

Consider a twisting moment M applied to the system of two cemented spherical grains (Figure 1). Shear stress components $q(r)$ acting on the grain-cement interface are axisymmetrical, and the only non-zero displacement of the grain surface $u(r)$ is perpendicular to the polar radius r (Figure A2.1).

The displacements $u(r)$ are related to stresses $q(r)$ as (Johnson, 1992):

$$u(r) = \frac{1}{\pi G} \int_0^{\pi} d\varphi \int_0^{r\cos\varphi + \sqrt{a^2 - r^2 \sin^2\varphi}} \frac{q\left(\sqrt{r^2 + s^2 - 2rs\cos\varphi}\right)}{\sqrt{r^2 + s^2 - 2rs\cos\varphi}} (r - s\cos\varphi)\, ds, \tag{A2.1}$$

where integration is inside the circle $|r| \le a$ in the plane of contact (see Figure 4).

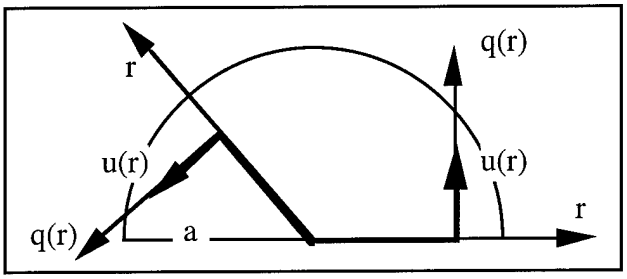

Figure A2.1. Torsional displacements and shear stresses in the plane of grain-cement-grain contact. The problem under consideration is treated in a linear approximation, so we assume the contact zone is planar.

The tangential displacement of the grain surface $u(r)$, and the tangential displacement of the cement layer surface relative to its median plane $U(r)$ are related to the respective angles of rotation $\beta(r)$ and $\mathrm{B}(r)$ as:

$$u(r) = r\beta(r), U(r) = r\mathrm{B}(r). \tag{A2.2}$$

The condition of displacement compatibility between the grain and the cement surface is:

$$\beta(r) = \mathrm{B}(r) + \gamma, \tag{A2.3}$$

where γ represents the grain's rigid rotation.

Treating the cement layer as an elastic foundation in torsion, we have the following relation between stress $q(r)$ and angle $\mathrm{B}(r)$:

$$q(r) = -G_c \frac{U(r)}{h(r)} = -G_c \frac{r\mathrm{B}(r)}{h(r)}, \tag{A2.4}$$

where $h(r)$ is the half-width of the cement layer. For a cement layer between two spheres:

$$h(r) = R[\varepsilon + \frac{1}{2}(\frac{r}{R})^2], \varepsilon = \frac{h_0}{R}, \tag{A2.5}$$

where h_0 is the minimum half-separation between the spheres.

Finally, equations (A2.1), (A2.2), (A2.3), (A2.4) , and (A2.5) yield the following integral equation for $\mathrm{B}(r)$:

$$r[\gamma + \mathrm{B}(r)] = -\frac{G_c}{\pi G}\int_0^{\pi} d\varphi \int_0^{r\cos\varphi + \sqrt{a^2 - r^2\sin^2\varphi}} \frac{\mathrm{B}(\sqrt{r^2+s^2-2rs\cos\varphi})(r - s\cos\varphi)}{R[\varepsilon + \frac{1}{2}(\frac{r^2}{R^2} + \frac{s^2}{R^2} - 2\frac{rs}{R^2}\cos\varphi)]} ds. \tag{A2.6}$$

The constant γ in equation (A2.6) can be found from the resulting twisting moment M:

$$M = -2\pi G_c \int_0^a \frac{\mathrm{B}(r) r^3}{R(\varepsilon + \frac{r^2}{2R^2})}\, dr. \qquad \text{(A2.7)}$$

The resulting distributions of the twisting shear stresses along the radius of a cement layer are qualitatively similar to those shown in Figure 2.

Precompacted Grains

The treatment of this problem is analogous to that used in the problems of normal and shear deformation of two precompacted grains. The resulting integral equation for the twisting shear stresses $q(r)$ in the contact zone is:

$$\frac{1}{\pi G}\int_0^{\pi} d\varphi \int_0^{r\cos\varphi+\sqrt{b^2-r^2\sin^2\varphi}} \frac{q(\sqrt{r^2+s^2-2rs\cos\varphi})(r-s\cos\varphi)}{\sqrt{r^2+s^2-2rs\cos\varphi}}\, ds = \begin{cases} \gamma r, & r \le a; \\ \gamma r - \dfrac{q(r)h_H(r)}{G_c}, & a < r \le b. \end{cases} \qquad \text{(A2.8)}$$

The constant γ here can be found from the resulting twisting moment:

$$M = 2\pi \int_0^b q(r) r^2\, dr. \qquad \text{(A2.9)}$$

The distributions of twisting shear stresses are similar to those shown in Figure 6.

This solution uses the no-slip condition in the direct grain-grain contact zone. The assumption is valid if shear stresses are small.

2.3. STRENGTH OF CEMENTED GRAINS

ABSTRACT

We conducted compaction tests (isotropic drained loading) on randomly packed glass beads that were a) uncemented and b) cemented by epoxy at their contacts. In the latter case, the volume of the epoxy accounted for 10 percent of the pore space. Intensive crushing of grains was observed in the first case at about 50 MPa. In the second case, the cemented grains stayed intact, the failure being localized within the epoxy. Therefore, even small amounts of cement at contacts prevent the failure of grains. Theoretically, this effect follows from our theory of cemented granular materials: stress concentration is high at the contacts of uncemented grains, whereas even small amounts of relatively soft cement result in a more uniform stress distribution over a larger contact area.

INTRODUCTION

The elastic moduli and the strength of granular media in general, and sedimentary rocks in particular, may be strongly affected by the properties and structure of intergranular bond material. The rocks of interest span a wide range from diagenetic sediments and sand-clay mixtures to tar sands.

In spite of significant progress achieved in modeling macroscopic deformation of granular media (e.g., Cundall and Strack, 1979; Nemat-Nasser, 1983; Nelson et al., 1988; Cundall et al., 1989), a challenge remains in predicting contact stiffness and strength from the geometry of a contact region and from the mechanical properties of grains and intergranular cement. Almost all theoretical investigations of deformation of granular aggregates are based on the classical solutions to the problems of normal (Hertz, 1882) or oblique (Mindlin, 1949; Walton, 1978) interaction of elastic spheres. Digby (1981) solved the problem of interaction of spherical particles that are initially bonded together across small areas. Trent (1989), and Trent and Margolin (1992) numerically investigated the behavior of cemented granular materials under both low-strain and high-strain loads. The materials are composed of circular particles which are glued together with elastic bonds. They show that the effective properties of samples are governed by the properties and distribution of individual intergranular bonds.

Significant attention has been paid to the experimental investigation of the geotechnical properties of cemented rocks (e.g., Gallagher et al., 1974, Clough et al., 1981, Saxena, 1982). Rad and Clough (1982) experimentally quantified the influence of cementation on the static and dynamic behavior of sands. Their conclusions state that cementation can be a very important parameter relative to the liquefaction resistance of sand. A recent experimental study by Bernabe et al. (1992), conducted on synthetic cemented granular materials (precompacted Ottawa sand with halite and silica glass as the cement), included triaxial compression tests. It has been found that a small amount of cement can significantly increase the strength of a granular material if it is deposited precisely at previously formed grain-to-grain contacts. The main conclusion of this work is that the cement strengthens the rock by preventing sliding and rotation of grains.

A different (from grain sliding and rotation) mode of rock failure is related to grain crushing. Gallagher et al. (1974) showed that because grains in rock aggregates are usually constrained at higher confining pressures and by stronger, stiffer cements than normally exists in soils, grain fracturing and crushing in rocks cannot be neglected. Bruno and Nelson (1991) numerically investigated rock failure under tensile, uniaxial compression, and biaxial loading. Their conclusion is that internal grain fracturing may affect the strength of the rock at high stresses. This theoretical result is supported by photographs showing internally cleaved grains.

Dvorkin et al. (1991), theoretically examined the normal interaction of two spherical elastic grains and an elastic cementation layer between them. Their results show that even with a small amount of cement, a contact force is distributed over an area that is larger than that in the uncemented case. Contact stress distribution becomes more uniform as compared to the uncemented case. These two factors lead to a significant reduction in stress concentration between cemented grains. Even very soft cement bears the load at grain contacts thus reducing stress concentration and preventing grain crushing.

Both theoretical and experimental results indicate that grain crushing does not normally occur at low stress level, but becomes an increasingly significant factor as stresses increase. This mode of rock failure may contribute to such instabilities as sanding and breakouts in deep wellbores. This is why we consider to be important to investigate the internal strength of grains in a granular material.

In this paper, we describe our compaction tests (isotropic drained loading) on cemented and uncemented glass beads. Uncemented beads were crushed (brittle failure) at about 50 MPa. The failure was associated with sharp porosity reduction and intensive acoustic emission. The grains appeared crushed on the photo taken after the loading cycle. Cemented grains were bonded together by epoxy at 10 percent epoxy saturation of the pore volume. These grains did not fail during the loading up to 80 MPa. The photo taken after the loading cycle shows that the grains stayed intact and only the epoxy cement failed.

We explain this effect from our theory of cemented granular materials: even small amounts of relatively soft cement result in a more uniform stress distribution over larger contact areas, as compared to the high stress concentration at small contact areas between uncemented grains.

Our conclusion is that even small amounts of cement deposited exactly at intergranular contacts significantly increase the strength of the grains. Cementing grains appears to be an effective way of creating strong high-porosity, high-permeability materials. Such an approach may be used in preventing grain crushing for stabilizing the bottom hole formation zone of a sand-producing well, or in manufacturing artificial aggregates.

EXPERIMENTS

In our experiments, we used spherical glass beads of 0.42 - 0.5 mm diameter. The material contains no more than two percent of irregularly-shaped grains, and is reasonably free of sharp angular particles, or particles showing milkiness, surface scoring, and foreign matter. The porosity of the uncemented glass bead sample, as measured before loading, was about 39 percent -- close to the porosity of a dense random pack of identical spheres. The cemented sample was prepared by mixing glass beads with a given volume of epoxy (in this case it was 10 percent of the pore space volume). The mixture was placed into a holder where the epoxy solidified. The liquid epoxy is a wetting fluid and thus it accumulated at grain contacts.

The bulk and shear moduli of the glass as calculated from the manufacturer's specifications are 50.0 GPa and 26.2 GPa, respectively. Those of the solidified epoxy (calculated from compressional and shear wave velocities, and density) are 6.8 GPa and 2.0 GPa, respectively.

Isotropic drained loading at confining pressure up to 80 MPa was conducted in a triaxial device on water saturated unjacketed samples. During the loading, porosity was measured through the volume of expelled pore water. We estimate the absolute error of these measurements at about ± 2 percent.

The porosity of the cemented sample showed a smooth decrease with increasing confining pressure, whereas the porosity of the uncemented sample sharply decreased from 35 to 31 percent at 50 MPa (Figure 1). This sharp decrease was probably associated with the crushing of glass beads. Another indication of the crushing was the intensive acoustic emission registered at about 50 MPa.

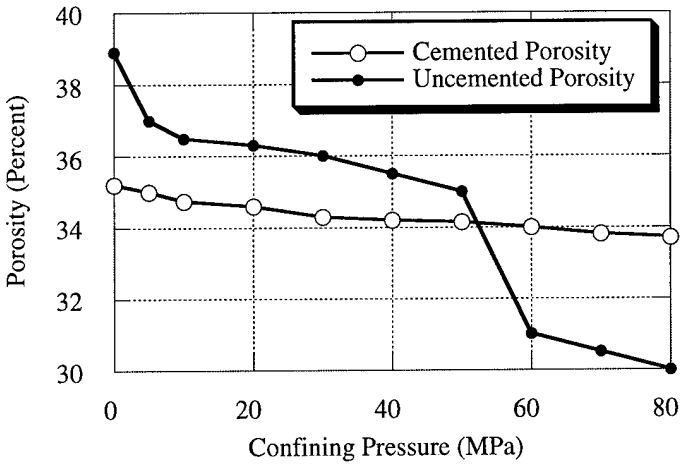

Figure 1. Porosity of glass beads versus pressure: open circles -- cemented beads, empty circles -- uncemented beads. Porosity was measured by the volume of pore fluid expelled.

The photo of the uncemented grains taken after the loading cycle showed their intensive brittle crushing. On the other hand, the cemented grains did not fail. This experiment showed that cementing fragile grains is an effective way of preventing their failure at high loading.

THEORY

Our theory of cemented granular materials is based on the solution of the contact problem of two cemented elastic grains (Dvorkin et al., 1991). The cement material is elastic and may be different from the grain material. There are two main conclusions following from the solution.

The first one is quite obvious: even a small amount of cement at a grain contact creates a contact zone that is much larger than that created by pressing together two uncemented grains. For example, at 10 percent epoxy saturation of the pore space, the ratio of the radius of the cement layer a (Figure 2a) to grain radius is 0.43. At the same time, the ratio of the radius of the contact area between uncemented grains (the Hertz solution) to grain radius is 0.11 at 50 MPa confining pressure.

The second conclusion is that the cement is load bearing in the case where there are only point glass/glass contacts. Normal contact stress (Figure 2b) is maximum at the center of the contact area when cement material is much softer than grain material, and is maximum at the periphery of the contact area when the cement is stiff.

An example of calculated normal contact stresses between two glass beads that are a) epoxy-cemented, and b) uncemented is given in Figure 3a. Contact stresses at the cemented interface are more uniformly distributed than those for the uncemented case. The maximum stress at the uncemented interface is 13.6 times as large as that at the cemented interface. Figure 3b shows a hypothetical case where the cement's bulk and shear moduli are four times smaller than those of the epoxy. In this case we can clearly see a maximum of the contact stresses at the center of the contact area. Even in this case of very soft cement, this maximum stress is about 0.32 of that at the cemented interface.

These theoretical calculations explain the experimentally observed effect of increasing strength of grains with cement at the contacts.

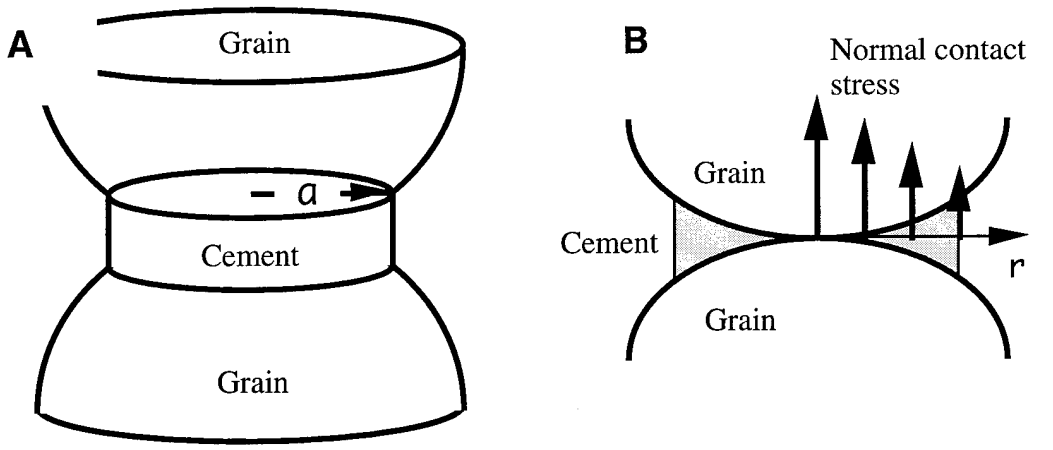

Figure 2. Two cemented grains: a. cement forms a circular-shaped contact area; b. normal contact stresses in cement.

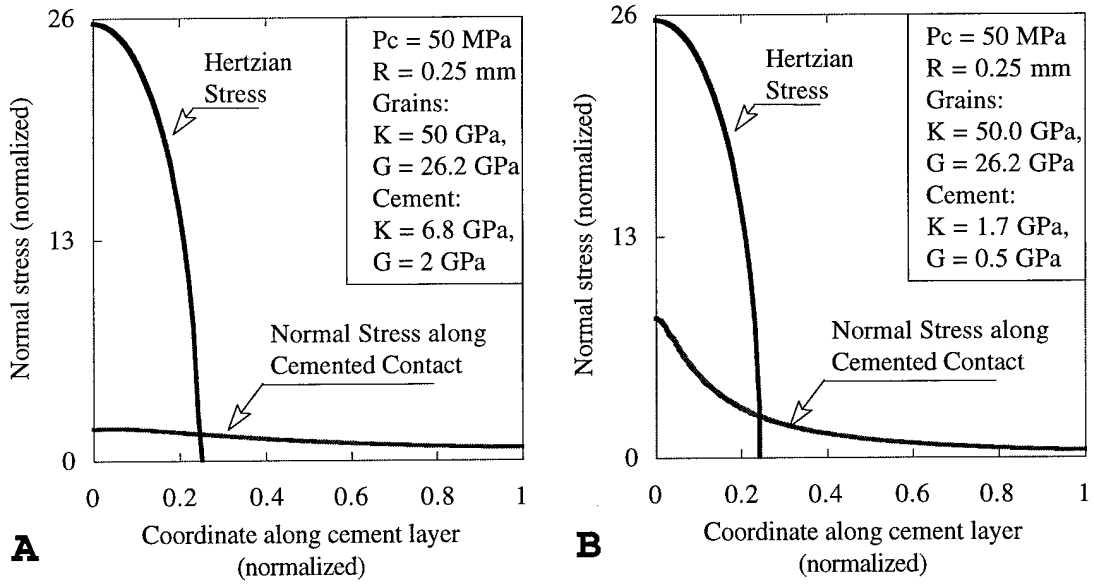

Figure 5. Theoretical prediction of stresses at grain contacts for cemented and uncemented beads: a. epoxy-cemented glass beads, b. glass beads with cement whose bulk and shear moduli are four times smaller than those of epoxy. Stresses are normalized by the average stress at the cemented contact. Coordinate along cement layer is normalized by the radius of the cement layer.

CONCLUSIONS

We show experimentally and explain theoretically that even soft intergranular cement, if deposited at grain contacts, significantly increases the strength of individual grains. This effect is due to a more uniform distribution of contact stresses in the load-bearing cement as compared to a high stress concentration at the uncemented interface. This effect holds even for the amount of cement as low as 10 percent of pore space volume. Therefore, cementing grains provides an effective means of creating strong high-porosity, high-permeability materials.

REFERENCES

Bernabe, Y., Fryer, D.T. and Hayes, J.A., 1992, The effect of cement on the strength of granular rocks, Geophys. Res. Let., 19, 1511 - 1514.

Bruno, M.S. and Nelson, R.B., 1991, Microstructural analysis of the inelastic behavior of sedimentary rock, Mechanics of Materials, 12, 95 - 118.

Clough, G.W., Sitar, N, Bachus, R.C., and Rad, N.S., 1981, Cemented sands under static loading, J. Geotech. Eng. Division, ASCE, 107, 799 - 817.

Cundall, P.A., Jenkins, J.T. and Ishibashi, I., 1989, Evolution of elastic moduli in a deforming granular assembly, Int. Conf. on Micromechanics of Granular Media, Clermont-Ferrand, France.

Cundall, P.A. and Strack, O.D.L., 1979, A discrete numerical model for granular assemblies, Geotechnique, 29, 47 - 65.

Digby, P.J., 1981, The effective elastic moduli of porous granular rocks, J. Appl. Mech., 48, 803 - 808.

Dvorkin, J., Mavko, G. and Nur, A., 1991, The effect of cementation on the elastic properties of granular material, Mechanics of Materials, 12, 207 - 217.

Gallagher, J.J., Friedman, M., Handin, J., and Sowers, G.M., 1974, Experimental studies relating to microfracture in sandstone, Tectonophysics, 21, 203 - 247.

Hertz, H., 1882, Uber die Beruhrung fester elastisher Korper (On the contact of elastic solids), J. Reine und Angewandte Mathematik, 92, 156 - 171.

Mindlin, R.D., 1949, Compliance of elastic bodies in contact, Trans. ASME, 71, A-259.

Nemat-Nasser, S., 1983, On finite plastic flow of crystalline solids and geomaterials, J. Appl. Mech., 50, 1114 - 1126.

Nelson, R.B., Lade, T.V., Issa, J., Chamieh, N. and Yamamuro, J., 1988, Micromechanical behavior of frictional geologic materials, Final Report AFOSR Grant 86-0290, Bolling AFB, Washington D.C.

Rad, N.S. and Clough, G.W., 1982, The Influence of Cementation on the Static and Dynamic Behavior of Sands, Dept. of Civil Engineering, Stanford University, Report 59, 315 p.

Saxena, S.K., 1982, Geotechnical properties of calcareous rocks of Southern Florida, in Geotechnical Properties, Behavior, and Performance of Calcareous Soils, eds. K.R. Demars and R.C. Chaney, 340 - 358.

Trent, B.C., 1989, Numerical simulation of wave propagation through cemented granular material, in AMD -- 101, Wave Propagation in Granular Media, eds. D. Karamanlidis and R.B. Stout, 9 - 15.

Trent, B.C. and Margolin, L.G., 1992, A numerical laboratory for granular solids, Eng. Comp., 9, 191 - 197.

Walton, K., 1978, The oblique compression of two elastic spheres, J. Mech. Phys. Solids, 26, 139 - 150.

2.4. SEISMIC DETECTION OF RESIDUAL CONTAMINANTS

ABSTRACT

The key to effective characterization and treatment of contaminated sites is our ability to delineate the spread of contaminants in the shallow subsurface. A promising non-invasive technique that allows one to identify contaminants is the geophysical three-dimensional mapping of seismic velocities, reflections, and attenuation. The physical principle of this technique is that the same rock, if filled with different fluids, transmits sound waves differently. There are two main reasons for this effect: (a) pore-fluid compressibility and (b) pore-fluid viscosity. While the effect of pore-fluid compressibility has been extensively used for hydrocarbon detection (bright spots), the latter, pore-fluid viscosity, effect has been neglected, mainly because it is noticeable at high frequencies only. We present theoretical models which show that at relatively high, but practically important, frequencies (1 - 10 kHz) the effect of pore-fluid viscosity becomes seismically visible and thus allows one to locate residual viscous contaminants left in thin pores and/or between sand grains. This conclusion is supported by a laboratory ultrasonic experiment where adding small amounts of viscous epoxy to a glass-bead pack resulted in increasing compressional-wave velocity.

INTRODUCTION

The cost of treatment of contaminated sites may be sufficiently reduced if the location of contaminants is accurately predicted. This task becomes especially complicated if there are only small amounts of a contaminant left in thin cracks and between grains. A promising non-invasive technique that allows one to locate contaminants in the shallow subsurface is the geophysical mapping of seismic velocities, reflections, and attenuation.

A critical missing ingredient in previous applications of seismic methods to contaminant and groundwater problems is the relations between the geophysical signatures (seismic velocities and attenuation) and physical properties of pore fluid -- its viscosity and compressibility. Finding, understanding and quantifying these relations is the key goal of rock physics.

Rock physics has been successfully used in the oil and gas industry in transforming high-resolution three- and two-dimensional maps of seismic velocities and attenuation into important physical properties of deep reservoirs and pore fluids. One important effect that allows for such transformations is that seismic velocities in rocks generally change with changing pore fluid, and with changing frequency. There are two principal reasons for this velocity versus saturation and frequency change: (1) Pore fluid, when placed inside the rock, acts as an elastic component that adds stiffness to the solid-fluid composite, and (2) At high frequencies, viscous pore fluid is unable (does not have time) to freely flow between highly compliant thin pores and large pores (unrelaxed state of pore fluid). Therefore, at high frequencies, pore fluid is trapped inside thin pores, thus reinforcing the most compliant elements of the rock (Figure 1a).

The first, pore-fluid-compressibility, effect has been widely used in prospecting for hydrocarbons: often compressional-wave velocity in gas-saturated or oil-saturated reservoirs is smaller than in surrounding brine-saturated rock. Such velocity contrast results in a bright spot that directly indicates the location of hydrocarbon (e.g., Clark, 1992). The second, frequency or pore-fluid-viscosity, effect cannot be used in hydrocarbon reservoirs because high-frequency waves cannot penetrate into the deep subsurface.

One important advantage of applying seismic imaging to environmental problems is that high-frequency signals can be used to characterize the shallow subsurface. For example, a

frequency of 1 kHz is routinely employed to obtain high-resolution velocity maps in well-to-well tomography.

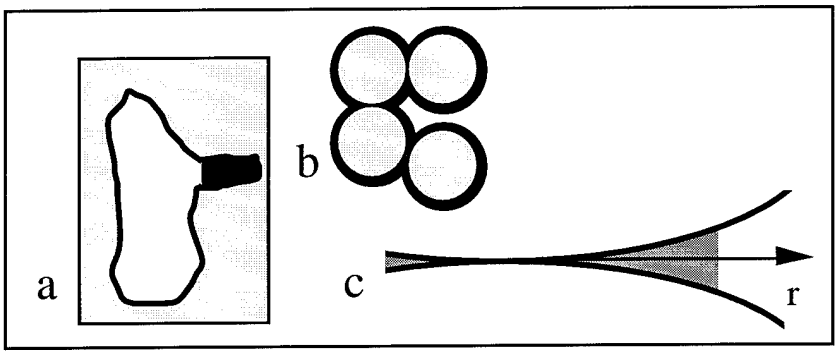

Figure 1. a. Contaminant (black) present in thin cracks. b. Contaminant (black) coating sand grains and creating cementation at the grain contacts. c. Contaminant filling the gap at a grain-to-grain contact.

In this paper, we show that high-frequency seismic imaging can be used to detect residual viscous contaminant left in thin cracks and/or at grain contacts. Our theoretical estimates are based on the squirt-flow mechanism: Stiff portions of the pore space have relatively small variations of pore pressure when the rock is loaded by a passing wave. Soft portions of the pore space tend to transfer more of the stress to the fluid, which results in high variations of induced pore pressure. At low frequencies, one expects these pressures to equilibrate -- an assumption leading to Gassmann's formula for the bulk modulus of saturated rock. At higher frequencies, intensive cross-flow between the soft and the stiff parts persists, resulting in wave-energy dissipation and velocity/frequency dispersion. At very high frequencies, the fluid is unrelaxed and blocked in the compliant pores.

We show that if the contaminant's viscosity is significantly larger than that of water, noticeable velocity dispersion may occur at frequencies of several kHz. Therefore, the effect of pore-fluid viscosity becomes seismically visible allowing one to locate residual viscous contaminant.

SANDSTONES: RESIDUAL CONTAMINANT IN CRACKS

The following theoretical formulas have been derived based on the squirt-flow model for wave-induced motion of the fluid present in thin cracks (Dvorkin et al., 1994). They can be used to calculate P- and S-wave velocities (V_p and V_s, respectively), and attenuation (inverse quality factors Q_p^{-1} and Q_s^{-1}, respectively) in fluid-saturated rock with residual contaminant left in the thin, compliant portions of the pore space (Figure 1a). In this model, the contaminant may differ from the saturating fluid.

$$V_p = \sqrt{\mathrm{Re}\,(K_r + \tfrac{4}{3} G_m)/\rho}, \quad V_s = \sqrt{\mathrm{Re}\,(G_m)/\rho},$$

$$Q_p^{-1} = \left|\mathrm{Im}\,(K_r + \tfrac{4}{3} G_m)\right| / \left|\mathrm{Re}\,(K_r + \tfrac{4}{3} G_m)\right|,$$

$$Q_s^{-1} = \left|\mathrm{Im}\,(G_m)\right| / \left|\mathrm{Re}\,(G_m)\right|.$$

In these formulas

$$K_r = K_m / (1 + \alpha_m \, {}^{dP}\!/_{d\sigma}), \; \alpha_m = 1 - K_m / K_{ms};$$

$$1/G - 1/G_m = (4/15)(1/K - 1/K_{md}),$$

$$1/K_{md} = 1/\tilde{K}_{ms} + 1/K_{hP} - 1/K_s,$$

$$\tilde{K}_{ms} = K_{msd} + \alpha K_s[1 - f(\xi)];$$

$$1/K_m = 1/K_{ms} + 1/K_{hP} - 1/K_s;$$

$$K_{ms} = \frac{K_{msd} + \alpha K_s [1 - f(\xi)]}{1 + \alpha f(\xi)^{dP/d\sigma}},$$

$$\alpha = 1 - K_{msd}/K_s,\ f(\xi) = 2J_1(\xi)/[\xi J_0(\xi)],\ \xi = \sqrt{i\omega\mu}\ Z;$$

$$\frac{dP}{d\sigma} = -[\alpha_0 (1 + \frac{K\phi}{\alpha_0^2 F_0})]^{-1},$$

$$1/F_0 = 1/K_f + 1/(\phi Q_0),\quad \alpha_0 = 1 - K/K_s,$$

$$Q_0 = K_s/(\alpha_0 - \phi);$$

$$1/K_{msd} = 1/K_s - 1/K_{hP} + 1/K;$$

where ρ is the saturated-rock density; K and G are the dry-rock bulk and shear moduli, respectively; K_{hP} is the bulk modulus of dry rock at high pressure; K_s is the bulk modulus of the mineral phase; K_f is the pore-fluid bulk modulus; μ is the dynamic viscosity of the contaminant; ϕ is porosity; and J_0 and J_1 are Bessel functions of zero and first order, respectively. All above quantities are in SI units. Parameter Z describes the wave-induced squirt flow of the contaminant in thin cracks and is frequency- and viscosity-independent. It can be found by matching one of the four parameters: V_p, V_s, Q_p^{-1}, or Q_s^{-1} with one experimental measurement (preferably V_p). The experiment can be performed on a clean water-saturated sample at ultrasonic frequency. Typically, Z ranges from 0.03 to 0.09.

We used these formulas to calculate P- and S-wave velocities in water-saturated Navajo sandstone of 11.8 percent porosity. The viscosity of the contaminant varied from 1 cPs to 10^4 cPs. The Z value calculated from ultrasonic-pulse-transmission experiments (Coyner, 1984) was 0.087.

Compressional-wave velocity versus frequency is shown in Figure 2a. We can see significant velocity/viscosity dispersion at 1 kHz -- a frequency commonly used in well-to-well tomography. If the contaminant's viscosity is as low as 100 cPs -- the viscosity of 30 deg. API oil (Batzle and Wang, 1992), the V_p difference between the clean and the contaminated rock is about 120 m/s. This difference approaches 290 m/s, and 330 m/s as the contaminant's viscosity becomes 10^3 cPs and 10^4 cPs, respectively. A strong velocity/viscosity dispersion at 1 kHz can be also observed for shear-wave velocity (Figure 2b). Here V_s increases from 2800 m/s to 2850 m/s, 2905 m/s, and 2915 m/s as the contaminant's viscosity increases from 1 cPs to 10^2 cPs, 10^3 cPs, and 10^4 cPs, respectively.

Based on these estimates, we conclude that even small amounts of viscous contaminant left in the thin, compliant portions of the pore space can be seismically detectable at frequency 1 kHz and larger.

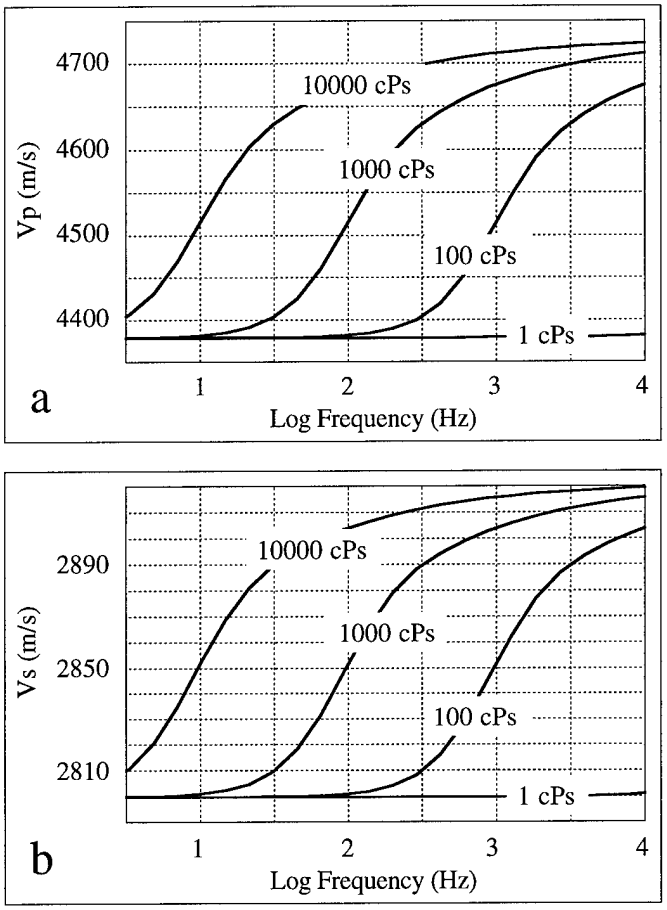

Figure 2. Compressional-and shear-wave velocities in water-saturated Navajo sandstone. Viscous contaminant is present only in thin, compliant cracks. The numbers indicate the contaminant's viscosity. a. V_p. b V_s.

SANDS: RESIDUAL CONTAMINANT AT GRAIN CONTACTS

Consider unconsolidated sand grains coated with viscous contaminant (Figure 1b). The rest of the pore space may be dry or water-saturated. As a result of such pore-space topology, the contaminant fills the gaps around grain-to-grain contacts. Loading of the grains by a passing seismic wave results in the squirting flow of the contaminant in these contact gaps (Figure 1c). If frequency (and/or viscosity of the contaminant) is high, the fluid in a contact gap will resist the squeezing action of the seismic excitation by developing substantial hydrodynamic pressure and creating contact stiffness. We calculate this stiffness by combining a model of fluid flow in a crack (Dvorkin et al., 1992) and a model of the normal deformation of two cemented grains (Dvorkin et al., 1991).

To obtain the stiffness, one has to numerically solve the following integro-differential equation:

$$-P''(1-\frac{\tanh\lambda}{\lambda})-\frac{P'}{r}(1-\frac{\tanh\lambda}{\lambda}+2\tanh^2\lambda)-P\frac{\omega^2}{c_0^2}=$$

$$\frac{2R\omega^2\rho_0}{r^2}[\frac{1-\nu}{\pi G}\int_0^{\pi}d\varphi\int_0^{r\cos\varphi+\sqrt{b^2-r^2\sin^2\varphi}}P(\sqrt{r^2+s^2-2rs\cos\varphi})ds-\delta],\quad \lambda=\frac{r^2}{2R}\sqrt{\frac{i\omega}{\eta}},$$

where P is hydrodynamic pressure in the fluid; ω is angular frequency; ρ_0 is the contaminant's density; η is its kinematic viscosity; c_0 is its acoustic velocity; R is the grain's radius; G and ν are its shear modulus and Poisson's ratio, respectively; b is the radius of the contaminant-filled gap between two grains, as measured along the r coordinate (Figure 1c); and δ is an arbitrarily-chosen non-zero constant. The b value can be calculated from the thickness of the contaminant layer h as $b = \sqrt{2Rh}$. The equation has to be solved with the boundary conditions $P = 0$ at $r = b$, and $P' = 0$ at $r = 0$.

After the equation is solved, the normal two-grain stiffness S_n can be calculated from

$$S_n = F / \delta, \quad F = \int_0^b 2\pi r P(r) dr.$$

Finally, assuming that the shear stiffness is small as compared to the normal stifness, the effective bulk and shear moduli of a random pack of identical spherical grains, K_{eff} and G_{eff}, can be calculated from

$$K_{eff} = \frac{C(1-\phi)}{12\pi R} S_n, \; G_{eff} = \frac{C(1-\phi)}{20\pi R} S_n,$$

where C is the coordination number, and ϕ is porosity (Winkler, 1983). This dry-frame moduli can be used in Gassmann's equation when calculating P-wave velocity in water-saturated sand.

We calculated P-wave velocity versus frequency and viscosity in unconsolidated water-saturated glass beads coated with viscous contaminant (Figure 3). In this case velocity/viscosity dispersion is not as large as in Navajo sandstone. For example, at frequency 1 kHz the velocity increase between clean beads and the beads coated with 10^5 cPs viscosity contaminant is only 48 m/s. This difference reaches 130 m/s at frequency 10 kHz. We conclude that in unconsolidated sands, residual contaminant is harder to detect than in Navajo-type sandstones. Nevertheless, using high-frequency high-resolution seismic techniques may help locate this type of residual contamination caused by high-viscosity substances.

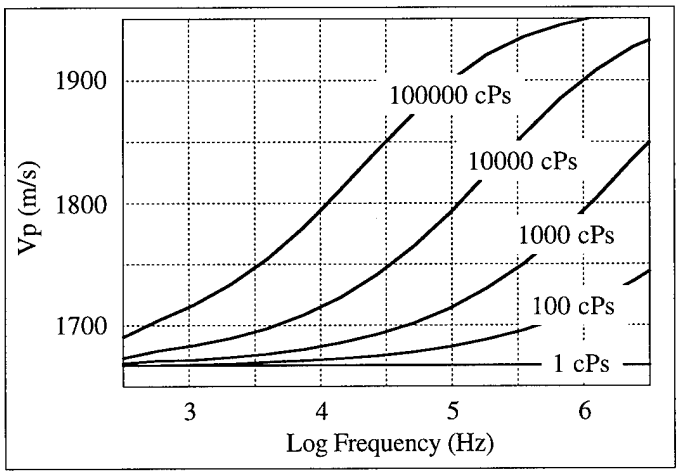

Figure 3. Compressional-wave velocity in unconsolidated water-saturated glass beads. The beads are coated with viscous contaminant. The ratio h / R is 0.05. The numbers indicate the contaminant's viscosity.

EXPERIMENTS

We have conducted ultrasonic pulse-transmission experiments (1 MHz) on dry glass beads partially saturated with epoxy. The viscosity of the epoxy was about 400 cPs. The confining pressure varied from 5 to 20 MPa. The microphotographs of the thin sections showed that the epoxy filled the intergranular contact gaps. The results (Figure 4) indicate that there is a small but noticeable velocity increase associated with the addition of epoxy. It is interesting that this increase (about 40 m/s) only weakly depends on saturation (if saturation is partial). The reason is that the most intensive squirt flow occurs in the direct vicinity of the contact and thus adding the epoxy does not significantly change wave-induced pressure in the contact gap. This effect is also predicted by our theoretical estimates.

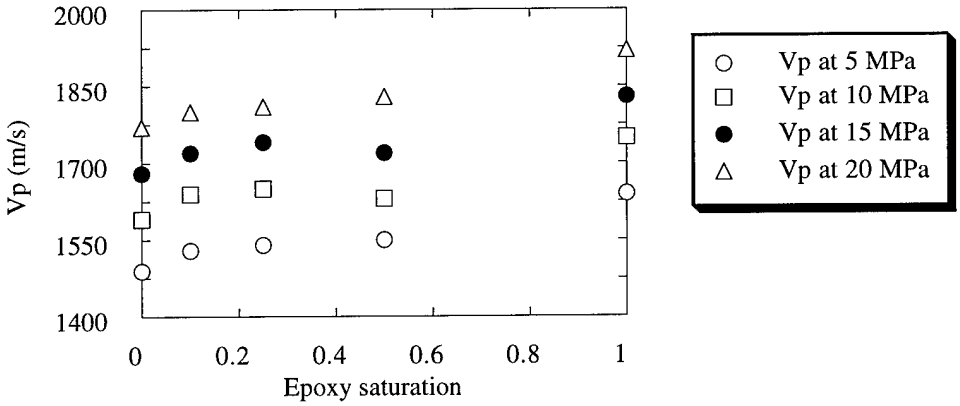

Figure 4. Ultrasonic compressional-wave velocity in compacted partially epoxy-saturated glass beads.

CONCLUSIONS

Small amounts of viscous contaminant, if located in thin compliant pores, or at grain contacts, may noticeably affect high-frequency (several kHz) seismic velocities in rocks. This effect is large in Navajo-type sandstones and is small in unconsolidated sands. Velocity increase in contaminated rocks (as compared to clean rocks) strongly depends on the viscosity of the contaminant: the larger viscosity, the larger the increase (at a given frequency).

This velocity/viscosity dispersion may serve as the theoretical foundation for a promising non-invasive geophysical technique that allows one to locate residual contaminants in the shallow subsurface.

REFERENCES

Batzle, M. and Wang, Z., 1992, Seismic properties of pore fluids: Geophysics, 57, 1396-1408.

Clark, V.A., 1992, The effect of oil under in-situ conditions on the seismic properties of rocks: Geophysics, 57, 894-901.

Coyner, K.B., 1984, Effects of stress, pore pressure, and pore fluids on bulk strain, velocity, and permeability in rocks: Ph.D. thesis, Massachusetts Inst. Tech.

Dvorkin, J., Mavko, G., and Nur, A., 1991, The effect of cementation on the elastic properties of granular materials: Mechanics of Materials, 12, 207-217.

Dvorkin, J., Mavko, G., and Nur, A., 1992, The dynamics of viscous compressible fluid in a fracture: Geophysics, 57, 720-726.

Dvorkin, J., Mavko, G., and Nur, A., 1993, Squirt flow in fully saturated rocks: Geophysics, in press.

Winkler, K.W., 1983, Contact stiffness in granular porous materials: Comparison between theory and experiment: Geophys. Res. Let., 10, 1073-1076.

2.5. ELASTICITY OF PARTIALLY SATURATED FROZEN SAND

INTRODUCTION

Seasonal thawing and freezing of near-surface sediments significantly affects the interpretation of seismic reflection surveys and vertical seismic profiling, as well as activity on the surface. Permafrost covers much of the Earth's colder regions and is also subject to periodic thawing and freezing. The significance of the regions with large seasonal temperature variations for exploration and engineering activities makes understanding the elasticity of frozen ground an important practical and scientific goal.

Previous theoretical and experimental studies of seismic velocities in frozen rocks (e.g., Timur, 1968) showed that P-wave velocity in fully water-saturated rocks increases with decreasing temperature whereas it is almost independent of temperature in dry rocks. As temperature decreases, saturated rocks become (given enough time) completely frozen and velocity reaches its constant (terminal) value. A theoretical scheme for estimating both P- and S-wave velocities in saturated freezing rocks has been proposed by Zimmerman and King (1986); the method accurately predicted the experimental data.

In this study we are concerned with velocities in partially saturated unconsolidated sands. Our experiments show that in hydrophilic granular materials velocities may be close to their full-saturation terminal values at saturations as small as 10 - 15 percent. The reason for this strong velocity increase from the dry state is the cementing action of ice that forms pendular rings at the grain contacts. This freezing effect is a special case of a more general phenomenon: even small amounts of relatively soft cement, if placed at the grain contacts, act to dramatically increase the stiffness of the aggregate.

By applying the Dvorkin et al. (1994) intergranular cementation theory we accurately predict the measured experimental values. These accurate predictions cannot be achieved by effective medium theories that do not take into consideration the specific location of the cement -- at the grain contacts.

EXPERIMENTS

The laboratory apparatus includes a 76 cm-long, 7.6 cm in diameter Plexiglas holder filled with the dry-matrix material (0.7 mm in diameter well-sorted glass beads, or Ottawa sand with average grain size 0.3 mm). P- and S-wave velocities are measured within the holder using transmitter and receiver transducers (both 2.5 MHz central frequency) placed 1.52 cm apart. The transducers are held within a rigid plastic frame, which is lowered into the Plexiglas tube by the cables. The holder is seated on a metal base with drainage holes.

The matrix materials were saturated by suctioning degassed water up the tube through the holes in the base. This technique allowed air to escape and prevented air bubbles from lodging in the matrix. Partial saturation was achieved by draining the fully-saturated matrix materials. The amounts of water held by capillary forces between the grains were uniform along the upper part of the holder and accounted for 13.1 and 13.5 percent saturation in glass beads and Ottawa sand, respectively. Both matrix materials appeared to be hydrophilic -- water formed pendular rings around grain contacts.

P- and S-wave velocities were measured in the samples (dry, saturated, and partially saturated) after they spent a day in a freezer at about -20° C (to ensure the complete freezing of water). The results of these measurements, as well as the experimental values for dry-matrix porosity and ice saturation of the pore space are summarized in Table 1.

The measured ultrasonic velocities are plotted versus ice saturation in Figure 1. At zero ice saturation both P- and S-wave velocities are zero since no confining pressure is applied to the samples. Apparent is a dramatic increase in the velocities as ice saturation increases

from zero to about 13 percent. This increase is much larger than that occurring between low and full saturation.

Table 1. Results of experimental measurements.

Matrix-Cement	Dry-Matrix Porosity	Ice Saturation	V_P (m/s)	V_S (m/s)
Glass-Ice	0.4066	1.0	4583.	2492.
Ottawa Sand-Ice	0.3875	1.0	4480.	2730.
Glass-Ice	0.4066	0.131	3418.	2100.
Ottawa Sand-Ice	0.3875	0.135	3040.	1900.
Glass-Ice	0.4066	0.0	0.	0.
Ottawa Sand-Ice	0.3875	0.0	0.	0.

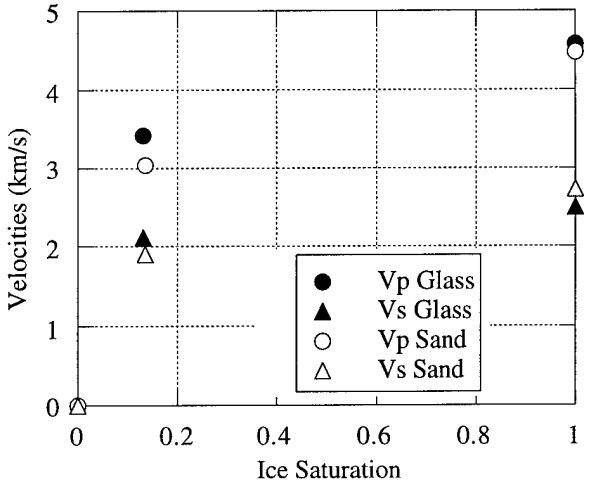

Figure1. Velocities in uncompacted frozen glass beads and Ottawa sand versus ice saturation.

EFFECT OF CEMENTATION

The observed strong velocity increase at low ice saturations is apparently due to the cementing effect of frozen pendular rings. Indeed, the theoretical and experimental results of Dvorkin et al. (1994) show that even small amounts of relatively soft cement, if placed at grain contacts, dramatically increase the stiffness of an aggregate. We applied the cementation theory of Dvorkin et al. (1994) to calculate the effective elastic moduli of ice-cemented glass beads and Ottawa sand (the algorithm is given in Appendix). Both aggregates were modeled as assemblies of randomly packed identical elastic spheres (glass and quartz) with elastic cement (ice) at the contacts. The material properties used in these calculations are summarized in Table 2.

All densities, as well as P- and S-velocities in ice, were measured by the authors. P- and S-velocities in glass were taken from Berge et al. (1993). The velocities in Ottawa sand grains were obtained indirectly, by using Hill's average (1952) to calculate the effective moduli of the fully-saturated sand-ice mixture, and adjusting those of the grains to match the experimental results. The equations for calculating an effective modulus (M_{Hill}) are:

$$M_{\text{Hill}} = (M_V + M_R)/2,\ M_V = (1-\phi_0)M_{\text{Sand}} + \phi_0 M_{\text{Ice}},$$
$$1/M_R = (1-\phi_0)/M_{\text{Sand}} + \phi_0/M_{\text{Ice}}, \qquad (1)$$

where M_{Sand} and M_{Ice} are the moduli of the sand grain material and ice, respectively, and ϕ_0 is the porosity of a dry matrix. These equations can be used to calculate bulk (K), shear (G), and P-wave (M) moduli. The latter is related to P-wave velocity as $M = \rho V_p^2$, where ρ is density.

Table 2. Material properties of ice, glass, and sand grains.

Substance	V_P (m/s)	V_S (m/s)	Density (kg/m^3)
Ice	3840.	1980.	900.
Glass	5860.	3480.	2505.
Sand Grains	5372.	3517.	2668.

The values thus obtained for V_p and V_s in the sand-grain material are about 86% to 89% those in pure quartz -- 6050 m/s and 4090 m/s, respectively (Carmichael, 1989). Nevertheless, we decided to use the calculated values because the elastic moduli of sand grains may be lower than those of pure quartz due to microcracks.

Our theoretical calculations are compared with the experimental values of the *P*-wave and shear moduli in Figures 2 and 3. The moduli are plotted versus the porosity ϕ of an aggregate -- $\phi = \phi_0(1 - S)$, where S is the volumetric ice saturation. The theoretical curves begin at porosity 0.2 because the cementation theory can be used only for small amounts of intergranular cement. We observe a very good match between the experimental data and the theoretical predictions for glass beads. In Ottawa sand, the accuracy of the theoretical prediction is still satisfactory (the error is 15 percent) for the *P*-wave modulus, whereas for the shear modulus the error reaches 34 percent. Notice, that for V_p and V_s, these errors become 7 percent and 16 percent, respectively. This difference between the predicted and the measured values is most likely due to the angularity of the sand grains: the cemented contact area between angular grains is smaller than that between two spheres (for the same amount of cement).

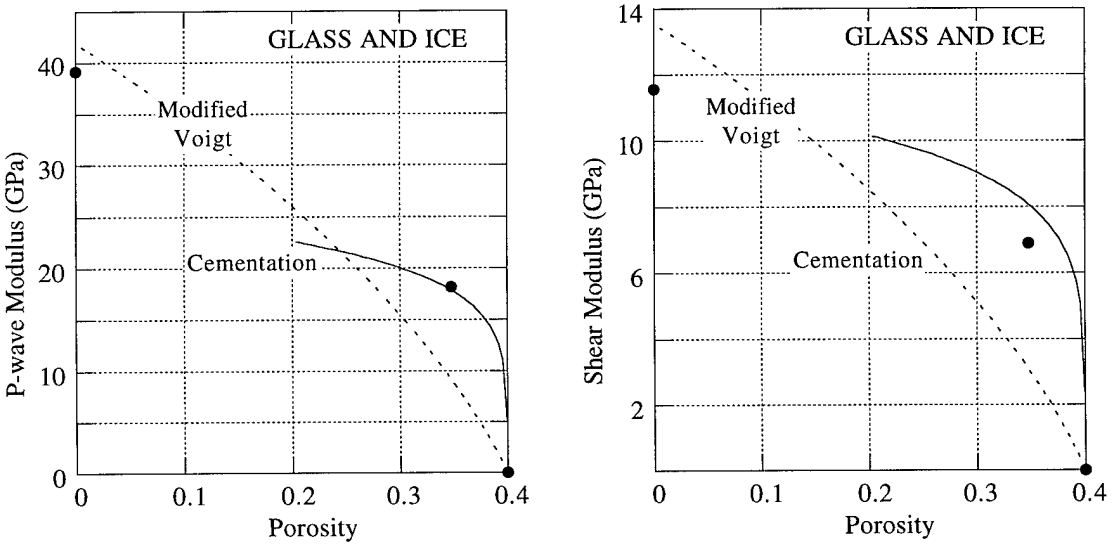

Figure 2. P-wave (left) and shear (right) moduli in ice-cemented glass beads. Circles -- experiments, solid lines -- the cementation theory, dashed line -- modified Voigt average. The porosity is that of the frozen sample, including ice as part of the matrix; then, the 0 porosity point is from the fully-saturated case, and the 0.4 porosity point is from the dry case, with the other point representing partial saturation.

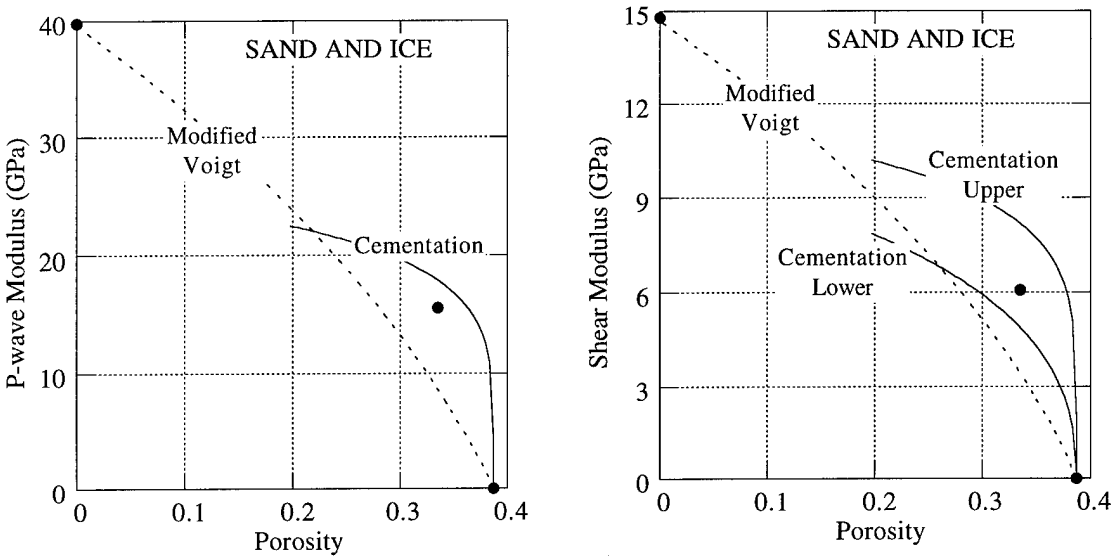

Figure 3. P-wave (left) and shear (right) moduli in ice-cemented Ottawa sand. Circles -- experiments, solid lines -- the cementation theory, dashed line -- modified Voigt average. Porosity is defined in Figure 2.

The second reason for the disparity may be a more uniform distribution of ice on the surface of the Ottawa sand grains. In this case only part of the ice -- the intersection of ice shells around the grains -- forms contact cement. We model the latter situation by representing Ottawa sand as a pack of identical spheres with ice uniformly distributed on their surfaces. This model gives a low-bound estimate for the effective elastic moduli. This lower bound is shown in Figure 3 for the effective shear modulus. The span between the upper and lower bounds is fairly large for elastic moduli. However, this span becomes much smaller for P- and S-wave velocities (Figure 4). Therefore, our theoretical bounds can be used for practical estimates of velocities in frozen partially saturated sands.

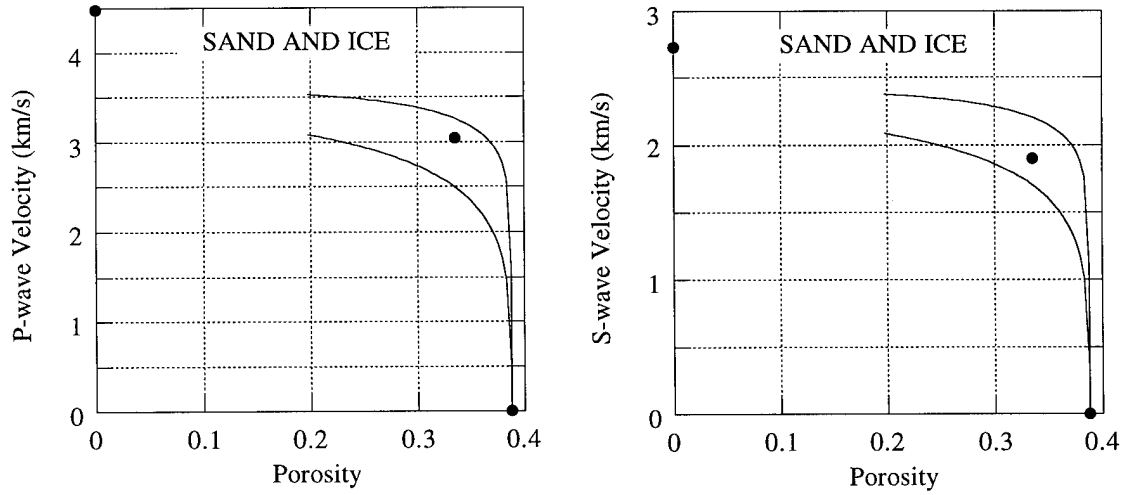

Figure 4. P- (left) and S-wave (right) velocities in ice-cemented Ottawa sand. Circles -- experiments, solid lines -- the cementation theory, upper and lower bounds.

CRITICAL POROSITY AND EFFECTIVE MEDIUM CALCULATIONS

Advanced effective medium theories, such as self-consistent approximation (e.g., Berryman, 1980; Berge et al., 1993) have been successfully used for modeling the effective properties of composites. However, these theories do not make explicit use of the fact that at zero confining pressure, in dry unconsolidated, uncemented granular materials elastic waves do not propagate, and elastic moduli are zero. In this case, the elastic modulus curves (in the modulus-porosity plane) have to intercept the porosity axis at a certain terminal (critical) porosity (ϕ_c). In sands, this critical porosity is about 0.38 -- the value close to the porosity of randomly packed identical spheres. Generally, in effective medium theories this intercept occurs at values higher than the realistic ϕ_c value for a given aggregate (e.g., Berge et al., 1993). Nur et al. (1991) propose that this critical porosity value is a natural physical boundary for using effective medium relations in sandstones and sands. They show that one can arrive at very accurate estimates for velocities in sandstones by using a heuristic, modified Voigt average, formula

$$M_{\text{Effective}} = M_{\text{Solid}}(1-\frac{\phi}{\phi_c}), \qquad (2)$$

where M_{Solid} may be the solid phase's bulk, shear, or P-wave modulus. The solid phase moduli have to be calculated from those of mineral components by using weighted averages, such as Hill's.

We now apply equation (2) to estimating the effective modulus of ice-cemented glass beads and Ottawa sand by assuming that the grains and the ice form a single solid phase whose effective moduli can be calculated from Hill's average -- equation (1). The latter assumption is supported by the fact that Hill's average gives fairly accurate estimates to the effective moduli of frozen glass beads at full ice saturation.

The results of these calculations are given in Figures 2 and 3. In many rocks the modified Voigt average formula can accurately predict the moduli at small and medium porosities (Nur et al., 1991). We show here that it may fail to predict the dramatic increase of these moduli that occurs as porosity slightly reduces from its initial (dry) value. The reason is that this average does not take into account the special arrangement of the ice cement among grains -- directly at their contacts. Practically, this arrangement is relevant to the case of frozen partially saturated sands.

Zimmerman and King (1985) give an important example of applying an effective medium theory (Kuster and Toksoz, 1974) to modeling velocities in fully saturated freezing sands, shales, and silts. The theoretical scheme is: First the elastic moduli of the ice-air mixture (the ice is the matrix) are computed by using the Kuster-Toksoz formula for spherical inclusions. Then the effective moduli of the frozen aggregate are computed by assuming that the ice-air mixture is the matrix, and the grains are spherical inclusions. By comparing these predictions with experimental data, Zimmerman and King show that this theoretical approach gives accurate estimates to velocities in permafrost. We applied the recommended theoretical scheme to calculating P-wave and shear moduli for partially saturated frozen glass beads (Figure 5).

The Kuster-Toksoz scheme gives adequate estimates for the moduli at full saturation. But again, it fails to mimic the high-porosity elastic properties of partially saturated frozen granular materials. A likely reason is that in fully saturated rocks ice forms first in the larger pore spaces, and then in progressively smaller ones (Williams and Smith, 1989). However, in partially saturated hydrophilic materials where water forms pendular rings, ice forms at grain contacts and acts as strong cement. In this case the cementation theory of Dvorkin et al. (1994) is apparently more appropriate.

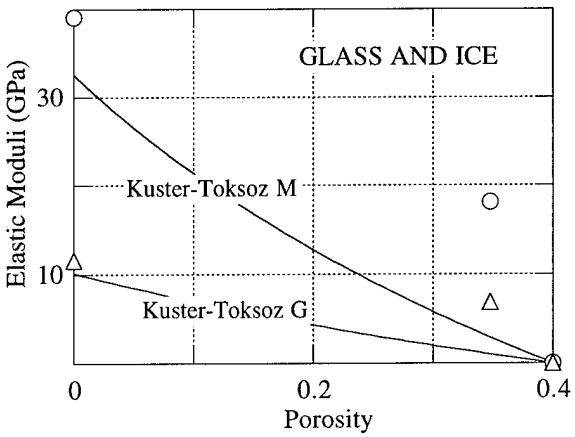

Figure 5. Kuster-Toksoz-Zimmerman estimates for elastic P-wave (M) and shear (G) moduli in frozen glass beads. Circles -- experimental points for M, triangles -- experimental points for G.

CONCLUSIONS

In hydrophilic partially saturated frozen sands, ice acts as intergranular cement by forming pendular rings around grain contacts. This arrangement leads to strong P- and S-wave velocity increase between dry and partially saturated frozen samples at low saturations. This velocity increase is much larger than that occurring between low and full saturation.

The experimental results can be accurately modeled by the theory of cementation that explicitly takes into account the special position of intergranular cement at grain contacts. The effective medium theories, while giving accurate estimates for velocities at high ice saturation, fail to predict the observed dramatic velocity increase occurring as small amounts of ice are added to grain contacts.

By assuming two geometrical schemes of ice distribution in the pore space (one in which ice is concentrated at the grain contacts, and another in which ice is uniformly distributed on the grain surface) the theory of cementation provides fairly narrow upper- and lower-bound estimates for P- and S-wave velocities in partially saturated frozen sands. These bounds can be used in practical estimates of the elastic properties of permafrost.

REFERENCES

Berge, P.A., Berryman, J.G., and Bonner, B.P., 1993, Influence of microstructure on rock elastic properties: Geophys. Res. Lett., 20, 2619-2622.

Berryman, J.G., 1980, Long-wavelength propagation in composite elastic media. I. Spherical inclusions: J. Acoust. Soc. Am., 68, 1809-1819.

Carmichael, R.S., 1989, Practical handbook of physical properties of rocks and minerals: CRC Press.

Delves, L.M. and Mohamed, J.L., 1985, Computational Methods for Integral equations: Cambridge University Press.

Dvorkin, J., Yin, H., and Nur, A., 1994, Effective properties of cemented granular materials: Mechanics of Materials, 18, 351-366.

Hill, R., 1952, The elastic behavior of crystalline aggregate: Proc. Phys. Soc. London, A65, 349-354.

Kuster, G.T., and Toksoz, M.N., 1974, Velocity and attenuation of seismic waves in two-phase media. Part 1. Theoretical formulations: Geophysics, 39, 587-606.

Nur, A., Marion, D., and Yin, H., 1991, Wave velocities in sediments, in Hovem, J.M., Richardson, M.D., and Stoll, R.D., eds., Shear waves in marine sediments: Kluwer Academic Publishers.

Timur, A., 1968, Velocity of compressional waves in frozen soils at permafrost temperatures: Geophysics, 33, 584-595.

Williams, P.J., and Smith, M.W., 1989, The frozen earth: Cambridge University Press.

Zimmerman, R.W., and King, M.S., 1986, The effect of the extent of freezing on seismic velocities in unconsolidated permafrost: Geophysics, 51, 1285-1290.

2.6. ELASTICITY OF HIGH-POROSITY SANDSTONES: THEORY FOR TWO NORTH SEA DATASETS

ABSTRACT

We have analyzed two laboratory datasets obtained on high-porosity rock samples from the North Sea. The velocities observed are unusual in that they seem to disagree with some simple models based on porosity. On the other hand, the rocks are unusually poorly-cemented (for laboratory studies, at least), and we investigate the likelihood that this is the cause of the disagreement. One set of rocks, from the Oseberg field, is made of slightly cemented quartz sands. We find that we can model their dry-rock velocities using a cementation theory where the grains mechanically interact through cement at the grain boundaries. This model does not allow for pressure-dependence. The other set of rocks, from the Troll field, is almost completely uncemented. The grains are held together by the applied confining pressure. In this case, a lower bound for the velocities can be found by using the Hertz-Mindlin contact theory (interaction of uncemented spheres) to predict velocities at a critical porosity, combined with the modified Hashin-Strikman lower bound for other porosities. This model, which allows for pressure-dependence, also predicts fairly large Poisson's ratios for saturated rocks, such as those observed in the measurements. The usefulness of these theories may be in estimating the nature of cement in rocks from measurements such as sonic logs. The theories could help indicate sand strength in poorly-consolidated formations and predict the likelihood of sand production. Both theoretical methods have analytical expressions and are ready for practical use.

INTRODUCTION

Exploring seismic-velocity-to-porosity transformations in various lithologies has been one of the important research areas in rock physics. The main application of this knowledge is to predict porosity from sonic logs and from seismic.

Often the elastic moduli of rock are used instead of velocities. Among them are the compressional-wave modulus (or the M-modulus) and the shear modulus (G). They can be expressed through V_p, V_s, and density ρ as

$$M = \rho V_p^2,$$

$$G = \rho V_s^2.$$

It has been established (Nur et al., 1991) that in consolidated sandstones elastic moduli depend approximately linearly on porosity. The straight line connects two end members: one has zero porosity and a modulus close to that of the solid phase, another has "critical" porosity and (for dry rock) a modulus close to zero. The critical porosity value for sandstones is between 0.36 and 0.4. Two groups of high-porosity sandstones from the Oseberg and the Troll fields defy this simple rule (Figure 1). They represent two different trends where the modulus changes with changing porosity not as dramatically as it does in consolidated sandstones. Our goal is to understand the physical principles that govern velocity-porosity relations in unconsolidated sandstones and to develop a predictive theory.

The two laboratory datasets have been obtained on high-porosity rock samples from the North Sea. The first set is from the Oseberg field (Strandenes, 1991). Some of these samples are shales and/or have strong intrinsic anisotropy. We select a subset that includes structurally and acoustically isotropic quartz sands with porosities between 0.13 and 0.32. Quartz volumetric content varies from 0.6 to almost 1.0. The thin section images reveal

slight quartz cementation among the grains. Two other dominant minerals here are mica (up to 0.15 volume fraction) and clay (up to 0.25 volume fraction).

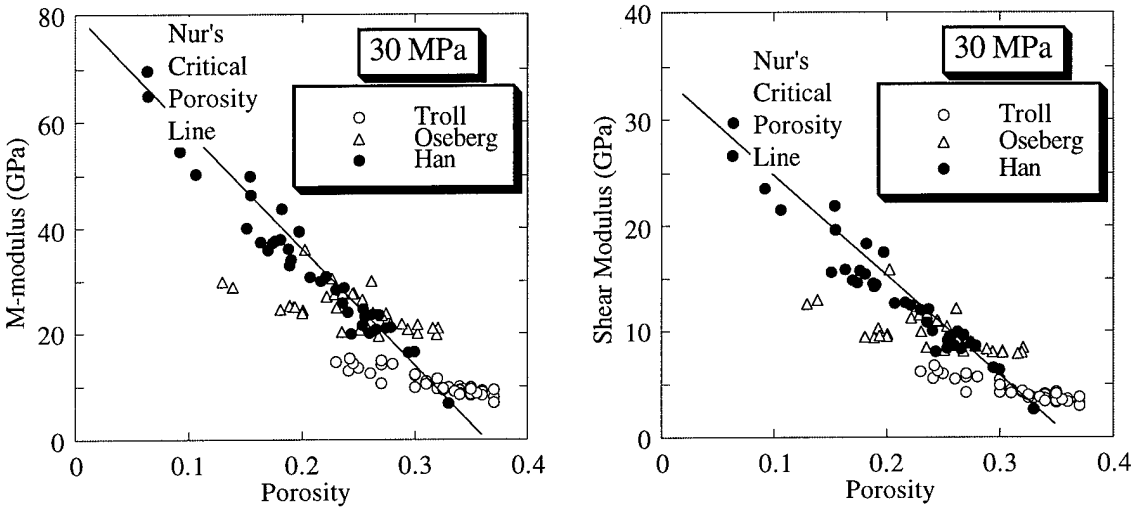

Figure 1. The compressional wave modulus (M-modulus) and the shear modulus versus porosity for three groups of dry rocks at 30 MPa confining pressure: consolidated sandstones without or with only small amounts of clay (Han, 1986), Oseberg sands (Strandenes, 1991), and Troll sands (Blangy, 1992).

The second set represents unconsolidated sands from the Troll field with porosities between 0.22 and 0.38 (Blangy, 1992; and Blangy et al., 1993). The thin section images show that intergranular cementation here is practically absent. Quartz is the dominant mineral in these sands with volume fraction varying between 0.5 and 0.8. Two other major mineral components are feldspar and mica.

Based on the apparent microstructure of the two rock groups we apply two theories to describe them. The first one is the cementation theory (Dvorkin et al., 1991 and 1994). This theory describes the mechanical interaction between grains that are bound together by intergranular cement without reliance on normal loading stresses to maintain contact. An important implication of this theory is that even very soft cement is load-bearing and thus very small amounts of cementation can significantly increase the stiffness of a granular composite. We use this theory to describe the Oseberg samples.

The second theory is based on the contact model of Hertz and Mindlin (Mindlin, 1949) that describes the mechanical interaction between two smooth uncemented elastic spheres based on friction and loading by normal stresses. We use this model to calculate the elastic moduli of sand at critical porosity. To extend it for different porosities, we use the modified Hashin-Strikman lower bound where one end member has zero porosity and the modulus of the solid phase and another end member has critical porosity and a pressure-dependent modulus given by the Hertz-Mindlin theory. This Hertz-Mindlin-Hashin-Strikman (HMHS) model allows us to account for the noticeable pressure dependence normally observed in sands. We apply it to describe the Troll samples.

CONTACT THEORIES

Cementation

The cementation theory by Dvorkin et al. (1991 and 1994) gives the normal and shear stiffnesses of a two-grain combination with elastic cement at the contact. Stiffnesses thus obtained can be used in various effective medium approximations. An appropriate approximation for sand is a random pack of identical spherical grains. The original theory

requires some computational effort to obtain the stiffnesses. By doing these computations in a broad range of the elastic constants of the grains and those of the cement, and for varying amounts of cement we have arrived at easily usable correlations as described below and in Appendix.

We assume that the starting framework of cemented sand is a dense random pack of identical spherical grains with porosity $\phi_0 \approx 0.36$ and the average number of contacts per grain $n \approx 9$. Adding cement to the grains acts to reduce porosity and to increase the effective elastic moduli of the aggregate. Then these effective dry-rock bulk (K_{eff}) and shear (G_{eff}) moduli are (Dvorkin et al., 1994)

$$K_{eff} = \frac{1}{6} n(1-\phi_0) M_c S_n, \quad G_{eff} = \frac{3}{5} K_{eff} + \frac{3}{20} n(1-\phi_0) G_c S_\tau;$$
$$M_c = \rho_c V_{pc}^2, \quad G_c = \rho_c V_{sc}^2; \tag{1}$$

where M_c and G_c are the compressional-wave and the shear moduli of the cement, respectively; ρ_c is its density; and V_{pc} and V_{sc} are its P- and S-wave velocities. Parameters S_n and S_τ are proportional to the normal and shear stiffness, respectively, of a cemented two-grain combination. They depend on the amount of the contact cement and on the properties of the cement and the grains (see Appendix).

The amount of the contact cement can be expressed through the ratio α of the radius of the cement layer a to the grain radius R:

$$\alpha = a / R.$$

The radius of the contact cement layer a is not necessarily directly related to the total amount of cement: part of the cement may be deposited away from the intergranular contacts (Figure 2a). However by assuming that porosity reduction in sands is due to cementation only, and by adopting certain schemes of cement deposition we can relate parameter α to the current porosity of cemented sand ϕ. For example, we can use Scheme 1 where all cement is deposited at grain contacts (Figure 2b):

$$\alpha = 2\left[\frac{\phi_0 - \phi}{3n(1-\phi_0)}\right]^{0.25} = 2\left[\frac{S\phi_0}{3n(1-\phi_0)}\right]^{0.25}, \tag{2}$$

or we can use Scheme 2 where cement is evenly deposited on the grain surface (Figure 2c):

$$\alpha = \left[\frac{2(\phi_0 - \phi)}{3(1-\phi_0)}\right]^{0.5} = \left[\frac{2S\phi_0}{3(1-\phi_0)}\right]^{0.5}. \tag{3}$$

In formulas (2) and (3) S is the cement saturation of the pore space. It is the fraction of the pore space (of the uncemented sand) occupied by cement (in the cemented sand).

It follows from the cementation theory that even soft contact cement is load-bearing. Thus even small amounts of cement, if deposited precisely at grain contacts, act to dramatically increase the stiffness of a particulate aggregate. This theoretical conclusion is well supported by experimental facts (Figure 3).

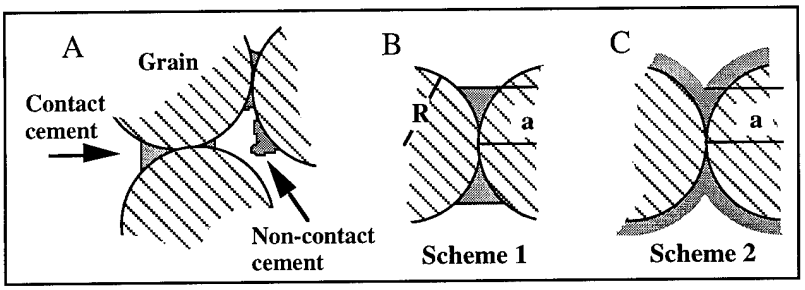

Figure 2. Cemented grains. a. Contact and non-contact cement. b. Scheme 1 of cement deposition. c. Scheme 2 of cement deposition.

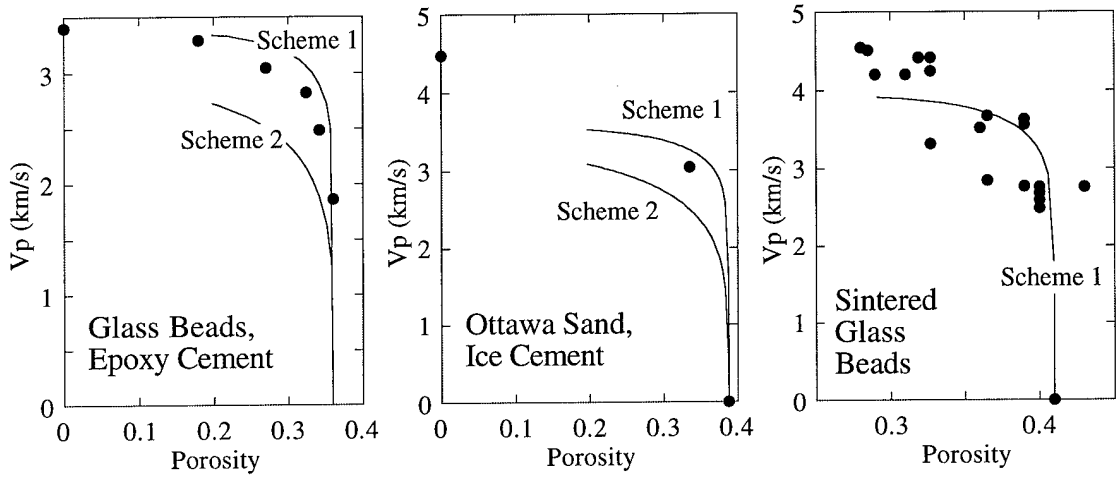

Figure 3. Examples of the theoretical and experimental values of velocities in cemented granular materials. Circles are from experiments, solid lines are theoretical predictions. From left to right: epoxy-cemented glass beads (data from Yin, 1993); ice-cemented Ottawa sand (data from Jacoby et al., 1995); and sintered glass beads (data from Berge et al., 1993).

Hertz-Mindlin Theory with the Modified Hashin-Strikman Lower Bound

The contact Hertz-Mindlin theory (Mindlin, 1949) gives the following expressions for the effective bulk (K_{HM}) and shear (G_{HM}) moduli of a dry dense random pack of identical spherical grains subject to a hydrostatic pressure P:

$$K_{HM} = \left[\frac{n^2(1-\phi_0)^2 G^2}{18\pi^2(1-\nu)^2} P\right]^{\frac{1}{3}},$$
$$G_{HM} = \frac{5-4\nu}{5(2-\nu)}\left[\frac{3n^2(1-\phi_0)^2 G^2}{2\pi^2(1-\nu)^2} P\right]^{\frac{1}{3}}, \quad (4)$$

where ν is the grain Poisson's ratio and G is the grain shear modulus.

Formula (4) describes the effective elastic properties of sand at critical porosity ϕ_0. In order to find the effective moduli (K_{eff} and G_{eff}) at a different porosity ϕ we propose a heuristic modified Hashin-Strikman lower bound based on the original Hashin-Strikman lower bound (1963):

$$K_{eff} = [\frac{\phi / \phi_0}{K_{HM} + \frac{4}{3} G_{HM}} + \frac{1 - \phi / \phi_0}{K + \frac{4}{3} G_{HM}}]^{-1} - \frac{4}{3} G_{HM},$$

$$G_{eff} = [\frac{\phi / \phi_0}{G_{HM} + \frac{G_{HM}}{6}\left(\frac{9K_{HM} + 8G_{HM}}{K_{HM} + 2G_{HM}}\right)} + \frac{1 - \phi / \phi_0}{G + \frac{G_{HM}}{6}\left(\frac{9K_{HM} + 8G_{HM}}{K_{HM} + 2G_{HM}}\right)}]^{-1} \quad (5)$$

$$- \frac{G_{HM}}{6}\left(\frac{9K_{HM} + 8G_{HM}}{K_{HM} + 2G_{HM}}\right),$$

where K is the grain bulk modulus.

This model connects two end members: one has zero porosity and the modulus of the solid phase and another has critical porosity and a pressure-dependent modulus as given by the Hertz-Mindlin theory (Figure 4). It is apparent that this contact theory allows one to describe the noticeable pressure dependence normally observed in sands. The Hashin-Strikman low bound is appropriate to describe materials close to suspensions. Blangy et al. (1993) show that such models give accurate estimates for velocities in unconsolidated sands. The applicability of contact theories to describing granular rocks has been explored by many authors. A detailed investigations was done by Murphy (1982).

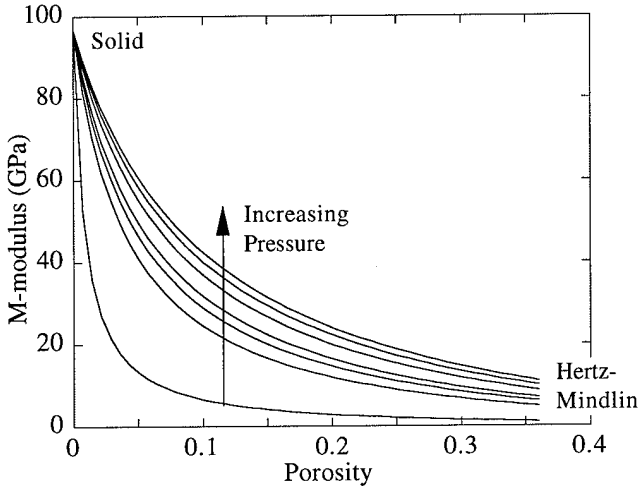

Figure 4. The modified Hashin-Strikman lower bound curves at varying confining pressure for pure quartz sand.

Notice that the dry-rock Poisson's ratios, as predicted by formula (4), do not vary with pressure. At the same time, porosity correction given by formula (5) makes the Poisson's ratio slightly pressure-sensitive.

APPLYING THE THEORY

Oseberg

The Oseberg samples have noticeable mineralogical diversity with quartz as the main component. Based on this last fact we model them as pure quartz sand bound by quartz or clay cement. We assume that cement is evenly deposited on the grain surface, as in Scheme 2, and calculate the dry-rock velocities from formulas (1) and (3). The bulk

modulus, shear modulus, and density of quartz are chosen as 38 GPa, 44 GPa, and 2.65 g/cm^3, respectively (Carmichael, 1990). Our estimates based on the cementation theory capture dry-rock velocity values reasonably well in the relatively clay-free Oseberg samples at confining pressure ranging from 20 MPa to 40 MPa (Figure 5). The theory explains the small variation of velocities with changing porosity.

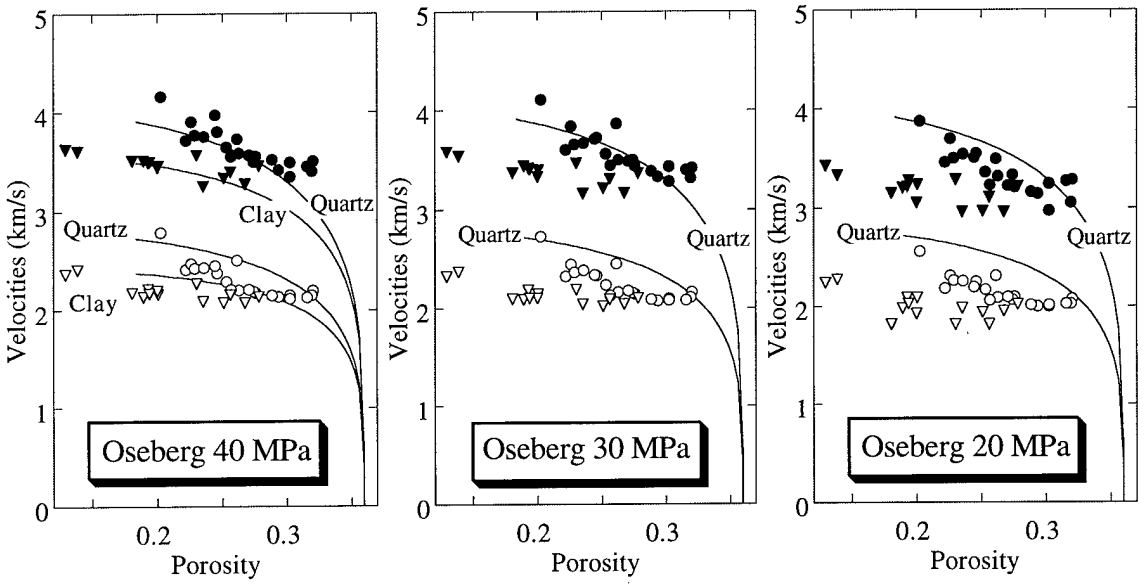

Figure 5. P-wave velocities (filled symbols) and S-wave velocities (open symbols) in the dry Oseberg samples at confining pressures 40, 30, and 20 MPa. Circles are for quartz-cemented rock, triangles are for clay-cemented rock. The solid lines are our theoretical estimates that are pressure-independent. In these estimates cement evenly envelopes the grains (Scheme 2). Cement is either quartz or clay.

We also calculate dry-rock velocities in the Oseberg samples by assuming that cement is clay. The bulk modulus, shear modulus, and density of clay are chosen as 21 GPa, 7 GPa, and 2.58 g/cm^3, respectively. The velocity values were derived by extrapolating the experimental linear velocity-porosity-clay relations obtained by Tosaya (1982) for clay-bearing Gulf sandstones. The density was calculated from the measured density of samples with high clay content, and known porosity and mineralogy. The theoretical line is close to the data points for the Oseberg samples with 10 - 25 volume percent of clay. It is interesting that reducing the cement's stiffness does not significantly reduce the stiffness of the cemented aggregate (Figure 5).

It is important to mention that the cementation theory currently does not account for velocity changes with changing confining pressure. The effective reservoir pressure in the Oseberg field is about 23 MPa. It is crucial that the theory works well at this confining pressure. In fact, the theoretical bounds slightly overestimate the observed values at 20 MPa. We speculate that one reason for this effect may be core damage during pressure release and thus a permanent velocity reduction. Holt et al. (1994) show that if a rock sample is unloaded and then reloaded to the initial pressure level, the velocities do not recover their initial values. Thus we conclude that the cementation theory has good predictive power for velocities in slightly cemented sands. It allows one to determine the cementing mineral (quartz or clay in this example).

The cementation theory lacks predictive power when applied to calculate Poisson's ratios in dry, as well as in saturated rock (Figure 6).

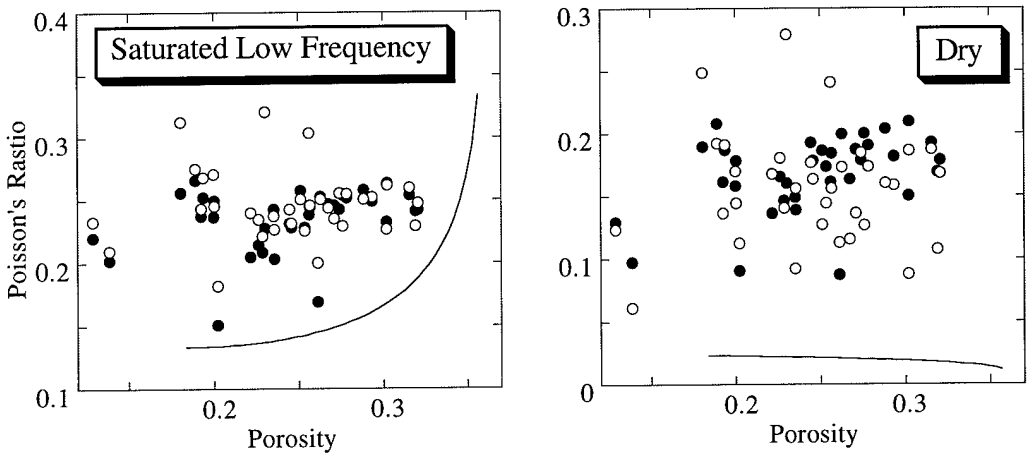

Figure 6. Poisson's ratios in the Oseberg samples at the confining pressures of 20 MPa (open circles) and 40 MPa (filled circles). Solid lines are our theoretical predictions (Scheme 2 of cement deposition). The water-saturated-rock values are calculated from the dry-rock values using Gassmann's (1951) formula.

Troll

Some of the Troll samples have large amounts of feldspar and mica. It would be logical to apply the HMHS scheme to grains made out of a "composite" solid phase that is a mixture of the dominant minerals present in the samples. We find that the theoretical velocities calculated using such mineral mixtures are very close to those calculated using pure quartz grains. The theoretical results for dry rock generally serve as an accurate lower bound for the Troll experimental values (Figure 7).

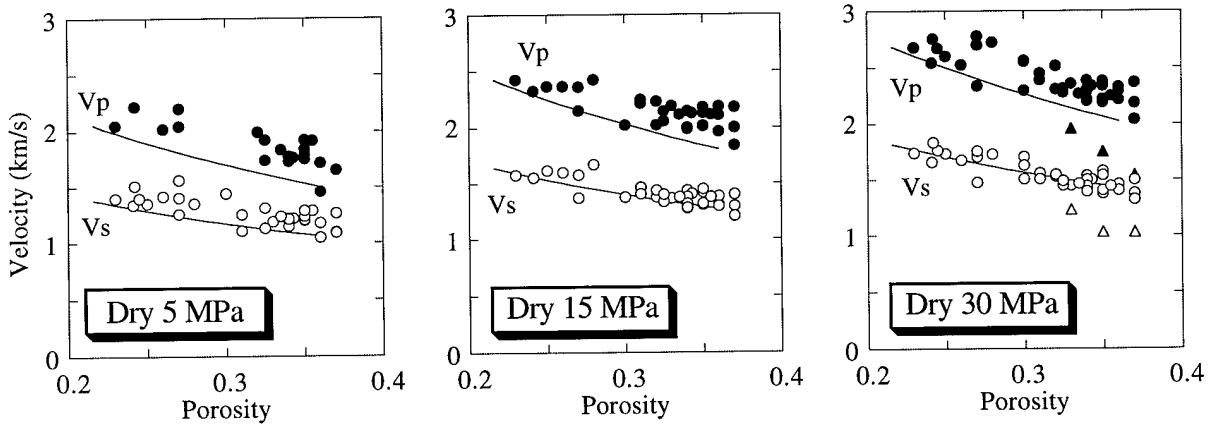

Figure 7. Dry-rock velocities in the Troll samples at the confining pressures of 5 MPa, 15 MPa, and 30 MPa. Filled symbols are for P-wave velocities, open symbols are for S-wave velocities. Solid lines are our theoretical estimates. Triangles are for Ottawa sand samples measured by Han (1986), Yin (1993), and Domenico (1984).

The data for dry Ottawa sand at 30 MPa confining pressure is plotted in these graphs for reference. There is a large disparity not only between the theoretical and the experimental values for Ottawa sand but also among the experimental values for the three samples. One reason may be a variation in compaction and sorting among these samples. As a result, the average number of contacts per grain may not always be 9 and may vary among the three samples of Ottawa sand.

Low-frequency water-saturated-rock velocities are computed from the dry-rock data using Gassmann's (1951) formula (Figure 8). The relative errors of the theoretical estimates are reduced as compared to the dry-rock results. There are two apparent reasons for this improvement. First, pore fluid acts to reduce the dry-rock velocity variation among low-velocity samples. Second, it acts to strongly increase P-wave velocities thus reducing relative errors.

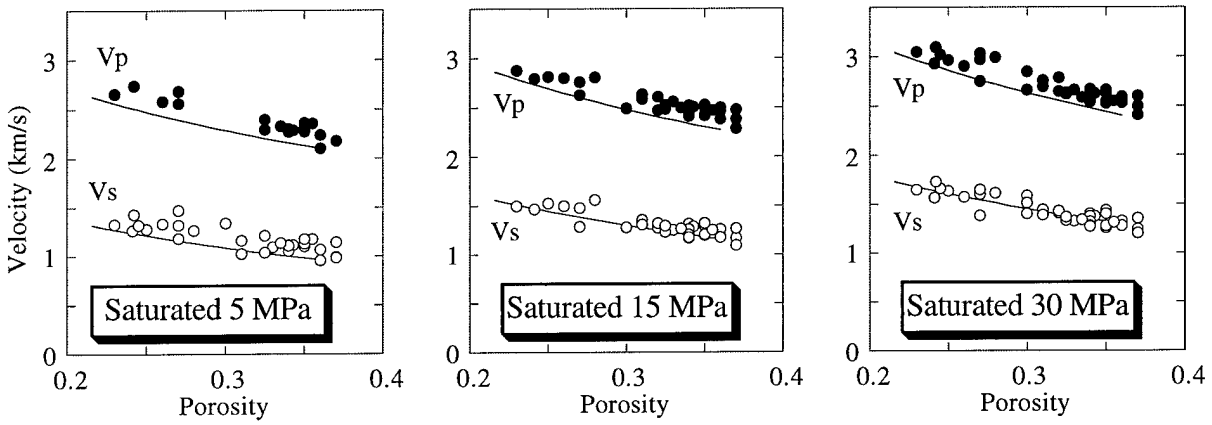

Figure 8. Low-frequency saturated-rock velocities (from Gassmann's formula) in the Troll samples at the confining pressures of 5 MPa, 15 MPa, and 30 MPa. Filled symbols are for P-wave velocities, open symbols are for S-wave velocities. Solid lines are our theoretical estimates.

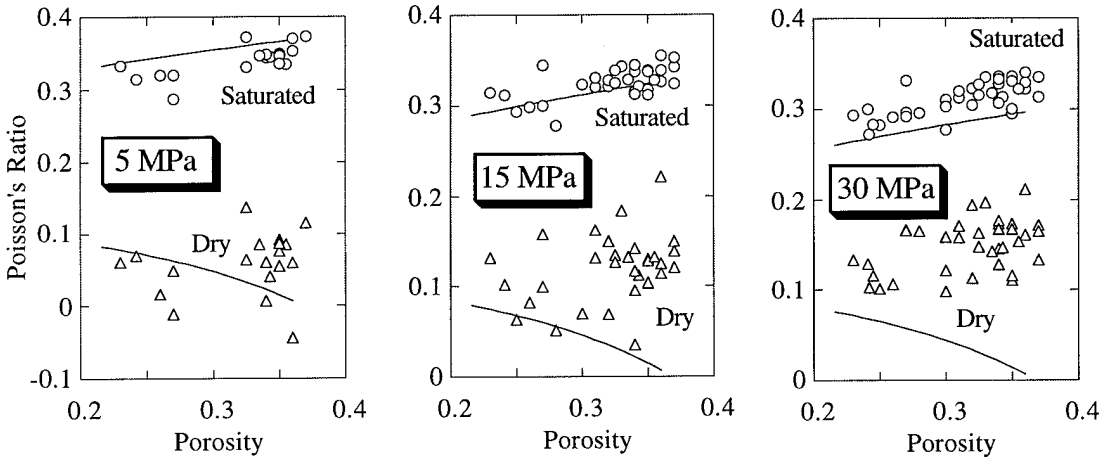

Figure 9. Dry-rock and low-frequency saturated-rock Poisson's ratios in the Troll samples at the confining pressures of 5 MPa, 15 MPa, and 30 MPa. Solid lines are our theoretical estimates.

The last reason is also responsible for the accurate predictions the HMHS model provides for saturated-rock Poisson's ratios (Figure 9). These values are high and match those generally observed in saturated loose sediments. The physical meaning of these high values is clear: saturated loose sediments, especially with no confining pressure, are close to suspensions where Poisson's ratios have their maximum value of 0.5.

In the HMHS model, the saturated-rock Poisson's ratio increases with increasing porosity. This trend qualitatively agrees with that in the data and has a clear physical meaning -- as porosity increases, the rocks approach the state of suspension and the Poisson's ratio approaches 0.5. At the same time, it is obvious that the Poisson's ratios of

saturated rock obtained from formula (4), which does not account for porosity variation, will do as good quantitative predictions as those obtained from formula (5) where porosity is accounted for.

An important feature of the HMHS model is that while the dry-rock Poisson's ratios are only slightly pressure-dependent, the saturated-rock Poisson's ratios have a noticeable pressure dependence (Figure 9).

We conclude that the HMHS model can be used to estimate and bound velocities in loose sands in the Troll field. It can accurately predict saturated-rock Poisson's ratios but should not be used to estimate dry-rock Poisson's ratios at high pressure.

DISCUSSION: PRACTICAL VALUE OF THE THEORIES

Oseberg

We learn from the above theoretical speculations that in the Oseberg rocks a significant part of cement is deposited at grain contacts. This cementation pattern ensures strong velocity increase with only small porosity decrease and is likely to be responsible for the high velocities measured on these high-porosity samples. We speculate that this result can be generalized to give a rule: If high-porosity rock has velocity values close to those given by the cementation theory then it is cemented at grain contacts. The amount of the contact cement can be estimated by varying parameter α in the cementation theory (see Appendix) to match the data point. Thus velocity measurements reveal the internal rock structure.

The latter information is important in assessing, for example, a rock's strength. Yin and Dvorkin (1994) show that even very small amounts of contact cement (even if it is as soft as, e.g., clay) prevent the grains from breaking at high confining pressure (Figure 10).

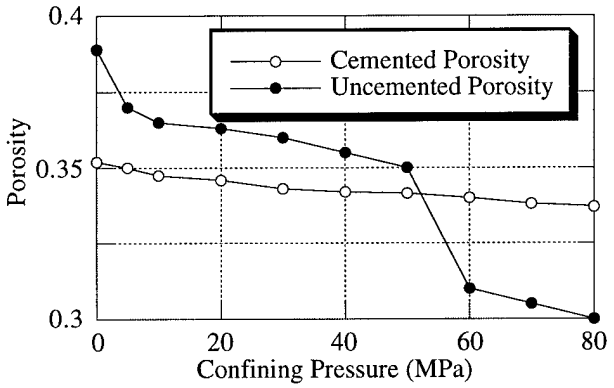

Figure 10. Porosity versus hydrostatic confining pressure in water-saturated randomly packed glass beads that were a) uncemented and b) cemented by epoxy at their contacts (Yin and Dvorkin, 1994). Porosity was measured by the volume of expelled fluid. In the uncemented case, a sharp porosity decrease is observed at about 50 MPa. The decrease is associated with the crushing of grains. The cemented grains (the volume of the epoxy accounted for only 10 percent of the pore space) did not crush. The photos showed that in the latter case, the grains stayed intact with the failure being localized within the epoxy.

We conclude that if high-porosity sandstones have velocities in the range predicted by the cementation theory they are mechanically stable and sanding is unlikely.

The practical significance of the cementation theory is not only in its predictive power -- it is likely that a simple linear velocity-porosity correlation obtained from the data will serve even better for the purpose of estimating porosity from seismic. The practical value is also in understanding the physical reasons for the measured velocities. This understanding may help assess a rock's mechanical stability and lead even further to estimating, for example, such a crucial parameter as permeability, once we are aware of the rock's internal structure.

Troll

Velocity values in the Troll samples can be adequately approximated by the HMHS model. This fact implies that the rock is held together by confining pressure only. The grains that are uncemented at high porosity stay uncemented as porosity decreases. Thus the additional material responsible for porosity reduction is deposited in the large pores, away from compliant contacts. This in turn implies that the rock is mechanically unstable and sanding is likely once uniform confining pressure is released. An important practical result is that the predicted very high Poisson's ratios in saturated rocks closely match the observed values. Thus by combining seismic and depositional history one can distinguish this unconsolidated and mechanically unstable rock from other types.

CONCLUSION

The cementation theory explains well why the high velocity values are encountered in the high-porosity Oseberg samples. This fact means that the grains mechanically interact through quartz cement that is deposited to strengthen the most compliant part of the pore space -- grain contacts. The main practical conclusion is that if at high porosities velocity values are close to those provided by the cementation theory then the grain contacts are cemented. This in turn means that the rock is mechanically stable and sanding is not likely.

Velocity values in the Troll samples can be estimated from a combination of the Hertz-Mindlin contact theory and the modified Hashin-Strikman lower bound, the latter being close to an isostress model for suspensions. Thus in this rock contact cement is almost absent and grains are held together primarily by confining pressure. The model accurately predicts the high Poisson's ratios generally observed in saturated loose sediments.

The main practical conclusion is that if at high porosities velocity values are close to those provided by the HMHS model then there is no contact cement and the rock is held together by confining pressure only. Therefore, the rock is mechanically unstable and sanding is likely to occur once uniform confining pressure is released.

By analyzing the data and finding the appropriate theories to explain the observed trends we gain understanding of the internal rock structure and of stress transfer patterns.

REFERENCES

Berge, P.A., Berryman, J.G., and Bonner, B.P., 1993, Influence of microstructure on rock elastic properties: Geophys. Res. Lett., **20**, 2619-2622.

Blangy, J.P., 1992, Integrated seismic lithologic interpretation: The petrophysical basis: Ph.D. thesis, Stanford University.

Blangy, J.P., Strandenes, S., Moos, D., and Nur, A., 1993, Ultrasonic velocities in sands -- revisited: Geophysics, **58**, 344-356.

Carmichael, R.S., 1990, Practical Handbook of Physical Properties of Rocks and Minerals: CRC Press.

Domenico, S.N., 1976, Effect of brine-gas mixture on velocity in an unconsolidated reservoir: Geophysics, **41**, 882-894.

Dvorkin, J., Mavko, G. and Nur, A., 1991, The effect of cementation on the elastic properties of granular material, Mechanics of Materials, **12**, 207-217.

Dvorkin, J., Nur, A. and Yin, H., 1994, Effective properties of cemented granular material, Mechanics of Materials, **18**, 351-366.

Gassmann, F., 1951, Elasticity of porous media: Uber die Elastizitat poroser Medien: Vierteljahrsschrift der Naturforschenden Gesselschaft in Zurich, Heft 1.

Han, D.-H., 1986, Effects of porosity and clay content on acoustic properties of sandstones and unconsolidated sediments: Ph.D. thesis, Stanford University.

Hashin, Z., and Shtrikman, S., 1963, A variational approach to the elastic behavior of multiphase materials: J. Mech. Phys. Solids, **11**, 127-140.

Holt, R.M., Brignoli, M., Fjaer, E., Unander, T.E., and Kenter, C.J., 1994, Core damage effects on compaction behavior, in Eurock '94: Balkema.

Jacoby, M., Dvorkin, J., and Liu, X., 1995, Elasticity of partially saturated frozen sand: Geophysics, in press.
Mindlin, R.D., 1949, Compliance of elastic bodies in contact, Trans. ASME, **71**, A-259.
Murphy, W.F., 1982, Effects of microstructure and pore fluids on the acoustic properties of granular sedimentary materials: Ph.D. thesis, Stanford University.
Nur, A., Marion, D., and Yin, H., 1991, Wave velocities in sediments, in Hovem, J.M., Richardson, M.D., and Stoll, R.D., eds., Shear waves in marine sediments: Kluwer Academic Publishers.
Strandenes, S., 1991, Rock physics analysis of the Brent Group Reservoir in the Oseberg Field: Stanford Rock Physics and Borehole Geophysics Project.
Tosaya, C.A., 1982, Acoustical properties of clay-bearing rocks, Ph.D. thesis, Stanford University.
Yin, H., 1993, Acoustic velocity and attenuation of rocks: Isotropy, intrinsic anisotropy, and stress induced anisotropy, Ph.D. thesis, Stanford University.
Yin, H., and Dvorkin, J., 1994, Strength of cemented grains: Geophys. Res. Lett., **21**, 903-906.

APPENDIX: EXPRESSIONS FOR STIFFNESSES

Parameters S_n and S_τ in formulas (1) are:

$$S_n = A_n(\Lambda_n)\alpha^2 + B_n(\Lambda_n)\alpha + C_n(\Lambda_n),$$
$$A_n(\Lambda_n) = -0.024153 \cdot \Lambda_n^{-1.3646},\ B_n(\Lambda_n) = 0.20405 \cdot \Lambda_n^{-0.89008},$$
$$C_n(\Lambda_n) = 0.00024649 \cdot \Lambda_n^{-1.9864};$$

$$S_\tau = A_\tau(\Lambda_\tau, \nu)\alpha^2 + B_\tau(\Lambda_\tau, \nu)\alpha + C_\tau(\Lambda_\tau, \nu),$$
$$A_\tau(\Lambda_\tau, \nu) = -10^{-2} \cdot (2.26\nu^2 + 2.07\nu + 2.3) \cdot \Lambda_\tau^{0.079\nu^2 + 0.1754\nu - 1.342},$$
$$B_\tau(\Lambda_\tau, \nu) = (0.0573\nu^2 + 0.0937\nu + 0.202) \cdot \Lambda_\tau^{0.0274\nu^2 + 0.0529\nu - 0.8765},$$
$$C_\tau(\Lambda_\tau, \nu) = 10^{-4} \cdot (9.654\nu^2 + 4.945\nu + 3.1) \cdot \Lambda_\tau^{0.01867\nu^2 + 0.4011\nu - 1.8186};$$

$$\Lambda_n = \frac{2G_c}{\pi G}\frac{(1-\nu)(1-\nu_c)}{1-2\nu},\ \Lambda_\tau = \frac{G_c}{\pi G},\ \alpha = \frac{a}{R};$$

where G and ν are the shear modulus and the Poisson's ratio of the grains, respectively; G_c and ν_c are the shear modulus and the Poisson's ratio of the cement, respectively; a is the radius of the contact cement layer (Figure 2b, c); and R is the grain radius.

These formulas are statistical approximations of the rigorous cementation theory solutions (Dvorkin et al., 1994). The error does not exceed one percent.

2.7. LARGE STRAINS IN CEMENTED GRANULAR AGGREGATES: ELASTIC-PLASTIC CEMENT

1.0. ABSTRACT

We describe large-strain behavior of cemented geomaterials by modeling the deformation of a random pack of identical cemented spheres. In this model we assume that the grains are elastic but that the intergranular cement becomes partly plastic as local stresses meet a plasticity condition. This plasticity condition for a thin elastic-plastic cement layer is derived based on the von Mises criterion. Next we solve the problems of large-strain deformation of two cemented spheres in compression and in shear. This solution allows for calculation of the normal and shear strain-dependent stiffnesses of two cemented grains. Finally, we derive effective stress-strain laws for an aggregate of cemented spheres where grain-to-grain contact stiffnesses are strain-dependent. These theoretical stress-strain laws are close to the relations typically observed in clay-cemented sands. An important result is that an initially isotropic aggregate may become anisotropic if the stress field is non-hydrostatic. This stress-induced anisotropy may lead to an up to 10-percent error in estimating, for example, an apparent isotropic bulk modulus from a uniaxial-strain experiment.

2.0. INTRODUCTION

2.1. Background

The large-strain mechanical properties of natural and artificial geomaterials are important in many geomechanical and engineering applications. Many granular geomaterials are cemented with, for example, clay (sand-clay mixtures) or asphalt (asphaltic concrete). Dvorkin et al. (1994), and Yin and Dvorkin (1994) show that intergranular cementation may strongly affect the elastic properties of particulate materials as well as their strength. It is natural to conclude that cementation affects the large-strain microscopic and macroscopic behavior of such materials as well.

This effect is apparent in the stress-strain curves from uniaxial-stress compression tests on two tight gas sandstone samples (Jizba, 1991). In one sample quartz grains are cemented by a clay matrix that occupies 63 percent of the sample's volume. In the second sample the volumetric content of the clay matrix is only 1 percent. The stress-strain behavior of these two samples is distinctively different (Figure 1). The low-clay-content sample deforms almost linearly up to about 2 percent strain and then exhibits brittle failure. The clay-cemented sample shows ductile (plastic) behavior with the stress-strain curves gently approaching failure.

Another argument that supports the importance of intergranular cementation is the difference between static and dynamic moduli in rocks. Static moduli are those obtained from appropriate stress-strain curves (e.g., static Young modulus is the derivative of the stress-strain curve in a uniaxial-stress experiment). Dynamic moduli are those calculated from P- and S-wave velocities in rocks. For example, dynamic bulk and shear moduli are:

$$K_{\text{Dynamic}} = \rho(V_p^{\,2} - \frac{4}{3}V_s^{\,2}),\ G_{\text{Dynamic}} = \rho V_s^{\,2},$$

where ρ is density, and V_p and V_s are P- and S-wave velocities, respectively.

Typically, dynamic moduli in dry rocks are larger than the corresponding static moduli. One reason is the effect of strain. A sound wave propagating through rock results in minor

stress excursions around a given point on the stress-strain curve. The slope of such an excursion curve is larger than that of the major stress-strain curve in loading and is very close to the corresponding dynamic modulus (Hilbert et al., 1994). This effect is due to the plastic behavior of rocks at high strain.

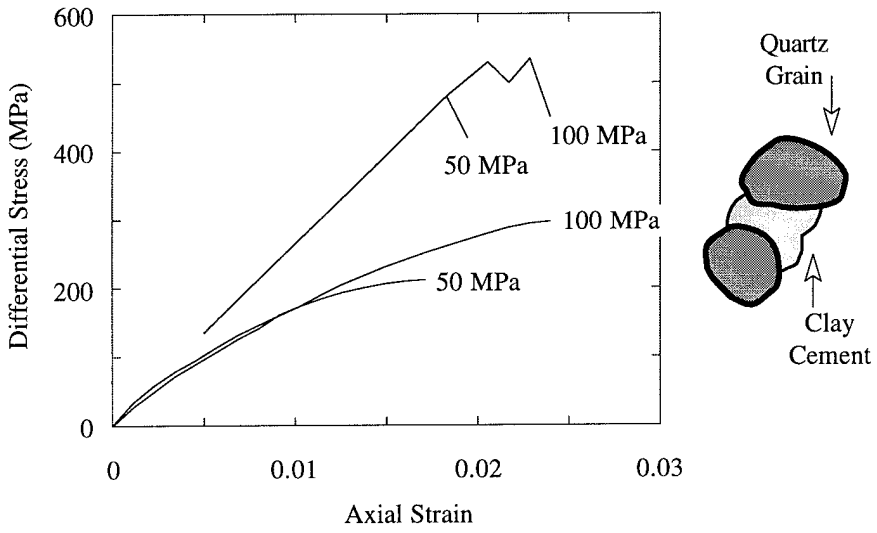

Figure 1. Stress-strain curves from uniaxial-stress compression tests on sandstone samples. In each test the radial stress is constant (labels on the curves). Two upper curves correspond to a low-clay-content sample which failed in a brittle manner. Two lower curves correspond to a sample with 63 percent volumetric clay content. The sample exhibited ductile deformation prior to failure. It eventually failed by shear localization.

If confining pressure is small, this plasticity is partly due to grain compaction, redistribution, and rotation. However at high confining pressure plasticity is mostly due to the plastic nature of intergranular cement. This effect can be clearly seen in Figure 2 where the ratios of dynamic to static bulk moduli (the latter from hydrostatic compaction experiments) are plotted versus hydrostatic pressure (Jizba, 1991).

In two samples with almost no clay this ratio quickly approaches unity as pressure increases. We conclude that once grain redistribution and rotation is finished, rock behaves elastically. However in clay-cemented samples this ratio stays above unity which means that the clay cement strongly contributes to the plasticity of such rocks.

2.2. Model and Assumptions

The goal of this paper is to theoretically describe the apparently important effect of cement's plasticity on the macroscopic behavior of an aggregate. Our principal approach is to model large strains in a cemented aggregate by assuming that cement is elastic-plastic, that is part of a cement layer becomes plastic as stress concentration increases.

Contact stresses (Figure 3a) between cemented grains are principally different from those calculated using traditional Hertzian models (e.g., Hertz, 1882; Mindlin, 1949; Walton, 1978; Digby, 1981). Dvorkin et al. (1994) show that if cement is soft as compared to grains, contact stress concentrations occur at the center of a cemented region (Figures 3b and 3c). It reasonable to assume that as the contact stresses at the center of a cemented region meet a plasticity condition, the central part of the cement becomes plastic and is surrounded by elastic cement (Figure 3d).

Stress distributions, such as shown in Figures 3b and 3c, are obtained under the assumption that the normal and shear stresses in the elastic cement can be estimated using the elastic foundation approximation (Dvorkin et al., 1991). This approximation neglects lateral strain within the cement layer and thus is not adequate to describe stress distribution at the periphery of the cement layer. As a result, there may be a possibility that plastic yield initiates from the periphery inward, instead of from the center outwards, as assumed here. It is clear that a rigorous analysis of contact stresses within cement is needed in order to refine the first-order approximation model presented here.

When deriving the plasticity condition for a thin cement layer we again assume that the normal and shear stresses in the elastic part can be estimated from the elastic foundation approximation. In the plastic part of the cement layer we use the von Mises yield criterion. A word of caution is that this isotropic criterion may be not accurate for geomaterials with layered cement, such as laminated clay.

Once the plasticity condition is established, we find elastic and plastic contact stresses between two grains. This problem requires solving an ordinary integral equation. The solution is numerical and straightforward. These contact stress distributions allow us to find normal and shear stiffnesses of a two-grain combination.

Intrinsic in this analysis is the assumption of local axisymmetry. Dvorkin et al. (1994) show that this assumption is accurate for an elastic cement layer. Additional future effort is needed to estimate the accuracy of the local axisymmetry assumption in elastic-plastic cement.

Next we use statistical modeling to calculate the effective macroscopic stresses in a random pack of identical cemented spheres subject to high strains. Theoretical stress-strain curve shapes are very close to those observed on real geomaterials.

One important effect is that an aggregate with elastic-plastic cement becomes anisotropic if macroscopic stresses are non-hydrostatic. This effect follows from the fact that the contact stiffnesses are strain-dependent since larger local strains result in larger plastic zones. This stress-induced anisotropy may produce an up to 10-percent error in estimating, for example, an apparent isotropic bulk modulus from a uniaxial-strain experiment.

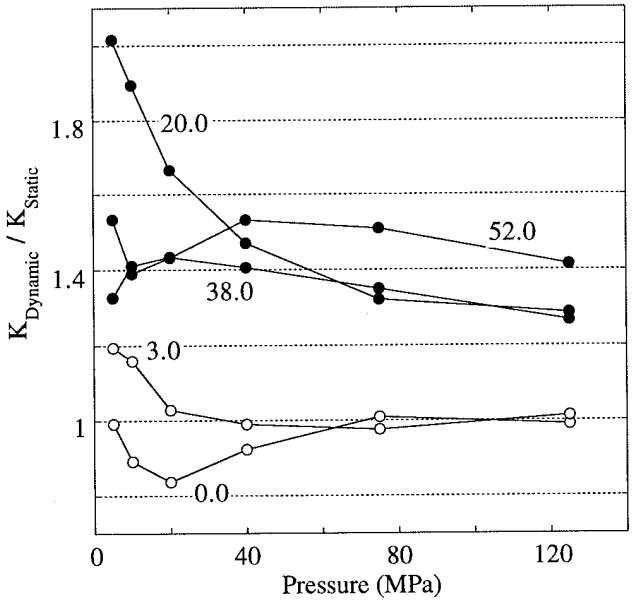

Figure 2. Dynamic-to-static bulk modulus ratios for sandstones. The labels on the curves indicate volumetric clay content.

3.0. ELASTIC-PLASTIC CEMENT LAYER

3.1. Yield Criterion

As a yield criterion we use the von Mises criterion of constant intensity of tangential stresses (Kachanov, 1971):

$$T = \sigma_s / \sqrt{3}, \tag{3.1}$$

where T is the intensity of tangential stresses:

$$T = \frac{1}{\sqrt{6}} \sqrt{(\sigma_{xx} - \sigma_{yy})^2 + (\sigma_{yy} - \sigma_{zz})^2 + (\sigma_{zz} - \sigma_{xx})^2 + 6(\sigma_{xy}^2 + \sigma_{xz}^2 + \sigma_{yz}^2)}, \tag{3.2}$$

σ_{ij} are the components of the stress tensor, and σ_s is the yield limit of the cement under tension.

Equations (3.1) and (3.2) give the following expression for the von Mises criterion:

$$\sigma_{xx}^2 + \sigma_{yy}^2 + \sigma_{zz}^2 + 3(\sigma_{xy}^2 + \sigma_{xz}^2 + \sigma_{yz}^2) - (\sigma_{xx}\sigma_{yy} + \sigma_{yy}\sigma_{zz} + \sigma_{zz}\sigma_{xx}) = \sigma_s^2. \tag{3.3}$$

This last equation can be also expressed in terms of principal stresses σ_x, σ_y, and σ_z:

$$(\sigma_x - \sigma_y)^2 + (\sigma_y - \sigma_z)^2 + (\sigma_z - \sigma_x)^2 = 2\sigma_s^2.$$

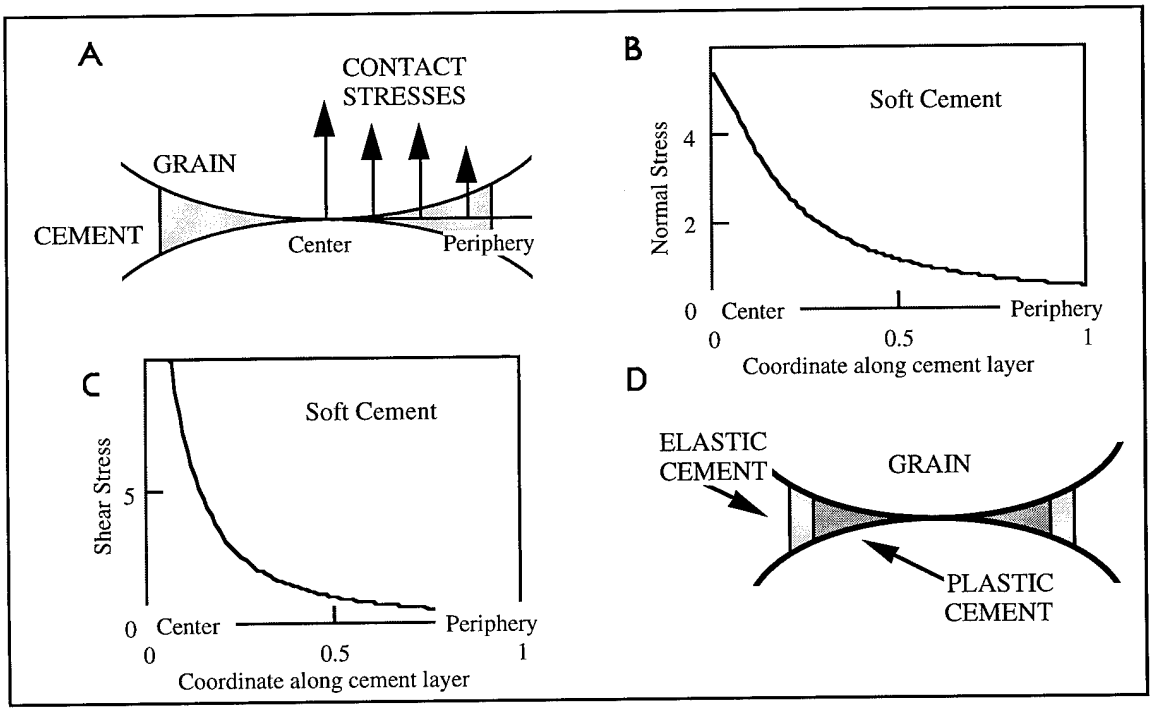

Figure 3. a. Contact stresses between two cemented grains. b. Normal stresses between two cemented grains with soft cement. c. Shear stresses between two cemented grains with soft cement. d. Cement layer with a plastic central kernel surrounded by elastic cement. Stresses are normalized by the average stress. Coordinate is normalized by the radius of the cement layer.

3.2. Thin Cement Layer in Extension and Shear

Consider a thin cement layer (Figure 4a) whose width $2h$ may gently change along its length: $h''(x) << 1$. The $z = 0$ plane of the rectangular (x, y, z) coordinate system is parallel to the layer. The layer's walls have displacements $W(x)$ that are parallel to the z axis. We assume that as long as the layer deforms elastically, stresses can be estimated from the elastic foundation approximation (Dvorkin et al., 1991 and 1994):

$$\sigma_{xx} = \sigma_{yy} = \frac{2G_c \nu_c}{1-2\nu_c}\frac{W(x)}{h(x)}, \sigma_{zz} = \frac{2G_c(1-\nu_c)}{1-2\nu_c}\frac{W(x)}{h(x)}, \sigma_{ij(i\neq j)} = 0, \tag{3.4}$$

where G_c and ν_c are the shear modulus and the Poisson's ratio of the cement, respectively.

By substituting equation (3.4) into the criterion (3.3) we arrive at the following plasticity condition for a thin cement layer in extension (or compression):

$$\left|\frac{W(x_0)}{h(x_0)}\right| = \frac{\sigma_s}{2G_c}. \tag{3.5}$$

where x_0 is the coordinate at the elastic-plastic boundary. In equation (3.5) we neglect hardening and assume that the yield limit in compression is the same as in tension.

Consider now a plastic zone surrounded by two elastic zones (Figure 4c). Again we assume that the elastic foundation formulas (3.4) are valid in the elastic zone. By doing so we neglect the condition of incompressibility that will influence stresses at the elastic-plastic boundary. The equations of balance

$$\frac{\partial \sigma_{xx}}{\partial x} + \frac{\partial \sigma_{yx}}{\partial y} + \frac{\partial \sigma_{zx}}{\partial z} = 0, \frac{\partial \sigma_{xy}}{\partial x} + \frac{\partial \sigma_{yy}}{\partial y} + \frac{\partial \sigma_{zy}}{\partial z} = 0, \frac{\partial \sigma_{xz}}{\partial x} + \frac{\partial \sigma_{yz}}{\partial y} + \frac{\partial \sigma_{zz}}{\partial z} = 0$$

will be satisfied if we assume that all stresses are constant within the plastic zone. If the plastic zone is symmetrical with respect to its center, then on its boundaries AA and BB (Figure 4c) where condition (3.5) is met, stresses will be the same:

$$\sigma_{xx} = \sigma_{yy} = \frac{2G_c \nu_c}{1-2\nu_c}\frac{W(x)}{h(x)} = \frac{\sigma_s \nu_c}{1-2\nu_c},$$

$$\sigma_{zz} = \frac{2G_c(1-\nu_c)}{1-2\nu_c}\frac{W(x)}{h(x)} = \frac{\sigma_s(1-\nu_c)}{1-2\nu_c}; \sigma_{ij(i\neq j)} = 0.$$

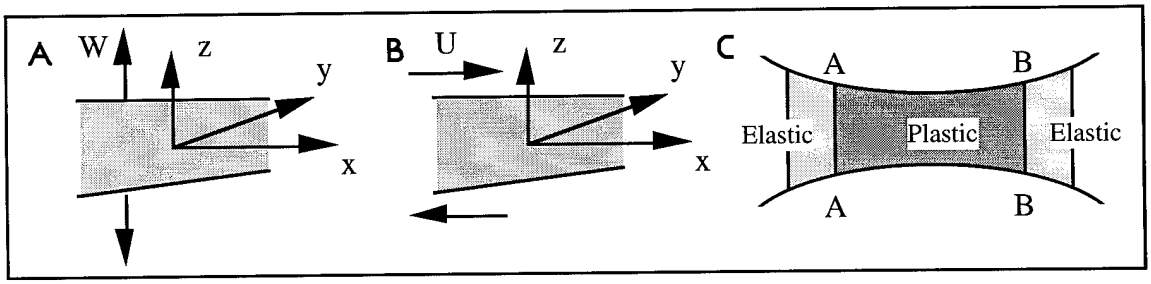

Figure 4. a. Thin cement layer in extension. b. Thin cement layer in shear. c. Thin cement layer -- plastic zone surrounded by elastic cement.

Therefore, within the plastic zone stresses are constant:

$$\sigma_{xx} = \sigma_{yy} = \frac{\sigma_s \nu_c}{1-2\nu_c},\ \sigma_{zz} = \frac{\sigma_s(1-\nu_c)}{1-2\nu_c};\ \sigma_{ij(i\neq j)} = 0. \tag{3.6}$$

Consider next a thin cement layer deforming in shear with tangential displacement $U(x)$ (Figure 4b). From the elastic foundation approximation we have the following stresses in the elastic part of the layer:

$$\sigma_{xz} = \frac{G_c U(x)}{h(x)}, \tag{3.7}$$

with all other stresses being zero. Now the von Mises criterion (3.3) yields the following plasticity condition:

$$\left|\frac{U(x_0)}{h(x_0)}\right| = \frac{\sigma_s}{\sqrt{3}G_c}. \tag{3.8}$$

Again, putting stresses in the plastic part of the layer constant, we find that within the plastic zone

$$\sigma_{xz} = \sigma_s / \sqrt{3}, \tag{3.9}$$

with all other stresses being zero.

3.3. Thin Cement Layer: Combined Extension and Shear

If the layer deforms simultaneously in extension and shear, the elastic foundation approximation gives the following stresses within the elastic part:

$$\sigma_{xx} = \sigma_{yy} = \frac{2G_c\nu_c}{1-2\nu_c}\frac{W(x)}{h(x)},\ \sigma_{zz} = \frac{2G_c(1-\nu_c)}{1-2\nu_c}\frac{W(x)}{h(x)},\ \sigma_{xz} = \frac{G_c U(x)}{h(x)}, \tag{3.10}$$

with all other stresses being zero. From equations (3.10) and (3.3) the plasticity condition follows as

$$4\left[\frac{W(x_0)}{h(x_0)}\right]^2 + 3\left[\frac{U(x_0)}{h(x_0)}\right]^2 = \frac{\sigma_s^{\,2}}{G_c^{\,2}}, \tag{3.11}$$

and the stresses within the plastic zone are

$$\sigma_{xx} = \sigma_{yy} = \frac{2G_c\nu_c}{1-2\nu_c}\frac{W(x_0)}{h(x_0)},\ \sigma_{zz} = \frac{2G_c(1-\nu_c)}{1-2\nu_c}\frac{W(x_0)}{h(x_0)},\ \sigma_{xz} = \frac{G_c U(x_0)}{h(x_0)}. \tag{3.12}$$

It is clear that if stresses are axisymmetrical then a plasticity kernel surrounded by the elastic material will be axisymmetrical as well. In this case we can use the radial coordinate r instead of x in equations (3.5), (3.6), (3.8), (3.9), (3.11), and (3.12).

4.0. TWO CEMENTED SPHERES

4.1. Assumptions

Consider two identical elastic spheres (grains) cemented at their contact. The cement layer is much thinner than the sphere radius. The configuration is axisymmetrical with respect to the line connecting the centers of the spheres. The spheres are subjected to normal and tangential displacements with respect to the contact point (Figure 5a). The cement may deform in both elastic and plastic modes (Figure 5b).

We assume that shear stresses that are imposed on the grain surfaces due to the tangential displacements of the spheres, and also produced by the normal displacements do not affect normal stresses on the grain surfaces. Also, normal stresses that are imposed on the grain surfaces due to the normal displacements of the spheres, and produced by the shear displacements do not affect shear stresses on the grain surfaces. A similar assumption is inherently contained in the elastic foundation model that we use for the cement layer. As far as the grains are concerned, the assumption can be supported by some contact mechanics solutions, e.g., a rigid punch on an elastic half-space (Johnson, 1985).

In addition we assume that all stresses are axisymmetrical with respect to the line connecting the centers of the spheres. Dvorkin et al. (1994) show that this assumption is accurate.

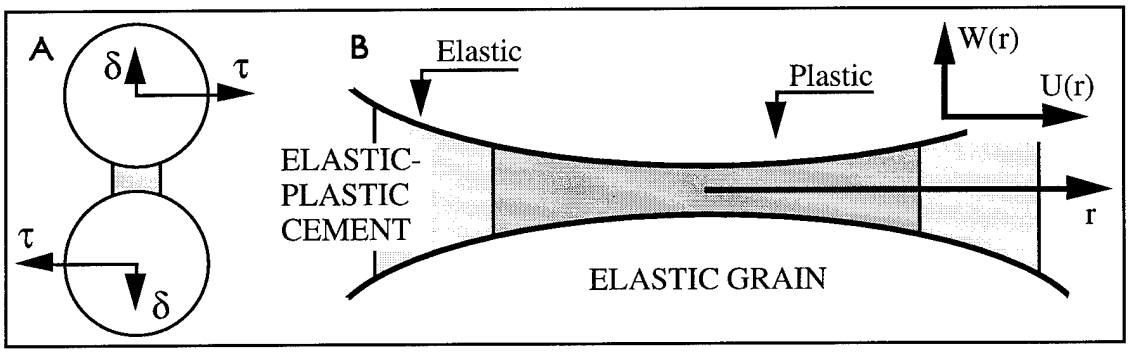

Figure 5. a. Two cemented elastic spheres subject to normal and tangential deformation. b. Thin cement layer between the spheres.

4.2. Stresses in Cement

The cement layer may have a plastic kernel and an elastic ring surrounding this kernel (Figure 5b). The normal $W(r)$ and the tangential $U(r)$ displacements of the surface of the cement layer are axisymmetrical (with respect to the line connecting the centers of the spheres, and depend on the radial coordinate r.

To relate $W(r)$ and $U(r)$ to the normal $p(r)$ and tangential $q(r)$ stresses acting on the grain surface in the cemented area, we use equations (3.10) and (3.12). In the elastic part of the cement we have

$$p(r) = -\frac{2G_c(1-\nu_c)}{1-2\nu_c}\frac{W(r)}{h(r)},\ q(r) = -\frac{G_c U(r)}{h(r)};\ h(r) = R[\varepsilon + \frac{1}{2}(\frac{r}{R})^2],\ \varepsilon = \frac{h(0)}{R}, \quad (4.1)$$

where ε is the minimum half-thickness of the cement layer. In the plastic region these stresses do not depend on the radial coordinate:

$$p(r) = -\frac{2G_c(1-\nu_c)}{1-2\nu_c}\frac{W(c)}{h(c)}, \; q(r) = -\frac{G_c U(c)}{h(c)}, \tag{4.2}$$

where c is the radius of the plastic region. This radius can be found from formula (3.11):

$$4\left[\frac{W(c)}{h(c)}\right]^2 + 3\left[\frac{U(c)}{h(c)}\right]^2 = \frac{\sigma_s^{\,2}}{G_c^{\,2}}. \tag{4.3}$$

4.3. Deformation of Grains and Cement

The normal displacement of the grain surface $w(r)$ and the tangential displacement of the grain surface $u(r)$ can be approximately related to the normal $p(r)$ and tangential $q(r)$ stresses as (Dvorkin et al., 1994)

$$\begin{aligned} w(r) &= \frac{1-\nu}{\pi G}\int_0^{\pi} d\varphi \int_0^{r\cos\varphi+\sqrt{b^2-r^2\sin^2\varphi}} p(\sqrt{r^2+s^2-2rs\cos\varphi})\,ds, \\ u(r) &= \frac{1}{\pi G}\int_0^{\pi} d\varphi \int_0^{r\cos\varphi+\sqrt{b^2-r^2\sin^2\varphi}} q(\sqrt{r^2+s^2-2rs\cos\varphi})(1-\nu\sin^2\varphi)\,ds, \end{aligned} \tag{4.4}$$

where G and ν are the grain shear modulus and Poisson's ratio, respectively. The integration is conducted inside the circle $r \le b$ (Figure 6), where b is the radius of the cement layer. Note that $w(r)$ and $u(r)$ are displacements relative to the sphere's center.

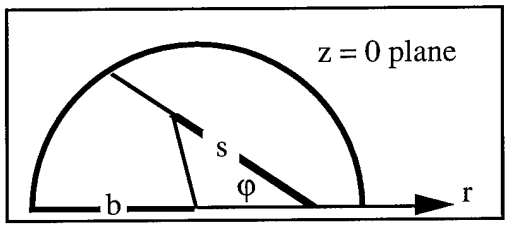

Figure 6. The region of cemented contact on the grain surface.

These displacements can be related to the displacements $W(r)$ and $U(r)$ of the surface of the cement layer as

$$w(r) = W(r) + \delta, \; u(r) = U(r) + \tau, \tag{4.5}$$

where δ and τ are the normal displacement and the tangential displacement, respectively, of the sphere's center relative to the contact point (Figure 5a).

4.4. Contact Stresses and Stiffnesses

By combining equations (4.1) - (4.5) we arrive at the following system of equations for the contact stresses $p(r)$ and $q(r)$:

$$\frac{\pi(1-2\nu_c)G}{2G_c(1-\nu_c)(1-\nu)}h(r)p(r)+\int_0^{\pi}d\varphi\int_0^{r\cos\varphi+\sqrt{b^2-r^2\sin^2\varphi}}p(\sqrt{r^2+s^2-2rs\cos\varphi})ds=$$

$$\frac{\pi G}{1-\nu}\delta \quad \text{at} \quad c<r\le b,$$

$$\frac{\pi G}{G_c}h(r)q(r)+\int_0^{\pi}d\varphi\int_0^{r\cos\varphi+\sqrt{b^2-r^2\sin^2\varphi}}q(\sqrt{r^2+s^2-2rs\cos\varphi})(1-\nu\sin^2\varphi)ds= \tag{4.6}$$

$$\pi G\tau \quad \text{at} \quad c<r\le b;$$

$$p(r)=p(c),\ q(r)=q(c) \text{ at } 0\le r\le c;$$

$$\left[p(c)\frac{1-2\nu_c}{1-\nu_c}\right]^2+3q^2(c)=\sigma_s{}^2.$$

System (4.6) can be easily solved numerically using, for example, the quadrature method (Delves and Mohamed, 1985).

We define the normal (S_n) and the tangential (S_τ) contact stiffnesses of a two-grain combination as

$$S_n=F_n/\delta,\ S_\tau=F_\tau/\tau, \tag{4.7}$$

where F_n and F_τ are the resulting normal and tangential forces, respectively:

$$F_n=2\pi\int_0^b p(r)rdr,\ F_\tau=2\pi\int_0^b q(r)rdr.$$

4.5. Examples

We explore contact stress distribution between two quartz grains cemented by clay. The ratio of the cement radius to the grain radius, b/R, is 0.7. The separation distance between the grains at their contact, ε, is zero. The elastic constants are chosen as follows: G = 45 GPa, ν = 0.064, G_c = 1.98 GPa, ν_c = 0.29 (Yin, 1993). The yield limit of the cement, σ_s,was chosen at 450 MPa, following the failure experiments by Jizba (1991) on high-clay-content sandstones.

In Figure 7 we present normal stresses along the radius of the cement layer at varying normal force F_n. As this force increases, the plastic kernel starts developing at the center of the contact. In this kernel normal stresses are constant as given by formula (3.6). Outside the plastic kernel normal stresses gradually decrease towards the periphery of the cement layer.

Similar shapes are obtained for tangential contact stresses at varying tangential force F_τ (Figure 8). In this case tangential stresses in the plastic kernel are constant as given by formula (3.9). The decrease of the tangential stresses towards the periphery of the cement layer is steeper than that of the normal stresses.

Next we explore the effect of grain separation, $\varepsilon=h(0)/R$, on the contact stresses. We compare the case with no separation ($\varepsilon=0$) to the case where $\varepsilon=0.1$ (Figure 9).

Normal stress distribution appears to be more uniform in the case where the grains are separated as compared to the no-separation case.

By changing the b / R ratio, and the yield stress value, one can arrive at the results qualitatively identical to those presented in Figures 7 - 9.

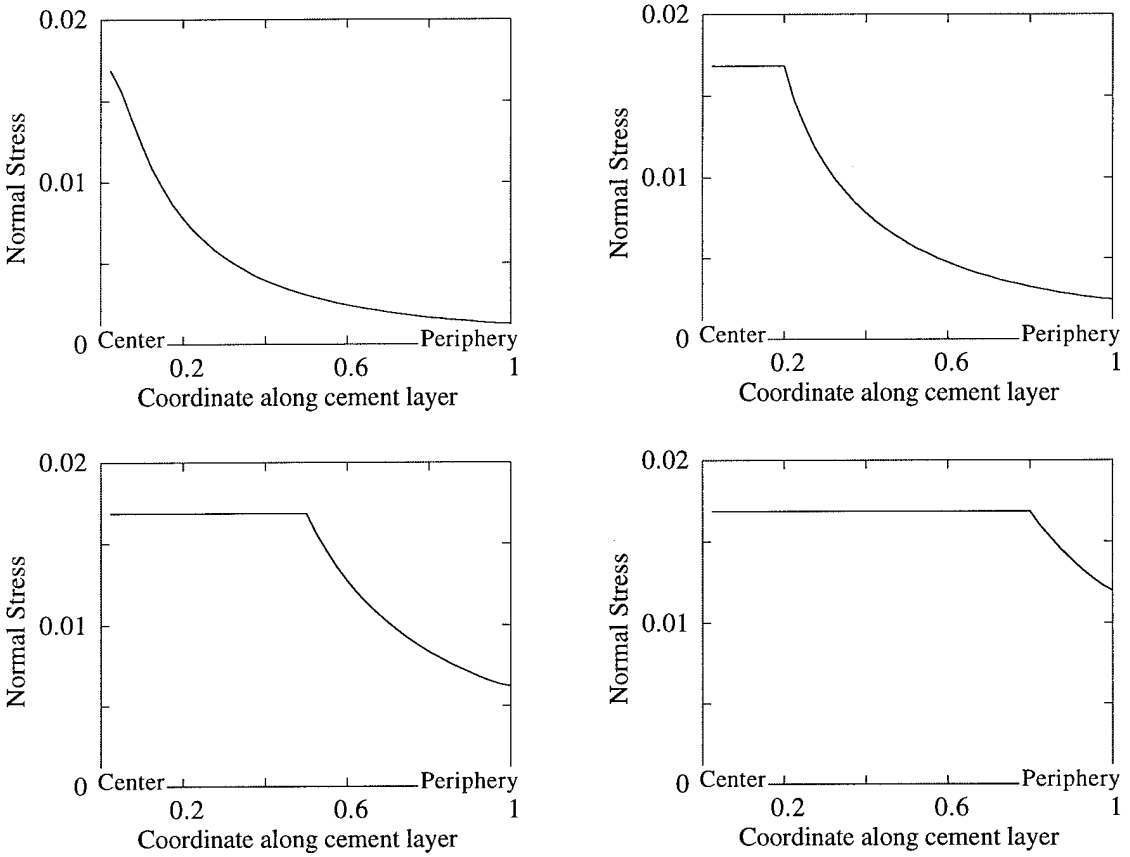

Figure 7. Normal stress distribution along a cement layer. The coordinate is normalized by the layer's radius. The stresses are normalized by the grain's shear modulus. The plastic kernel progresses with increasing load (left to right, top to bottom).

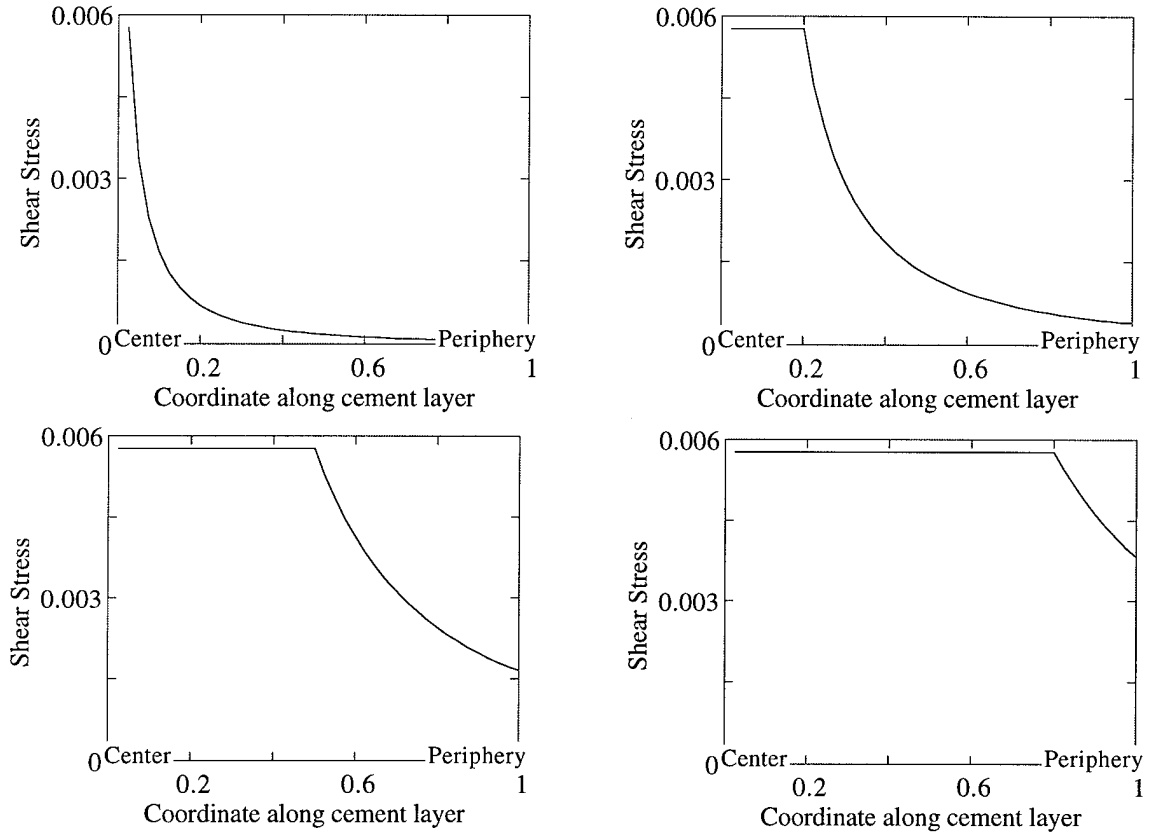

Figure 8. Tangential stress distribution along a cement layer. The coordinate is normalized by the layer's radius. The stresses are normalized by the grain's shear modulus. The plastic kernel progresses with increasing load (left to right, top to bottom).

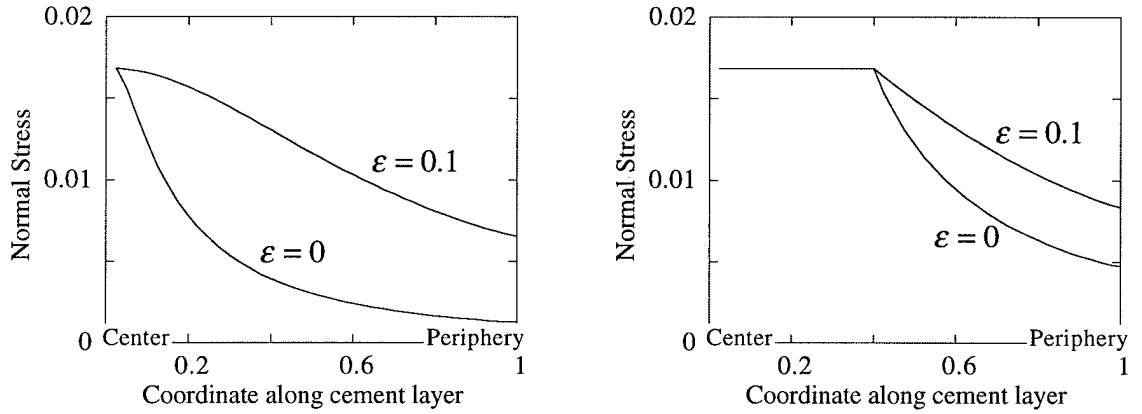

Figure 9. Normal stress distribution along a cement layer. Grains are separated ($\varepsilon = 1$) or have a point contact ($\varepsilon = 0$). The coordinate is normalized by the layer's radius. The stresses are normalized by the grain's shear modulus. The plastic kernel progresses with increasing load (left to right).

5.0. EFFECTIVE MODULI OF AN AGGREGATE

5.1. Assumptions and Definitions

Consider a random pack of identical elastic spheres of radius R cemented with elastic-plastic cement. The pack is statistically homogeneous and isotropic. The average number

n of contacts per sphere (coordination number) is about 9. The spheres occupy approximately 64 percent of the pack's volume which means that porosity of the pack (not counting cement) is about 0.36 (Bourbie et al., 1987). In our further derivations we follow the statistical scheme used by Walton (1987).

The i-th sphere's center has position vector $\vec{X}^{(i)}$ in the rectangular (1,2,3) coordinate system (Figure 10a). The displacement of the i-th center is $\vec{u}^{(i)}$. The unit vector $\vec{I}^{(nm)}$ that connects the center of the m-th sphere and the center of the n-th sphere (Figure 10b) is

$$\vec{I}^{(nm)} = \frac{\vec{X}^{(n)} - \vec{X}^{(m)}}{2R}. \tag{5.1}$$

We also assume that the displacements of the sphere centers are consistent with the applied uniform strain field e_{ij}:

$$u_i^{(n)} = e_{ij} X_j^{(n)}. \tag{5.2}$$

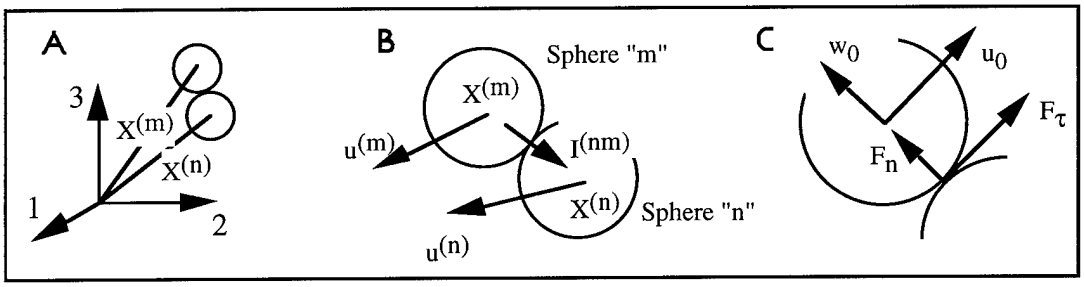

Figure 10. Displacements and forces in a sphere pack.

5.2. Relative Deformation of Grains

The displacement vector of the m-th sphere's center relative to the contact point is

$$\frac{\vec{u}^{(m)} - \vec{u}^{(n)}}{2}$$

By decomposing this vector into the normal part $\vec{w}_0$, along $I^{(nm)}$, and into the tangential part $\vec{u}_0$, normal to $I^{(nm)}$, we find:

$$\vec{w}_0 = \vec{I}^{(nm)} \frac{(\vec{u}^{(m)} - \vec{u}^{(n)})\vec{I}^{(nm)}}{2}, \vec{u}_0 = \frac{\vec{u}^{(m)} - \vec{u}^{(n)}}{2} - \vec{I}^{(nm)} \frac{(\vec{u}^{(m)} - \vec{u}^{(n)})\vec{I}^{(nm)}}{2}. \tag{5.3}$$

Formulas (5.1) - (5.3) yield the following expressions for the absolute values and for the components of vectors $\vec{w}_0$ and $\vec{u}_0$:

$$w_0 = \delta = -Re_{pq} I_p^{(nm)} I_q^{(nm)}, u_0 = \tau = R\sqrt{\sum_{i=1}^{3} (e_{ip} I_p^{(nm)} - e_{pq} I_p^{(nm)} I_q^{(nm)} I_i^{(nm)})^2};$$
$$w_{0i} = -Re_{pq} I_p^{(nm)} I_q^{(nm)} I_i^{(nm)}, u_{0i} = -Re_{ip} I_p^{(nm)} + Re_{pq} I_p^{(nm)} I_q^{(nm)} I_i^{(nm)}. \tag{5.4}$$

5.3. Contact Forces

We define the normal contact stiffness S_n between two spheres as the ratio of the normal component of the contact force F_n to the normal displacement w_0 (Figure 10c). The tangential contact stiffness is defined similarly:

$$S_n = F_n / w_0, S_\tau = F_\tau / u_0. \tag{5.5}$$

Generally, each of these stiffnesses depends on both normal and tangential displacement.

It follows from formulas (5.4) and (5.5) that the components of the contact force vector in the $(1,2,3)$ coordinate system are

$$F_i^{(nm)} = S_n w_{0i} + S_\tau u_{0i} = -R[(S_n - S_\tau)e_{pq} I_p^{(nm)} I_q^{(nm)} I_i^{(nm)} + S_\tau e_{ip} I_p^{(nm)}]. \tag{5.6}$$

5.4. Macroscopic Stresses

We define average macroscopic stresses in volume V that is occupied by a sphere pack as

$$\langle \sigma_{ij} \rangle = \frac{1}{V} \int_V \sigma_{ij} dV.$$

Any average value is meant to be a volumetric average as in the latter equation. By means of the Gauss theorem this volume integral can be transformed into a surface integral as:

$$\langle \sigma_{ij} \rangle = \frac{1}{V} \int_V \sigma_{ij} dV = \frac{1}{2V} \int_S (x_i t_j + x_j t_i) dS,$$

where S is the surface of volume V, x_i are coordinates on the surface, and t_i are surface traction components.

Consider now volume V_n that contains the n-th sphere. By integrating the stress-tensor components $\sigma_{ij}^{(n)}$ inside this volume we find:

$$\int_{V_n} \sigma_{ij}^{(n)} dV_n = \frac{1}{2} \int_{S_n} (x_i t_j + x_j t_i) dS_n = \frac{1}{2} \int_{S_n} (x'_i t_j + x'_j t_i) dS_n, \tag{5.7}$$

where $\vec{x}' = \vec{x} - \vec{X}^{(n)}$. The last equity in equation (5.7) is due to the fact that surface tractions are self-equilibrating and thus their surface integral is zero. Tractions on the sphere's surface are contact forces that act at the contacts only. Therefore,

$$x'_i = (X_i^{(m)} - X_i^{(n)}) / 2 = -R I_i^{(nm)}, \tag{5.8}$$

as follows from equation (5.1). By substituting equation (5.8) into equation (5.7) we find that for one sphere

$$\int_{V_n} \sigma_{ij}^{(n)} dV_n = -R \sum_{\text{Contacts}} (I_i^{(nm)} F_j^{(nm)} + I_j^{(nm)} F_i^{(nm)}) / 2. \tag{5.9}$$

Therefore, average stress in the aggregate is

$$\langle \sigma_{ij} \rangle = -\frac{R}{V} \sum_{\text{All Contacts}} (I_i^{(nm)} F_j^{(nm)} + I_j^{(nm)} F_i^{(nm)}), \tag{5.10}$$

where the factor 1/2 from equation (5.9) disappears since the summation in equation (5.10) is through all spheres and all contacts on each sphere, and thus each contact is counted twice. Next we substitute equation (5.6) into equation (5.10) and find that average stress in the aggregate is

$$\langle \sigma_{ij} \rangle = -\frac{R^2}{V} \sum_{\text{All Contacts}} [2(S_n - S_\tau) e_{pq} I_p^{(nm)} I_q^{(nm)} I_i^{(nm)} I_j^{(nm)} + S_\tau (e_{jp} I_p^{(nm)} I_i^{(nm)} + e_{ip} I_p^{(nm)} I_j^{(nm)})]. \tag{5.11}$$

If the average number of contacts per sphere is n and the number of spheres is N, then the total number of contacts is $nN/2$. The volume occupied by N spheres is

$$\frac{4}{3} \frac{N\pi R^3}{1-\phi}$$

where ϕ is the porosity of the aggregate. Now, by introducing statistically average quantities, we can replace equation (5.11) with the following equation for the macroscopic stress tensor components:

$$\sigma_{ij} = \frac{3n(1-\phi)}{8\pi R} \{\langle 2[S_n(w_0,u_0) - S_\tau(w_0,u_0)] e_{pq} I_p I_q I_i I_j \rangle + \langle S_\tau(w_0,u_0)(e_{jp} I_p I_i + e_{ip} I_p I_j) \rangle\}; \tag{5.12}$$

$$w_0 = -R e_{pq} I_p I_q, \; u_0 = R \sqrt{\sum_{i=1}^{3} (e_{ip} I_p - e_{pq} I_p I_q I_i)^2}.$$

5.5. Averaging Technique

The expression that has to be averaged in equation (5.12) is a scalar function of a unit vector $\vec{I} = (I_1, I_2, I_3)$. Consider such a function $\Phi(\vec{I}) = \Phi(I_1, I_2, I_3)$ in a spherical coordinate system (r, θ, φ) (Figure 11a). In this coordinate system

$$I_1 = \sin\theta\cos\varphi, \; I_2 = \sin\theta\sin\varphi, \; I_3 = \cos\theta.$$

We assume that the position of the head of the vector $\vec{I}$ is uniformly distributed on the surface of a unit-radius sphere (Figure 11b). Then the average of function Φ is

$$\langle \Phi \rangle = \frac{1}{\Sigma} \int_{\Sigma} \Phi d\upsilon = \frac{1}{4\pi} \int_0^{2\pi} \int_0^{\pi} \Phi(I_1, I_2, I_3) \sin\theta d\varphi d\theta = \frac{1}{4\pi} \int_0^{2\pi} \int_0^{\pi} \Phi(\sin\theta\cos\varphi, \sin\theta\sin\varphi, \cos\theta) \sin\theta d\varphi d\theta, \tag{5.13}$$

where Σ is the surface of the unit sphere, and ϑ is an element of the surface (Figure 11b).

By using formula (5.13) we can find, for example, that

$$\langle I_i I_j \rangle = \frac{1}{3}\delta_{ij}, \langle I_1^2 I_2^2 \rangle = \frac{1}{15}. \tag{5.14}$$

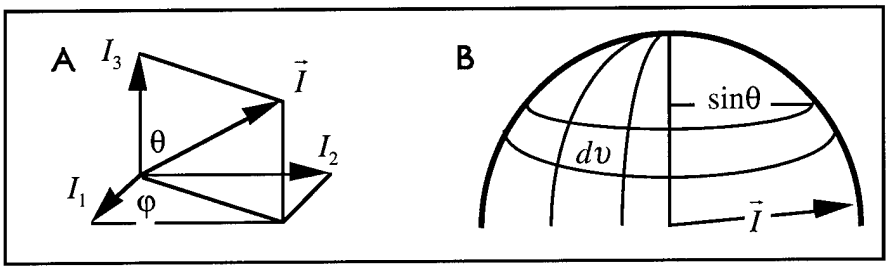

Figure 11. Spherical coordinate system for averaging a function of a unit vector.

5.6. Constant Contact Stiffnesses

In this section we derive the effective elastic constants of an aggregate where cement is purely elastic and thus contact stiffnesses S_n and S_τ are stress-independent (Dvorkin et al., 1994). In this case formula (5.12) can be written as

$$\sigma_{ij} = \frac{3n(1-\phi)}{8\pi R}[2(S_n - S_\tau)\langle e_{pq} I_p I_q I_i I_j \rangle + S_\tau(\langle e_{jp} I_p I_i \rangle + \langle e_{ip} I_p I_j \rangle)]. \tag{5.15}$$

Consider a hydrostatic stress field where strain-tensor components are given by $e_{ij} = e\delta_{ij}$. Then formulas (5.14) and (5.15) yield

$$\sigma_{11} = \frac{3n(1-\phi)}{4\pi R} S_n e \langle I_1^2 \rangle = \frac{n(1-\phi)e}{4\pi R} S_n,$$

Thus the effective bulk modulus is

$$K_{eff} = \frac{n(1-\phi)S_n}{12\pi R}. \tag{5.16}$$

Consider now a pure shear field where $e_{12} = e_{21} = \tau$, and all other strain-tensor components are zero. Formula (5.15) now yields

$$\sigma_{12} = \frac{3n(1-\phi)}{8\pi R}[4(S_n - S_\tau)\tau\langle I_1^2 I_2^2 \rangle + S_\tau \tau \langle I_1^2 + I_2^2 \rangle] = e_{12}\frac{n(1-\phi)}{10\pi R}(S_n + \frac{3}{2}S_\tau).$$

Thus the effective shear modulus is

$$G_{eff} = \frac{n(1-\phi)}{20\pi R}(S_n + \frac{3}{2}S_\tau). \tag{5.17}$$

Formulas (5.16) and (5.17) are consistent with those given by Winkler (1983).

6.0. EXAMPLES OF AGGREGATE DEFORMATION

6.1. Hydrostatic Compression

Consider a random pack of identical elastic spheres cemented at their contacts. The cement is initially elastic but becomes plastic as contact loads increase. Consider hydrostatic compression where strain-tensor components are given as $e_{ij} = -e\delta_{ij}$. Equation (5.12) gives in this case:

$$w_0 = \delta = Re, u_0 = \tau = 0, \sigma_{ij} = -\frac{n(1-\phi)e}{4\pi R} S_n(Re,0)\delta_{ij}.$$

Therefore, it follows from equations (5.12) and (4.6) that

$$\frac{\sigma_{11}}{G} = -\frac{n(1-\phi)e}{2}\bar{S}_n, \quad \bar{S}_n = \frac{1}{\bar{\delta}}\int_0^{\beta} f(t)tdt, \tag{6.1}$$

and function $f(t)$ can be found from equation

$$\Lambda_n(\varepsilon + \frac{t^2}{2})f(t) + \int_0^{\pi} d\varphi \int_0^{t\cos\varphi + \sqrt{\beta^2 - t^2\sin^2\varphi}} f(\sqrt{t^2 + \xi^2 - 2t\xi\cos\varphi})d\xi = \lambda_n\bar{\delta}, \quad \chi < t \le \beta; \tag{6.2}$$

$$f(t) = f(\chi), \quad 0 \le t \le \chi.$$

where χ is found from equation

$$f(\chi)\frac{1-2\nu_c}{1-\nu_c} = \frac{\sigma_s}{G}. \tag{6.3}$$

The notations in equations (6.1) - (6.3) are:

$$\Lambda_n = \frac{\pi(1-2\nu_c)G}{2(1-\nu_c)(1-\nu)G_c}, \lambda_n = \frac{\pi}{1-\nu}, \beta = \frac{b}{R}, \chi = \frac{c}{R}, \bar{\delta} = \frac{\delta}{R},$$

$$f(t) = \frac{p(Rt)}{G}, t = \frac{r}{R}, \xi = \frac{s}{R}, \bar{S}_n = \frac{S_n}{2\pi RG}.$$

We use equation (6.1) to calculate the hydrostatic deformation of a random pack of identical cemented spheres with elastic and plastic parameters as in the example in Section 4.5. Again, we explore the effect of grain separation, $\varepsilon = h(0)/R$, on the stress-strain laws (Figure 12a).

Separation of grains with $\varepsilon = 0.1$ results, as could be expected, in smaller macroscopic stresses at given strain, as compared to the no-separation case $\varepsilon = 0$. The elasticity region in the stress-strain plane is larger for $\varepsilon = 0.1$ than for $\varepsilon = 0$. This is a result of reduced contact stress concentration at the center of contact in the former case (Figure 9).

The effective bulk modulus is constant in the elastic region and gradually decreases as the plastic kernel progresses from the center of the cement layer (Figure 12b). This modulus is small where the grains are separated as compared to the case of contacting grains.

6.2. Uniaxial-Strain Compression

Consider a uniaxial-strain compression of a random sphere pack with $e_{33} = -e$ and all other strain-tensor components vanishing. Equations (5.12) and (4.6) give in this case (using the averaging technique described in Section 5.6):

$$\frac{\sigma_{11}}{G} = \frac{\sigma_{22}}{G} = -\frac{3n(1-\phi)e}{4} \times$$
$$\int_0^{\pi/2} [\bar{S}_n(e\cos^2\theta, e\cos\theta\sin\theta) - \bar{S}_\tau(e\cos^2\theta, e\cos\theta\sin\theta)]\cos^2\theta\sin^3\theta d\theta,$$

$$\frac{\sigma_{33}}{G} = -\frac{3n(1-\phi)e}{2} \times$$
$$\int_0^{\pi/2} [\bar{S}_n(e\cos^2\theta, e\cos\theta\sin\theta)\cos^2\theta + \bar{S}_\tau(e\cos^2\theta, e\cos\theta\sin\theta)\sin^2\theta]\cos^2\theta\sin\theta d\theta.$$

where

$$\bar{S}_n = \frac{1}{e\cos^2\theta}\int_0^\beta f(t)tdt, \bar{S}_\tau = \frac{1}{e\cos\theta\sin\theta}\int_0^\beta g(t)tdt.$$

Functions $f(t)$ and $g(t)$ are found from equations

$$\Lambda_n(\varepsilon + \frac{t^2}{2})f(t) + \int_0^\pi d\varphi \int_0^{t\cos\varphi+\sqrt{\beta^2-t^2\sin^2\varphi}} f(\sqrt{t^2+\xi^2-2t\xi\cos\varphi})d\xi = \lambda_n e\cos^2\theta,$$
$$\chi < t \le \beta;$$

$$\Lambda_\tau(\varepsilon + \frac{t^2}{2})g(t) + \int_0^\pi d\varphi \int_0^{t\cos\varphi+\sqrt{\beta^2-t^2\sin^2\varphi}} g(\sqrt{t^2+\xi^2-2t\xi\cos\varphi})(1-\nu\sin^2\varphi)d\xi =$$
$$\lambda_\tau e\cos\theta\sin\theta, \quad \chi < t \le \beta;$$

$$f(t) = f(\chi), \quad g(t) = g(\chi), \quad 0 \le t \le \chi.$$

The value of χ is found from equation

$$f^2(\chi)(\frac{1-2\nu_c}{1-\nu_c})^2 + 3g^2(\chi) = (\frac{\sigma_s}{G})^2.$$

We use the above equations to calculate macroscopic stresses in a random pack of identical cemented spheres from the previous example. The grains are in direct contact. The axial and radial stresses are plotted versus the axial strain in Figure 13. The plastic deformation region is clearly visible in the σ_{33} versus strain curve. However the σ_{11} versus strain curve is practically straight, apparently due to smaller stresses acting in the radial direction.

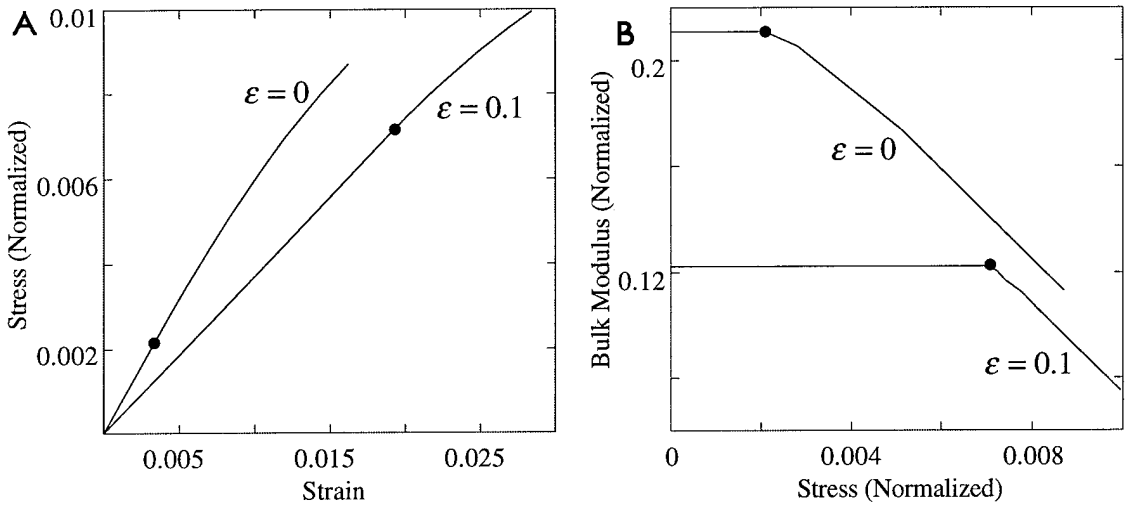

Figure 12. Hydrostatic compression of a random pack of cemented elastic grains. Grains are in direct contact ($\varepsilon = 0$) or are separated ($\varepsilon = 0.1$). a. Stress-strain curves. b. Effective bulk modulus. Dots indicate the boundary of the elastic deformation region.

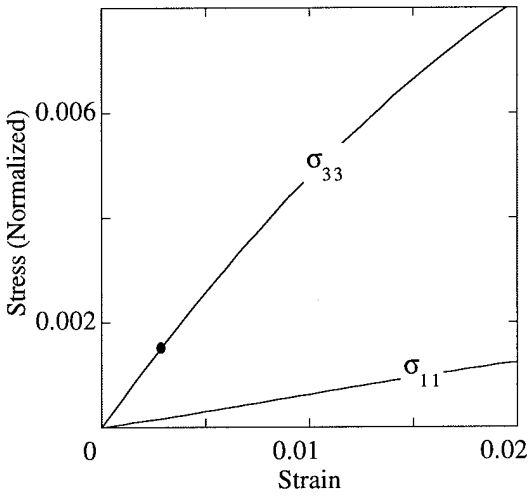

Figure 13. Uniaxial-strain compression of a random pack of cemented elastic grains. Grains are in direct contact. The axial and radial stresses are plotted versus the axial strain. The dot indicates the boundary of the elastic deformation region.

6.3. Complex State of Stress, Real Geomaterials

Formula (5.12) gives a straightforward expression for macroscopic stresses if the boundary conditions are formulated in strains, such as in the above examples of hydrostatic compression and uniaxial-strain compression. The situation becomes more complicated if the boundary condition is formulated partly in stresses as, for example, in a uniaxial-stress compression experiment. In this case the lateral stress, σ_{Lateral}, is constant. A scheme of solving such a problem is as follows. Use equation (5.12) with $e_{33} = -e_3$, $e_{11} = e_{22} = e_1$, and all other strain-tensor components vanishing. By computing σ_{11} select e_1 (at fixed e_3) such that $\sigma_{11} = \sigma_{\text{Lateral}}$. The axial stress computed at the determined e_{11} and e_{33} is the desired $\sigma_{33}(e_{33})$.

Expressions (4.7) for the normal and tangential contact stiffnesses of a two-grain combination can be directly plugged into a numerical discrete element scheme to calculate the effective macroscopic laws in realistic geomaterials under a complex state of stress (e.g., Trent and Margolin, 1992).

Certain confidence in the appropriateness of our micromechanical model for an elastic-plastic deformation of cemented grains follows from the fact that the solution produces stress-strain laws similar to those experimentally obtained in ductile rocks (Figure 1).

6.4. Stress-Induced Anisotropy

Due to cement's plastic deformation, normal and tangential contact stiffnesses are stress-dependent. This effect may lead to stress-induced anisotropy in an otherwise isotropic aggregate. Consider two experiments performed on the same sample: hydrostatic compression, and uniaxial-strain compression. In the first experiment the effective bulk modulus can be calculated from the stress-strain curve as

$$K_{\text{Hydrostatic}} = \frac{d\sigma_{11}}{3de_{11}} = \frac{d\sigma_{22}}{3de_{22}} = \frac{d\sigma_{33}}{3de_{33}}. \tag{6.4}$$

If we assume that the aggregate is isotropic in the second experiment, then the effective bulk modulus is:

$$K_{\text{Uniaxial}} = \frac{d(\sigma_{33} + 2\sigma_{11})}{3de_{33}}. \tag{6.5}$$

By comparing the "hydrostatic" stress from the uniaxial-compression experiment, $\sigma_{33} + 2\sigma_{11}$, with the true hydrostatic stress, σ_{11}, from the hydrostatic-compression experiment (Figure 14a) we see that the uniaxial-compression "hydrostatic" stress is larger. The results of calculating the effective moduli as given by formulas (6.4) and (6.5) show that the uniaxial bulk modulus is larger than the "true" hydrostatic-compression bulk modulus (Figure 14b). At high strain this difference may become as large as 10 percent. This observed disparity is an indication of stress-induced anisotropy in the uniaxial-compression experiment.

7.0. CONCLUSION

A theoretical solution is given to the problems of normal and tangential elastic-plastic deformation of two cemented elastic grains. Cement serves as an elastic-plastic element. As resulting forces between two grains increase, stress concentration develops in the center of the cement layer. Then a plastic kernel develops as local stresses meet a plasticity condition. This plasticity condition for a thin elastic-plastic cement layer is derived from the von Mises criterion. The plastic kernel in the cement layer is surrounded by an elastic ring where stresses and strains are linked through the elastic foundation model. The solution is reduced to ordinary integral equations. It gives normal and tangential stiffnesses of a two-grain combination for large microscopic strains.

This microscopic model is used to obtain macroscopic stress-strain laws in elastic-plastic packs of identical cemented spheres. To do so we statistically derive effective stress-strain laws for an aggregate of cemented spheres where grain-to-grain contact stiffnesses are strain-dependent.

Theoretical stress-strain laws thus obtained are close to the relations typically observed in clay-cemented sands. Therefore, our microscopic model can be used to realistically model large-strain deformation of cemented geomaterials.

An important result is stress-induced anisotropy in initially isotropic aggregates. Such an aggregate may become anisotropic if the stress field is non-hydrostatic. This stress-induced anisotropy may lead to an up to 10-percent error in estimating, for example, an apparent isotropic bulk modulus from a uniaxial-strain experiment.

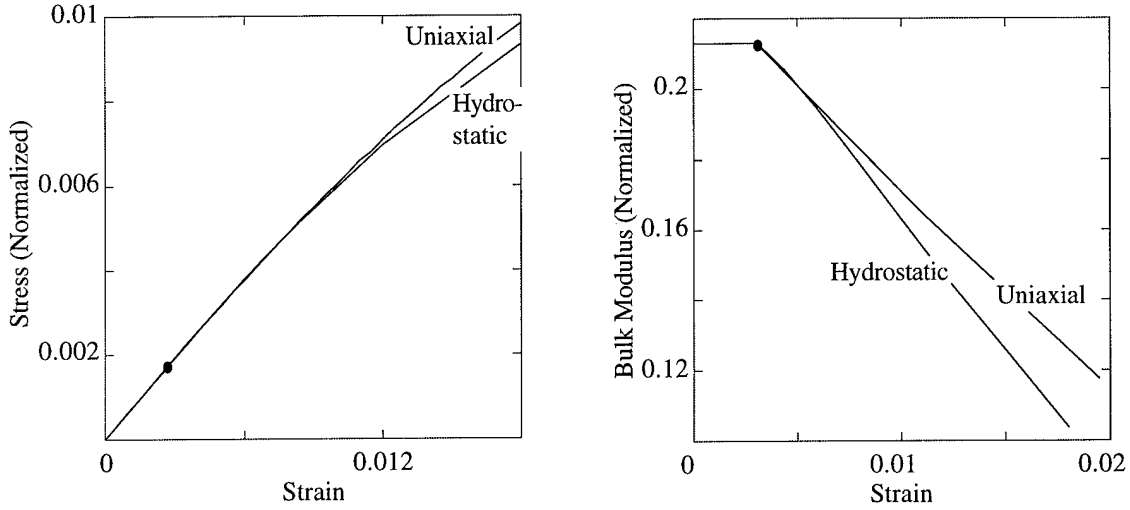

Figure 14. Stress-induced anisotropy in a random pack of identical cemented spheres. a. "Hydrostatic" stress versus strain from the uniaxial compaction and the hydrostatic compaction experiments. b. Bulk moduli from the uniaxial compaction and the hydrostatic compaction experiments. The dots indicate the boundary of the elastic deformation region.

9.0. REFERENCES

Bourbie, T., Coussy, O., and Zinszner, B., 1987, Acoustics of Porous Media, Gulf Publishing Company.

Delves, L.M. and Mohamed, J.L., 1985, Computational Methods for Integral equations, Cambridge University Press.

Digby, P.J., 1981, The effective elastic moduli of porous granular rocks, J. Appl. Mech., 48, 803-808.

Dvorkin, J., Mavko, G. and Nur, A., 1991, The effect of cementation on the elastic properties of granular material, Mechanics of Materials, 12, 207-217.

Dvorkin, J., Nur, A. and Yin, H., 1994, Effective properties of cemented granular material, Mechanics of Materials, 18, 351-366.

Hertz, H., 1882, Uber die Beruhrung fester elastisher Korper (On the contact of elastic solids), J. reine und angewandte Mathematik, 92, 156-171.

Hilbert, L.B., Jr., Hwong, T.K., Cook, N.G.W., Nihei, K.T., and Myer, L.R., 1994, Effects of strain amplitude on the static and dynamic nonlinear deformation of Berea sandstone, in Rock Mechanics, Nelson and Laubach (eds.), Balkema, 497-504.

Jizba, D.L., 1991, Mechanical and Acoustical Properties of Sandstones and Shales, Ph.D. thesis, Stanford University.

Johnson, K.L., 1985, Contact Mechanics, Cambridge University Press.

Kachanov, L.M., 1971, Foundations of the Theory of Plasticity, North-Holland.

Mindlin, R.D., 1949, Compliance of elastic bodies in contact, Trans. ASME, 71, A-259.

Trent, B.C. and Margolin, L.G., 1992, A numerical laboratory for granular solids, Eng. Comp., 9, 191 - 197.

Walton, K., 1978, The oblique compression of two elastic spheres, J. Mech. Phys. Solids, 26, 139-150.

Walton, K., 1987, The effective elastic moduli of a random packing of spheres, J. Mech, Phys. Solids, 35, 213-226.

Winkler, K.W., 1983, Contact stiffness in granular porous materials: comparison between theory and experiment, Geophys. Res. Let., 10, 1073 - 1076.

Yin, H., 1993, Acoustic Velocity and Attenuation of Rocks: Isotropy, Intrinsic Anisotropy, and Stress Induced Anisotropy, Ph.D. thesis, Stanford University.

Yin, H., and Dvorkin, J., 1994, Strength of cemented grains, Geophysical Research Letters, 21, 903-906.

2.8. PRESSURE SENSITIVITY OF CEMENTED GRANULAR MATERIALS

ABSTRACT

In this paper, we explore the mechanical contact interaction of two identical elastic spheres uniformly coated with thin layers of a different elastic material. These two coating layers intersect over a finite contact area thus bonding the spheres. The normal contact stiffness and the shear contact stiffness increase when the spheres are axially pressed together, due to the increasing contact area. We calculate the dependence of these stiffnesses on the axial load by using a new approximate analytical solution. The solution also gives the distributions of the normal and shear stress components on the cemented contact. We use this solution to calculate the pressure dependence of the effective elastic moduli of a random pack of identical cemented spheres. This pressure dependence may be large if the initial contact radius is small. It is insignificant for large contact radii. If the spheres are in direct contact and the initial contact radius is small, the elastic properties of the cement have little effect on the pack's elastic moduli. However, if the spheres are separated by even a small cemented gap, the elastic properties of the cement may have a considerable effect on the pack's elastic moduli.

1. INTRODUCTION

The mechanical properties of brittle granular materials are strongly affected by local intergranular effects, such as the geometrical nonlinearity due to pressure dependence of the contact area. These nonlinear effects prevail even if the material consists of linearly elastic grains. Granular materials are often modeled as a pack of linearly elastic spheres, and the fundamental problem of the contact between two elastic spheres has been the focus of many studies for over a century. Notable are the solutions of stress distribution and contact force-displacement relations for the problems of a relative axial displacement (Hertz, 1882); a relative tangential displacement (Mindlin, 1949); and a relative oblique displacement between two elastic spheres (Walton, 1978). Digby (1981) gives a solution of the contact problem for two elastic spheres initially bonded over a finite area.

A problem that is relevant to geologic granular materials is the contact between two elastic spheres cemented by a different elastic material. Dvorkin et al. (1991) showed that the cement layer may be approximately treated as an elastic foundation, and used this result to solve for the stress distribution and contact force-displacement relations for cemented grains (Dvorkin et al., 1994). These solutions did not account for any geometrical nonlinearity because the area of a cemented contact was constant and independent of pressure.

Once a two-sphere contact problem is solved, the effective elastic constants of a dense random pack of identical spheres can be related to the average number of contacts per sphere, the pack's porosity, and the normal and tangential contact stiffnesses (e.g., Digby, 1981; Walton, 1987). These relations are based on a statistical approach assuming that no relative roll or torsion occurs between any pair of spheres in contact, and that the displacements of the sphere centers are consistent with the uniform displacement field applied to the pack.

In this paper we give an approximate analytical pressure-dependent solution for the contact problem of two cemented spheres. Specifically, we assume that the spheres are uniformly coated with elastic cement layers (different from the sphere material), which intersect over a finite contact area thus bonding the spheres. As the spheres are axially pressed together, the contact area increases resulting in increasing normal and shear

stiffnesses. We use this solution to calculate the pressure dependence of the effective elastic moduli of a cemented pack.

The solution shows that this pressure dependence may be large if the contact radius is small and becomes insignificant for large contact radii. If the spheres are in direct contact and the contact radius is small, the elastic constants of the pack are hardly affected by the elastic properties of the cement. In this case Digby's (1981) solution can be used as a close approximation. However, if two contacting spheres are separated by soft cement, its properties strongly affect the elastic constants of the pack.

2. TWO COATED SPHERES

2.1. Axial Loading

Consider two identical elastic spheres of radius R separated by a gap 2ε and uniformly coated by an elastic cement (Figure 1). The contact area is the circular cross-section of the cement coatings at the mid plane A-A. The radial coordinate originating at the center of the contact is r, and the initial radius of the contact area is $r=a$. When the spheres are axially pressed together the radius of the contact area increases to $r=b$. Due to this axial compaction, the relative displacement of the mid plain with respect to the sphere center is δ_z. The resulting displacement $u_z(r)$ of the surface of a sphere relative to its center is given by (Johnson, 1985):

$$u_z(r)=\frac{1-\nu}{2\pi\mu}\int_{t=0}^{t=b}dt\int_{\theta=0}^{\theta=2\pi}\frac{q_z(t)}{s(t,r)}td\theta, \tag{1}$$

where ν and μ are Poisson's ratio and the shear modulus of the elastic spheres, respectively; $q_z(r)$ is the normal axisymmetric contact traction on the surface of the spheres; and s is the distance between t and r (Figure 2):

$$s(t,r)=\sqrt{t^2+r^2-2tr\cos\theta}. \tag{2}$$

The angular integration in equation (1) can be solved analytically (Gradshteyn and Ryzhik, 1980):

$$u_z(r)=\frac{1-\nu}{\pi\mu}\int_{t=0}^{t=b}q_z(t)f^*(\frac{r}{t})dt, \tag{3}$$

where

$$f^*(x)=\begin{cases}2K(x), & x<1;\\ \frac{2}{x}K(\frac{1}{x}), & x>1;\end{cases} \tag{4}$$

and $K(k)$ is the complete elliptic integral of the first kind:

$$K(k)=\int_0^{\pi/2}\frac{d\theta}{\sqrt{1-k^2\sin^2\theta}}, \tag{5}$$

with the series representation

$$K(k)=\frac{\pi}{2}\{1+[\frac{1}{2}]^2k^2+[\frac{1\cdot 3}{2\cdot 4}]^2k^4+\ldots+[\frac{(2n-1)!!}{2^n n!}]^2k^{2n}+\ldots\}. \tag{6}$$

A different form of integral equation (3) appears in Johnson (1985). In Appendix we show that the form used here is computationally more efficient.

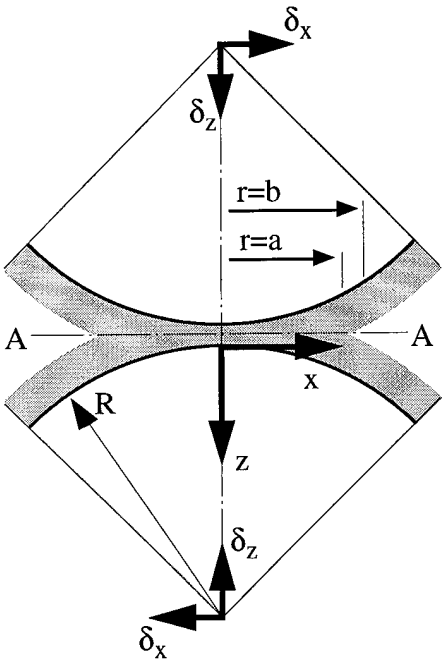

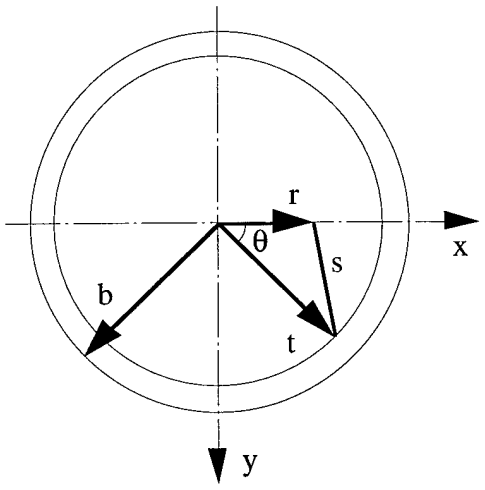

Figure 1 (left). The contact between two elastic spheres coated by elastic cement. Figure 2 (right). The coordinate system of the contact.

Dvorkin et al. (1991) show that the contact stress in the cement can be approximated by the elastic foundation model:

$$q_z(r)=-\frac{2\mu_c(1-\nu_c)}{1-2\nu_c}\frac{u_z(r)+g(r)-\delta_z}{h(r)-g(r)}, \tag{7}$$

where ν_c and μ_c are Poisson's ratio and the shear modulus of the elastic cement, respectively; $h(r)$ is half the distance between the surfaces of the spheres (without the coating); and $g(r)$ is half the distance between the external surfaces of the coated layers:

$$h(r)=\varepsilon+1-\sqrt{1-r^2}, \tag{8}$$

$$g(r)=\begin{cases}1+\varepsilon-\sqrt{(1+\varepsilon)^2+a^2-r^2}, & r>a;\\ 0 & r<a.\end{cases} \tag{9}$$

Notice that at $r=b$ we have

$$\delta_z = u_z(b) + g(b). \tag{10}$$

By substituting equations (7) and (10) into equation (3) we arrive at

$$u_z(r) = -\frac{\Lambda}{\pi}\int_{t=0}^{t=b} \frac{u_z(t) + g(t) - u_z(b) - g(b)}{h(t) - g(t)} f * (\frac{r}{t})dt, \tag{11}$$

where

$$\Lambda = \frac{2\mu_c(1-\nu_c)(1-\nu)}{\mu(1-2\nu_c)}. \tag{12}$$

We solve equation (11) for a given b to find $u_z(r)$. Then we use equations (7) and (10) to calculate the resultant contact force F_z and the contact normal stiffness D_z defined by:

$$F_z = \int_{r=0}^{r=b} q_z(r) 2\pi r dr, \tag{13}$$

$$D_z = \frac{dF_z}{d\delta_z}. \tag{14}$$

In this way we relate the contact stiffness and the new radius of contact to the applied axial force.

2.2. Tangential Loading

Let us now consider a small relative tangential displacement $2\delta_x$ (in the x direction) between the centers of the axially pressed spheres, such that there is no relative torsion or rolling between the spheres. In this case the normal and shear contact tractions can be treated independently, and therefore the tangential loading does not change the shape or size of the contact area. We also assume that the free surface of the cement is infinitely rough and that no slip occurs. Finally, we use approximations suggested by Dvorkin et al. (1994): (1) both the tangential displacement u_x of the surface of the sphere relative to the sphere's center, and the resulting tangential traction q_x are axisymmetric; and (2) the induced surface displacement and traction in the y direction are relatively small and may therefore be ignored. Note that for the special case of $\nu = \nu_c = 0$ these two assumptions are strictly correct.

Accordingly, the displacement u_x due to the stress q_x is given by (Johnson, 1985)

$$u_x(r) = \frac{1}{2\pi\mu}\int_{t=0}^{t=b} dt \int_{\theta=0}^{\theta=2\pi} \frac{q_x(t)}{s(t,r)}\{1 - \nu + \nu[\frac{r - t\cos\theta}{s(t,r)}]^2\} t d\theta, \tag{15}$$

where s is defined by equation (2).

The angular integration in equation (15) can be solved analytically (Gradshteyn and Ryzhik, 1980):

$$u_x(r) = \frac{1}{\pi\mu}\int_{t=0}^{t=b} q_x(t)[f^*(\frac{r}{t}) - \nu f^{**}(\frac{r}{t})]dt, \tag{16}$$

where f^* is given by equation (4),

$$f^{**}(x) = \begin{cases} \frac{2}{x^2}[K(x) - E(x)], & x < 1; \\ \frac{2}{x}[K(\frac{1}{x}) - E(\frac{1}{x})], & x > 1; \end{cases} \tag{17}$$

and $E(k)$ is the complete elliptic integral of the second kind,

$$E(k) = \int_0^{\pi/2} \sqrt{1 - k^2 \sin^2\theta}\, d\theta, \tag{18}$$

with the following series representation:

$$E(k) = \frac{\pi}{2}\{1 - \frac{1}{2^2}k^2 + \frac{1^2 \cdot 3}{2^2 \cdot 4^2}k^4 - \ldots - [\frac{(2n-1)!!}{2^n n!}]^2 \frac{k^{2n}}{2n-1} + \ldots\}. \tag{19}$$

From the elastic foundation approximation (Dvorkin et al., 1991) we find that the contact stress $q_x(r)$ is:

$$q_x(r) = -\mu_c \frac{u_x(r) - \delta_x}{h(r) - g(r)}, \tag{20}$$

where $h(r)$ and $g(r)$ are defined by equations (8) and (9).

By substituting formula (20) into equation (16) we arrive at

$$u_x(r) = -\frac{\mu_c}{\pi\mu}\int_{t=0}^{t=b} \frac{u_x(r) - \delta_x}{h(r) - g(r)}[f^*(\frac{r}{t}) - \nu f^{**}(\frac{r}{t})]dt. \tag{21}$$

Once integral equation (21) is solved, equation (20) is used to calculate the resultant contact force F_x and the contact tangential stiffness D_x defined by

$$F_x = \int_{r=0}^{r=b} q_x(r) 2\pi r dr, \tag{22}$$

$$D_x = \frac{dF_x}{d\delta_x}. \tag{23}$$

2.3. Numerical Procedure

In order to solve integral equations (11) and (21) we uniformly divide domain $0 \le r \le b$ into small intervals. Within each of these intervals $u_z(r)$ and $u_x(r)$ are

approximated by quadratic functions. The integration in every interval is carried out by a four-point Gauss-Legendre quadrature. The error $\|e\|_\ell$ in F_z and F_x is evaluated as a function of the interval size ℓ in the form

$$\|e\|_\ell = c\ell^\alpha, \tag{24}$$

where c and α are constants. For the example problems considered in this work, it was found that the order of convergence is $\alpha \approx 1.1$ regardless of high gradients in the solution.

3. EFFECTIVE MEDIUM MODEL

We use the solutions obtained in the previous section to calculate the pressure dependence of the wave velocities of a random pack of identical cemented spheres. We assume that the wavelength is sufficiently larger than the grain size, so that the material can be considered continuum.

The normal contact forces between the particles can be related to the macroscopic pressure applied to the aggregate (Digby, 1981):

$$p = \frac{C(1-\phi)}{4\pi R^2(1+\varepsilon/R)^2} F_z. \tag{25}$$

The effective bulk modulus (K_{eff}) and the effective shear modulus (μ_{eff}) can be presented as functions of the pack's porosity ϕ, the coordination number C (the average number of contacts per sphere), the radius R of a sphere, and the normal D_z and tangential D_x stiffnesses of a two-sphere combination (Digby, 1981). Then the compressional-wave velocity (V_p) and the shear-wave velocity (V_s) are

$$V_p^2 = \frac{C(1-\phi)}{4\pi R(1+\varepsilon/R)\rho}(D_z + \frac{2}{3}D_x), \tag{26}$$

$$V_s^2 = \frac{C(1-\phi)}{20\pi R(1+\varepsilon/R)\rho}(D_z + \frac{3}{2}D_x), \tag{27}$$

where ρ is the density of the aggregate, and D_z and D_x are given by (14) and (23).

It is important to mention that equations (25), (26) and (27) are based on the displacement affinity assumption, i.e., that the displacements of the sphere centers are consistent with the uniform displacement field applied to the pack.

4. EXAMPLES

Some limitations of our theoretical solution are related to the size of the initial contact radius. Specifically, if this radius is large the spheres may not be treated as elastic half spaces and the cement may not be treated as an elastic foundation. In addition we find from our solutions that for the case of large initial radii, yielding of the cement may be expected to occur before any noticeable pressure dependence can be observed. This is why in all presented examples the initial cemented contact radii are small with respect to the grain radius.

We use the above solutions to model the elastic wave velocities in cemented sand. To do so we assume that the grains are identical spheres arranged in a random dense pack with

porosity $\phi = 0.36$ and coordination number $C = 9$. There is experimental evidence that these assumptions are valid when estimating the effective elastic properties of well-sorted cemented sand (Jacoby et al., 1995; and Dvorkin and Nur, 1995).

We fix Poisson's ratio of the spheres and the cement at $\nu = \nu_c = 0.2$ and compute the wave velocities for the ratios μ / μ_c = 0.1, 1.0, and 10.0. To explore the effect of initial grain separation we consider two cases of the initial gap size: $\varepsilon / R = 0$ and $\varepsilon / R = 0.01$.

4.1. Contact Stresses

The distributions of normal contact stresses are given in Figure 3 for increasing (due to pressure) contact radii. In all cases the contact radius is initially $r / R = 0.05$, and it increases up to three times its initial value as the external pressure increases. When the cement is as stiff as the grain material, or stiffer, the stress distributions are nearly independent of the cement-to-grain stiffness ratio, or on the gap size (Figure 3b, c, e, and f). On the other hand, when the cement is significantly softer than the grain material (Figure 3a and d), stress distribution curves are different from those with the stiff cement. Also, a non-zero gap yields smaller normal contact stresses for the same contact radii.

The distributions of shear contact stresses are given in Figure 4 for increasing (due to pressure) contact radii. When the cement is as stiff as the grain material (Figure 4b and e), or stiffer (Figure 4c and f), shear stress concentrations are well pronounced at the circumference of the contact region. These stress concentrations resemble singularities at the edge of a rigid punch on an elastic half-space (Johnson, 1985). The gap acts to reduce these stress concentrations. In the soft cement case (Figure 4a and d) we observe stress concentrations at the center of the contact, similar to those observed by Dvorkin et al. (1994).

4.2. Pressure-Sensitivity of Velocities

If the cement and the grain materials are identical, our results (Figure 5a) are in close agreement with those of Digby (1981), as expected. It is apparent that if no gap exists between the grains, and the initial contact radius is small, the properties of the cement material have little effect on the elastic wave velocities in a cemented pack. In this case Digby's solution is a good approximation. In contrast, even a small gap between the grains may affect the velocities if the cement is relatively soft (Figure 5b). At the same time if the cement is stiff, its properties, as well as the gap size, hardly affect the velocities.

It is important to note that when the cement stiffness is equal to that of the grain, the results should be identical to those of Digby -- the gap size should not affect the velocities. However, there is a disparity between the results shown in Figure 5a and Figure 5b (solid lines). The error in the velocities (about 10%) may be attributed to the elastic foundation approximation.

APPENDIX

Integral equation (3) appears in Johnson (1985) in the alternative form

$$u_z(r) = \frac{2(1-\nu)}{\pi\mu} \int_{t=0}^{t=b} \frac{t}{t+r} q_z(t) K(k) dt, \qquad \text{(A1)}$$

where

$$k = \frac{4tr}{(t+r)^2}. \qquad \text{(A2)}$$

The difference between the two forms is that for any given r and t, the argument of K in (3) is always smaller than the argument of K in (A1). Consequently, for any given r and t, the evaluation of the integrand of equation (3) will converge faster and require less computation effort than the evaluation of the integrand of equation (A1). Since the integration in t is carried out numerically there is a clear advantage in using form (3) of the integral equation.

REFERENCES

Digby, P.J., 1981, The effective elastic moduli of porous granular rocks, J. Appl. Mech., 48, 803 - 808.

Dvorkin, J., G. Mavko and A. Nur, 1991, The effect of cementation on the elastic properties of granular material, Mechanics of Materials, 12, 207 - 217.

Dvorkin, J. and A. Nur, 1995, Elasticity of high-porosity sandstones: Theory for two North Sea datasets, Geophysics, in press.

Dvorkin, J., A. Nur and H. Yin, 1994, Effective properties of cemented granular materials, Mechanics of Materials, 18, 351 - 366.

Gradshteyn, I.S. and I.M. Ryzhik, 1980, Tables of Integrals, Series, and Products, Academic Press, San Diego, USA.

Hertz, H., 1882, Uber die Beruhrung fester elastisher Korper (On the contact of elastic solids), J. reine und angewandte Mathematik, 92, 156 - 171.

Jacoby, M., J. Dvorkin and X. Liu, 1995, Elasticity of partially saturated frozen sand, Geophysics, 61, 288-293.

Johnson, K.L., 1985, Contact Mechanics, Cambridge University Press, Cambridge, UK.

Mindlin, R.D., 1949, Compliance of elastic bodies in contact, Trans. ASME, 71, A-259.

Walton, K., 1978, The oblique compression of two elastic spheres, J. Mech. Phys. Solids, 26, 139-150.

Walton, K., 1987, The effective elastic moduli of a random packing of spheres, J. Mech. Phys. Solids, 35, 213-226.

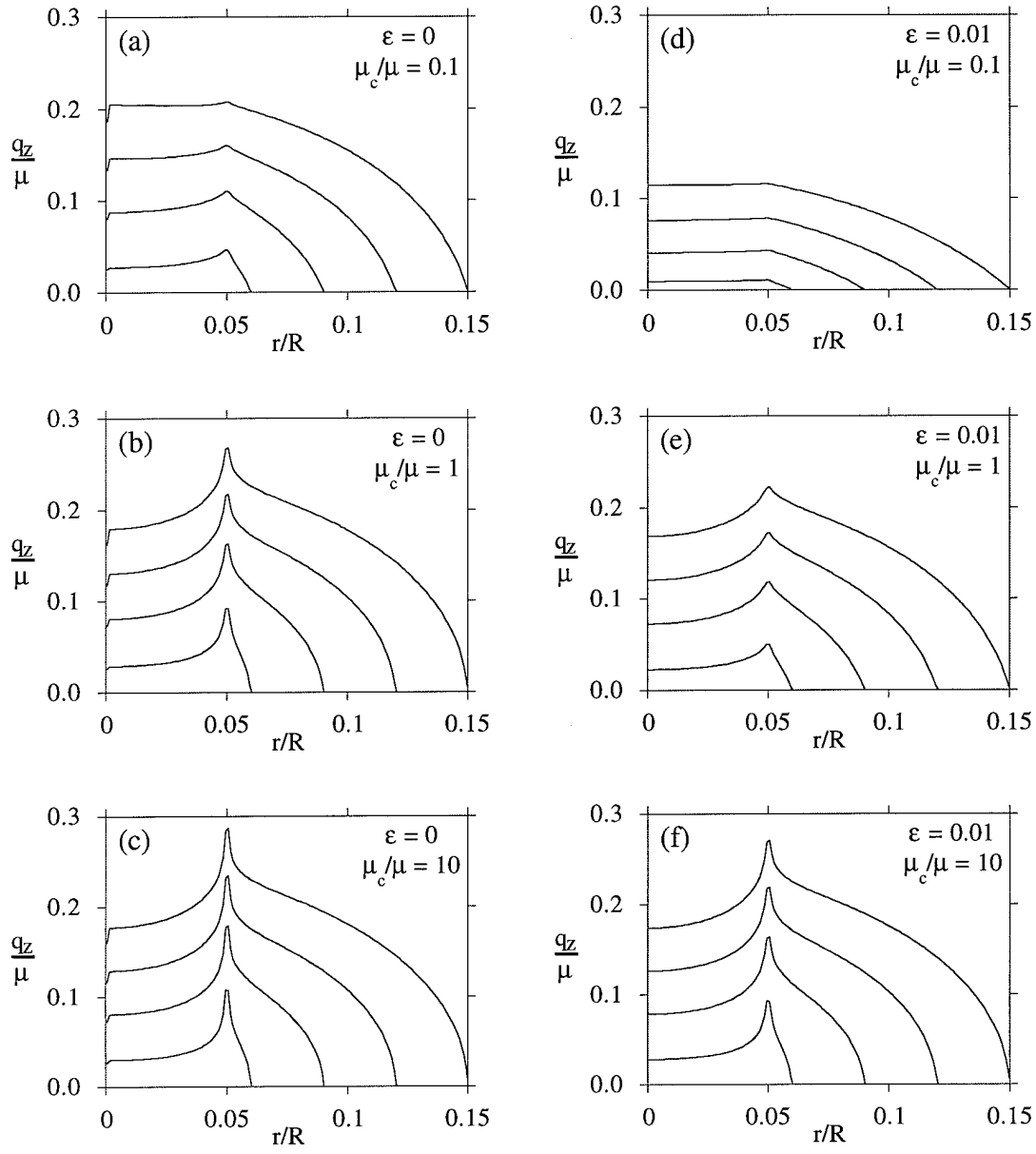

Figure 3. Normalized normal stress distribution in the cemented contact as a function of normalized distance from the contact center.

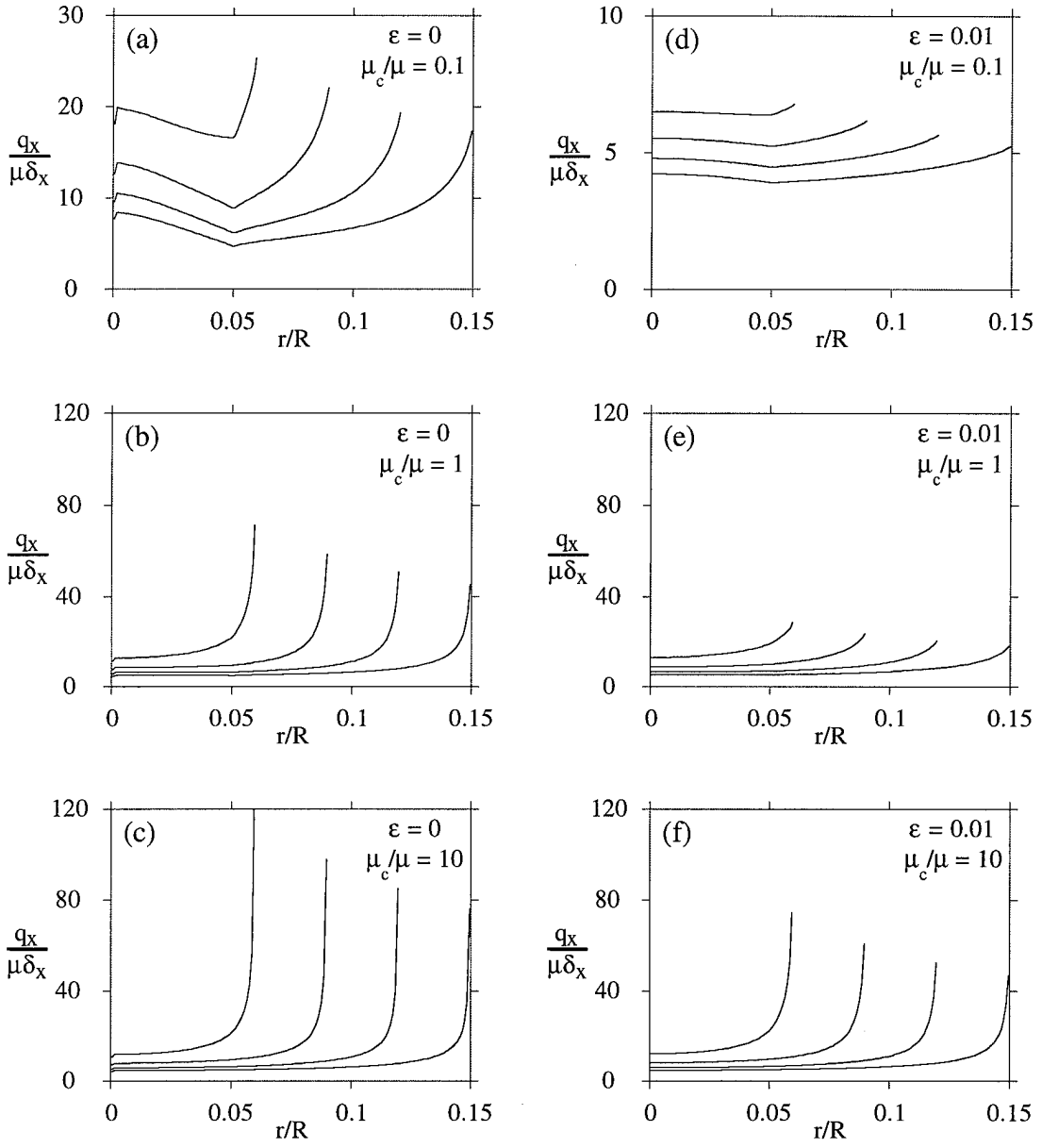

Figure 4. Normalized shear stress distribution in the cemented contact as a function of normalized distance from the contact center.

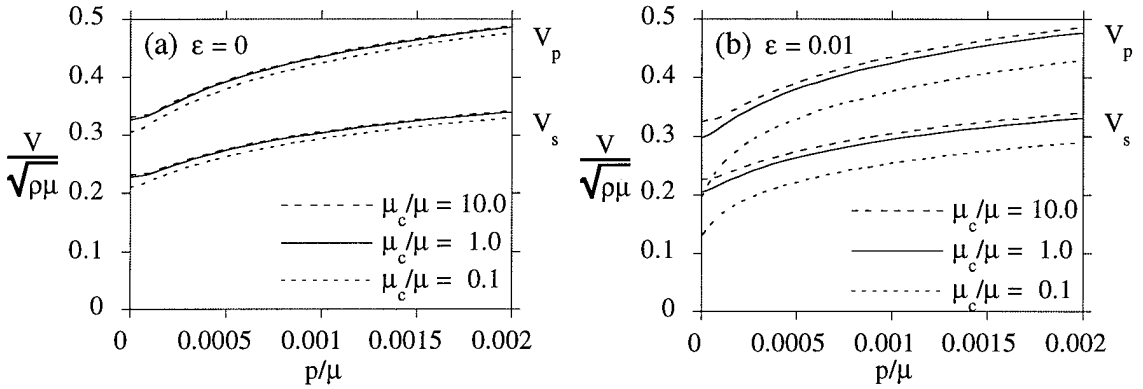

Figure 5. Normalized wave velocities in a pack of cemented spheres as a function of normalized pressure.

2.9. PLASTIC COMPACTION OF CEMENTED GRANULAR MATERIALS

ABSTRACT

We analytically relate hydrostatic stress to strain in a random dense pack of identical spheres cemented at their contacts. The spheres are elastic and the cement is perfectly plastic. This solution for the sphere pack is based on a solution for the normal interaction of two cemented spheres. Initially, the two spheres touch each other at a point. We show that as loading increases and cement becomes plastic, a finite (Hertzian) direct-contact area between the spheres necessarily has to develop and progress. The stress-strain behavior of the pack depends on the cement's yield limit and on the amount of cement. At the same hydrostatic stress, the deformation of the cemented aggregate is smaller than that of the uncemented one. This difference becomes large as the yield limit increases. We calculate the bulk modulus of an aggregate from the stress-strain curve. In the plasticity domain, the bulk modulus of the cemented aggregate is smaller than that of the uncemented one. The difference between the two may easily reach 50 percent. Of course, as the cement's yield limit decreases, the aggregate's stress-strain curve and the bulk modulus approach those of the uncemented sphere pack. This theoretical conclusion is qualitatively supported by experiments on epoxy-cemented glass beads. The maximum contact stress in the cemented aggregate may be less than a half of that in the uncemented one. This result explains an experiment where an uncemented glass bead sample failed at the hydrostatic stress of 50 MPa, whereas an epoxy-cemented sample stayed intact.

INTRODUCTION

Calcite-, quartz-, and clay-cemented sands carry static structural loads and may be subjected to dynamic earthquake or explosive stresses. Asphalt concrete is often used for air strips. Understanding the mechanical behavior of such natural and artificial cemented particulate materials is important in geomechanics and engineering.

A theory for calculating the effective elastic properties of cemented aggregates where grains and cement are elastic was developed by Dvorkin et al. [1, 2]. The results indicate that intergranular cement may strongly affect stress distribution at the contacts (Figure 1a). If cement is soft, contact stress concentration occurs, as could be expected, at the center of the contact (Figure 1c). For stiff cement, however, contact stress concentration occurs at the periphery of a cemented contact (Figure 1d). This conclusion is supported by photoelastic images of Sienkiewicz et al. [3].

The effective elastic moduli, as calculated from the cementation theory, are close to those measured in artificial cemented aggregates (Figure 2). Of course, particles in natural granular materials are rarely spheres. Nevertheless, the sphere pack approximation proves to be reliable in calculating the elastic moduli of natural rocks made out of well-sorted grains (Figure 3).

Dvorkin [4] describes large-strain behavior of cemented particulate materials by assuming that the grains are elastic and the cement becomes partly plastic as local stresses meet a plasticity condition. This plasticity condition for a thin elastic-plastic cement layer is derived based on the von Mises criterion. The stresses in the elastic part of the cement are modeled using the elastic foundation approximation. It is natural to assume that in this case the cement is softer that the grains. Then the plasticity zone in the cement initiates at the center of the contact and propagates outwards as the load increases (Figure 1b).

In this paper we explore the process of hydrostatic compaction of a cemented particulate aggregate where all cement becomes plastic. The theoretical stress-strain law in such an

aggregate is based on a solution for the normal compaction of two identical elastic spheres with plastic cement at their contact.

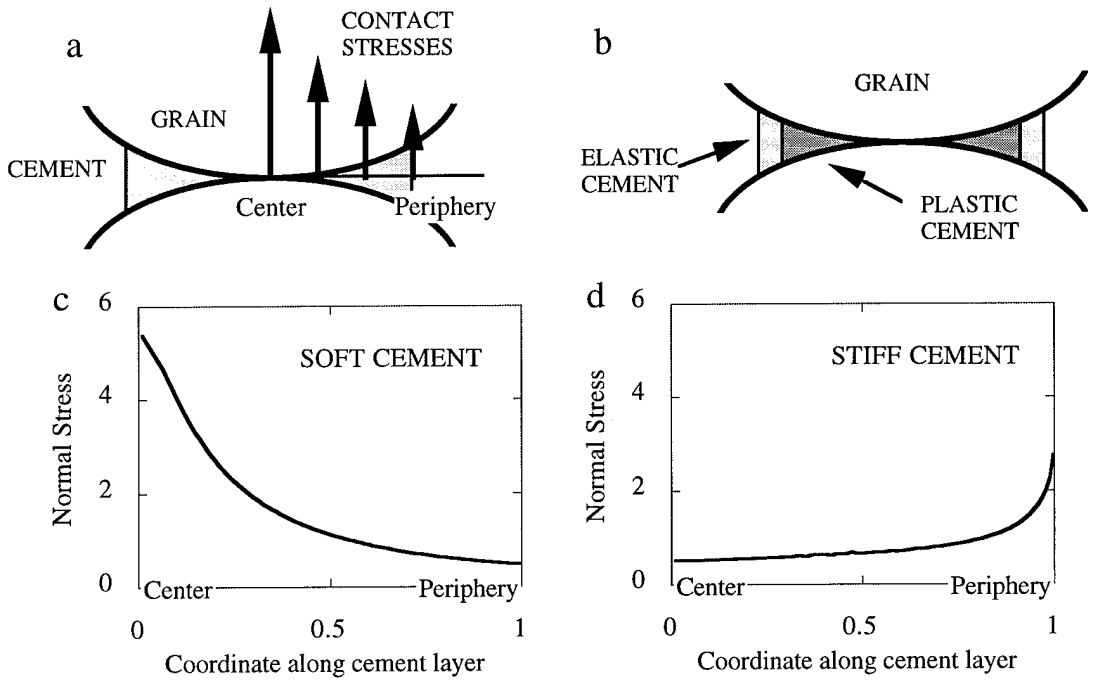

Figure 1. a. Contact stresses between two cemented grains. b. Cement layer with a plastic central kernel surrounded by elastic cement. c. Normal stresses between two cemented grains with soft cement. d. Normal stresses between two cemented grains with stiff cement. Stresses are normalized by the average stress. Coordinate is normalized by the radius of the cement layer.

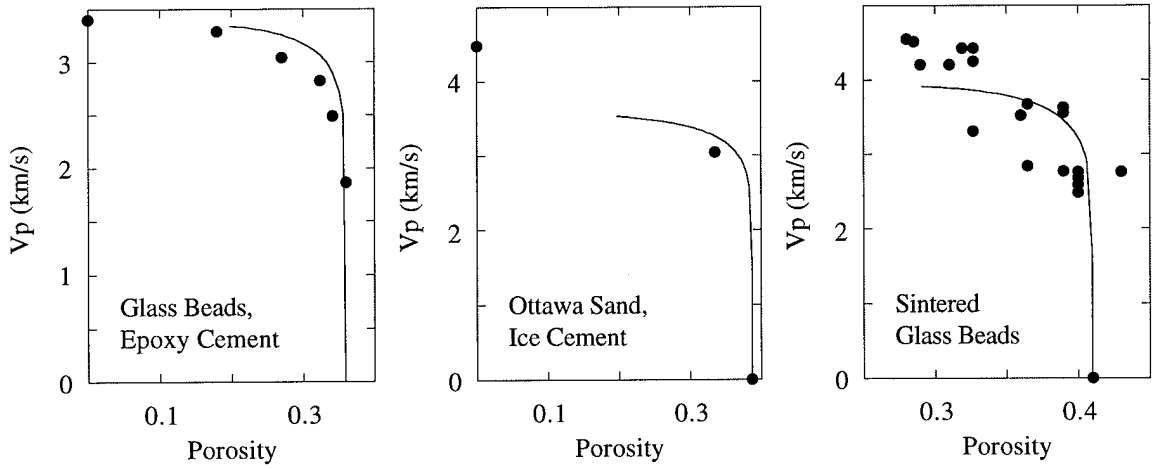

Figure 2. Examples of theoretical and experimental values of P-wave velocity in cemented granular materials. Circles are from the experiments, solid lines are theoretical predictions. From left to right: epoxy-cemented glass beads, data from Yin [5]; ice-cemented Ottawa sand, data from Jacoby et al. [6]; and sintered glass beads, data from Berge et al. [7].

We show that if the yield limit of the cement is high, the stress-strain curve noticeably differs from that for the non-cemented aggregate with Hertzian grain-to-grain interaction. Consequently, the bulk moduli calculated from the stress-strain curves differ as well: in the plasticity domain, the bulk modulus of the cemented aggregate is smaller than that of the

uncemented one. The difference may become as large as 50 percent. If the yield limit of the cement is small, the stress-strain curve and the bulk modulus are close to those in the uncemented aggregate. This theoretical conclusion is qualitatively supported by experiments on epoxy-cemented glass beads.

We find that plastic cement acts to reduce the contact stresses between two grains. This result explains an experiment where an uncemented glass bead sample failed at the hydrostatic stress of 50 MPa, whereas an epoxy-cemented sample stayed intact [8].

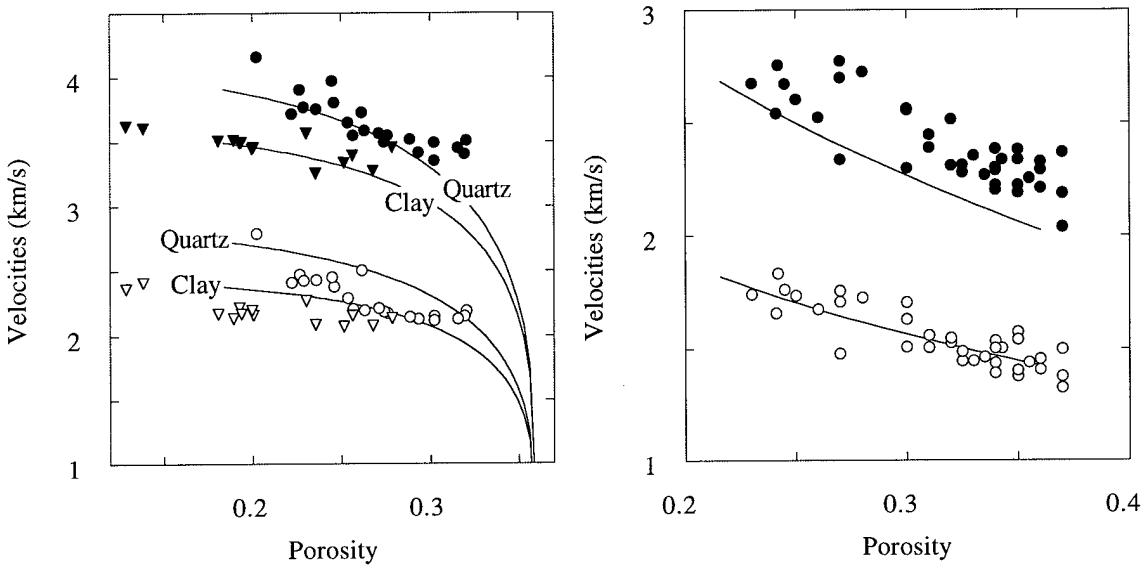

Figure 3. P-wave velocity (filled symbols) and S-wave velocity (open symbols) in dry high-porosity rock samples. Solid lines are our theoretical predictions. Examples are from [9]. a. Samples cemented by quartz and clay (as indicated on the lines). The lines are obtained from the cementation theory. b. Uncemented samples. Theoretical lines are based on the Hertz-Mindlin contact theory.

FORMULATION OF THE PROBLEM

Plastic Cement Layer: Geometry and Stresses

Consider two identical undeformed elastic spheres in contact. The space around the point of contact is filled with cement in a way that the cement layer is axisymmetrical with respect to the line connecting the centers of the spheres. Let z be the coordinate along this line with the origin at the point of contact. Then r is the radial coordinate in the plane perpendicular to the z axis. The radius of the cement layer is a_0 (Figure 4a).

A confining force F is applied to the spheres along the z axis. As this force increases, the cement becomes plastic and is squeezed sideways. The periphery of the cement layer assumes a new position at $r = a$.

Let us assume that the cement is soft as compared to the spheres, and is linear elastic, perfectly plastic. Its yield limit is σ_s. As force F increases, a plastic zone develops around the center of the contact (Figure 1b). This zone propagates outwards [4] and finally reaches the free surface of the cement. At this moment of equilibrium which precedes the cement's plastic flow, the equations of balance in the cement can be satisfied if we assume that all stresses are constant. Then from the von Mises criterion [10] we conclude that the normal stress in the z direction is $-\sigma_s$, and all other stresses disappear. As the cement flows sideways, a finite direct contact area may develop between the spheres. The radius

of this area is b (Figure 4b). If the loading now is kept constant, the plastic flow stops and the cement comes to equilibrium with

$$\sigma_{zz} = -\sigma_s, \quad b < r \le a, \tag{1}$$

and all other stresses vanishing.

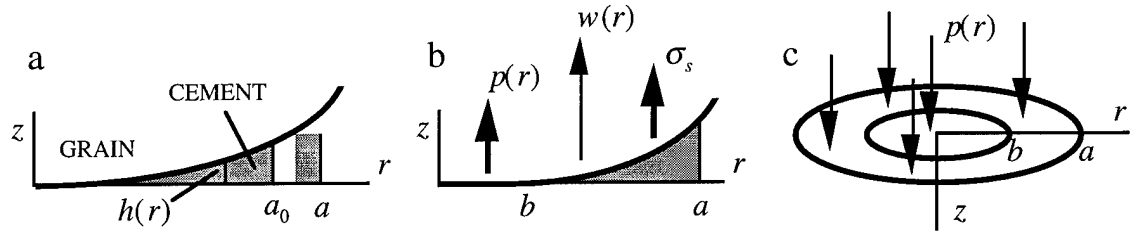

Figure 4. Cemented contact between two spheres.

Deformation of the Sphere

We adopt a common contact mechanics approximation that if the cemented contact is small (as compared to the sphere), the deformation of the sphere can be approximately calculated as that of an elastic half-space subjected to the contact stresses on its surface (Figure 4c). Then the displacement of the sphere's surface $w(r)$ due to axisymmetrical pressure $p(r)$ is [11]

$$w(r) = \frac{2(1-\nu)}{\pi G}\int_0^a p(t)\frac{t}{t+r}K[\frac{4tr}{(t+r)^2}]dt, \tag{2}$$

where G and ν are the shear modulus and Poisson's ratio of the sphere, respectively; and $K(r)$ is the complete elliptic integral of the first kind.

In the direct contact area $r \le b$ the displacement of the sphere's surface satisfies the Hertzian condition

$$w(r) = w(0) - \frac{r^2}{2R}, \tag{3}$$

where R is the sphere's radius.

Governing Equations

Equations (1), (2), and (3) can be combined to obtain the following governing equations for the pressure acting on the sphere's surface:

$$\frac{2(1-\nu)}{\pi G}\int_0^a p(t)\{\frac{\pi}{2} - \frac{t}{t+r}K[\frac{4tr}{(t+r)^2}]\}dt = \frac{r^2}{2R}, \quad r \le b;$$
$$p(r) = \sigma_s, \quad b < r \le a; \qquad p(r) = 0, \quad r > a. \tag{4}$$

Contact Force and Hydrostatic Pressure

If hydrostatic pressure P is applied to a dry random pack of identical spheres of porosity ϕ, the stress exerted on the solid phase is $P/(1-\phi)$. Then the total force acting on the surface of a sphere is $4\pi R^2 P/(1-\phi)$. This force is evenly divided among C contacts (the coordination number C is assumed to be the same for each sphere). Therefore, contact force F is related to hydrostatic pressure P as

$$F = \frac{4\pi R^2 P}{C(1-\phi)}. \tag{5}$$

The porosity of a random pack of identical spheres is about 0.36, and the coordination number is between 8 and 9 (e.g., [12]).

SOLUTION OF THE PROBLEM

Direct Contact Area Development

Consider the case where the cement is in plastic equilibrium and $b = 0$. The contact pressure acting on the grain surface is σ_s. For such constant pressure, the displacement of the grain surface is [11]

$$w(r) = \frac{2(1-\nu)\sigma_s a}{\pi G} E(\frac{r}{a}), \quad r \le a, \tag{6}$$

where $E(r)$ is the complete elliptic integral of the second kind. Then the half-thickness of the cement layer (Figure 4a) is

$$h(r) = \frac{r^2}{2R} + w(r) - w(0) = \frac{r^2}{2R} + \frac{2(1-\nu)\sigma_s a}{\pi G}[E(\frac{r}{a}) - \frac{\pi}{2}]. \tag{7}$$

The half-volume of the cement at a contact is

$$V = \int_0^a 2\pi r h(r) dr = \frac{\pi a^4}{4R} + (\frac{2}{3} - \frac{\pi}{4})\frac{4(1-\nu)\sigma_s a^3}{G}. \tag{8}$$

Provided that cement is incompressible, this volume is the same as the initial volume:

$$\frac{\pi a_0^4}{4R} = \frac{\pi a^4}{4R} + (\frac{2}{3} - \frac{\pi}{4})\frac{4(1-\nu)\sigma_s a^3}{G}. \tag{9}$$

From Equation (9) and for $a_0 / a << 1$ we find that

$$\frac{a}{a_0} = 1 + \frac{A}{4-3A}, \quad A = (1 - \frac{8}{3\pi})\frac{4(1-\nu)\sigma_s R}{G a_0}. \tag{10}$$

The corresponding contact force F is $\sigma_s \pi a^2$, and the hydrostatic pressure, as given by formula (5) is

$$P_y = \sigma_s(1+\frac{A}{4-3A})^2(\frac{a}{R})^2\frac{C(1-\phi)}{4}. \tag{11}$$

If hydrostatic pressure exceeds P_y , a finite zone of direct contact between the grains necessarily has to develop.

Complete Solution

After a finite direct contact zone between the spheres has developed, pressure distribution on the sphere's surface can be found from Equations (4). By using Equation (6) we can transform the integral in Equations (4) as

$$\begin{aligned}&\frac{2(1-\nu)}{\pi G}\int_0^a p(t)\{\frac{\pi}{2}-\frac{t}{t+r}K[\frac{4tr}{(t+r)^2}]\}dt\\&=\frac{2(1-\nu)}{\pi G}\int_0^b[p(t)-\sigma_s]\{\frac{\pi}{2}-\frac{t}{t+r}K[\frac{4tr}{(t+r)^2}]\}dt+\frac{2(1-\nu)\sigma_s a}{\pi G}[\frac{\pi}{2}-E(\frac{r}{a})].\end{aligned} \tag{12}$$

The complete elliptic integral of the second kind has the following series representation [13]:

$$E(\frac{r}{a})=\frac{\pi}{2}(1-\frac{1}{4}\frac{r^2}{a^2}-\frac{3}{64}\frac{r^4}{a^4}-\frac{5}{256}\frac{r^6}{a^6}-\ldots). \tag{13}$$

By calculating a polynomial approximation of $E(r/a)$

$$E_2(\frac{r}{a})=\frac{\pi}{2}(1-\frac{1}{4}\frac{r^2}{a^2}), \tag{14}$$

we find that the relative error $(E-E_2)/E$ does not exceed 5 percent if $r/a<0.4$ (Figure 5). Therefore, approximation (14) is accurate as long as $b/a<0.4$.

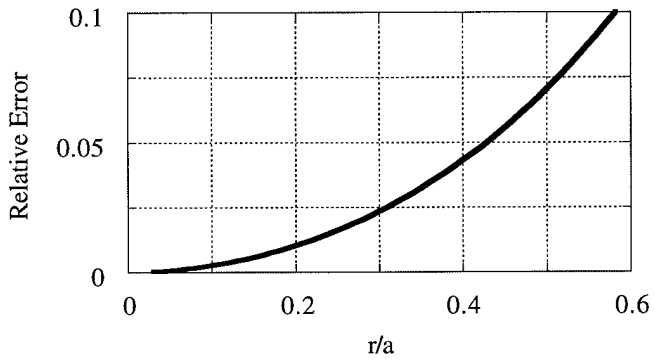

Figure 5. Relative error of using approximation (14) for the complete elliptic integral of the second kind.

Now Equations (4) can be presented as

$$\frac{2(1-\nu)}{\pi G}\int_0^b f(t)\{\frac{\pi}{2}-\frac{t}{t+r}K[\frac{4tr}{(t+r)^2}]\}dt=\frac{r^2}{2R}-\frac{r^2}{2R_1},\quad r\le b; \tag{15}$$
$$f(r)=0,\quad r>b;$$

where

$$f(r)=p(r)-\sigma_s,\quad r\le a;\qquad f(r)=0,\quad r>a; \tag{16}$$

and

$$R_1=\frac{2aG}{(1-\nu)\sigma_s}. \tag{17}$$

Equations (15) can be satisfied by the Hertzian pressure distribution [11]. Therefore, we arrive at the following solution of the problem:

$$p(r)=\frac{4G\sqrt{b^2-r^2}}{\pi R(1-\nu)}(1-\varepsilon)+\sigma_s,\quad r\le b; \tag{18}$$
$$p(r)=\sigma_s,\quad b<r\le a;\qquad p(r)=0,\quad r>a;$$

where

$$\varepsilon=\frac{(1-\nu)\sigma_s}{2G}\frac{R}{a}. \tag{19}$$

The sphere's surface displacement due to pressure given by Equation (18) is for $b<r\le a$ [11]:

$$w(r)=\frac{1-\varepsilon}{\pi R}[(2b^2-r^2)\arcsin(\frac{b}{r})+br\sqrt{1-(\frac{b}{r})^2}]+\varepsilon\frac{4a^2}{\pi R}E(\frac{r}{a}), \tag{20}$$

and the half-thickness of the cement layer is

$$h(r)=\frac{r^2}{2R}-\frac{b^2}{R}-\frac{\varepsilon}{R}(2a^2-b^2)$$
$$+\frac{1-\varepsilon}{\pi R}[(2b^2-r^2)\arcsin(\frac{b}{r})+br\sqrt{1-(\frac{b}{r})^2}]+\varepsilon\frac{4a^2}{\pi R}E(\frac{r}{a}). \tag{21}$$

Stress-Strain Law

The total force F at a contact can be calculated from Equations (18) and then related to the hydrostatic pressure P using Equation (5). The resulting force-balance equation is:

$$\beta^3=\frac{3\pi\varepsilon}{4(1-\varepsilon)}[\frac{4R^2P}{Ca^2(1-\phi)\sigma_s}-1], \tag{22}$$

where $\beta = b / a$.

The cement volume can be calculated by integrating the half-thickness of the cement layer, as given by Equation (21). By assuming that the cement is incompressible and its current volume is the same as its initial volume, we arrive at the following equation:

$$\frac{a_0^4}{a^4} = (1-\beta^2)[(1-8\varepsilon)-\beta^2(3-4\varepsilon)]$$
$$+\frac{1-\varepsilon}{\pi}[2\beta(1+2\beta^2)\sqrt{1-\beta^2}-3\pi\beta^4-2(1-4\beta^2)\arcsin(\beta)] \quad (23)$$
$$+\frac{32\varepsilon}{3\pi}[2-(1+\beta^2)E(\beta)+(1-\beta^2)K(\beta)].$$

Equations (22) and (23) can be used to find a and b at a given hydrostatic pressure P exerted on the aggregate. Once a and b are known, we can calculate the sphere's deformation e as

$$e = \frac{w(0)}{R} = (1-\varepsilon)\frac{b^2}{R^2} + \varepsilon\frac{2a^2}{R^2}. \quad (24)$$

Finally, the aggregate's bulk modulus is

$$K = \frac{1}{3}\frac{\partial P}{\partial \varepsilon}. \quad (25)$$

EXAMPLES

Stresses and Strains

Let us assume that the spheres are glass with G = 26.2 GPa and ν = 0.277. First consider a case where the amount of cement is small (a / R = 0.1). The results of calculating strain in the aggregate versus hydrostatic stress are given in Figure 6a. All curves initiate at pressure P_y, as given by Formula (11), and terminate when the ratio b / a becomes large and the approximation for E, as given by Formula (14), is not valid. The corresponding stress-strain curves are given in Figure 6b. The results for a case where the amount of cement is relatively high (a / R = 0.3) are given in Figure 7.

At the same stress, the deformation of a cemented aggregate is smaller than that of the uncemented one. As the yield limit of the cement becomes smaller, the strain-stress curves approach the curve for the uncemented aggregate. At the same yield limit and at a given pressure, the smaller the amount of cement, the larger the deformation (Figure 8).

Bulk Modulus

The bulk modulus of the glass bead pack, as given by Formula (25), is calculated for the case a / R = 0.3 for varying yield limit (Figure 9). The bulk modulus strongly depends on the cement yield limit and may significantly deviate from the modulus of the uncemented aggregate.

Notice that the bulk modulus decreases with the increasing cement yield limit. The reason is that at a given pressure the radius b of the direct contact area between the spheres decreases with the increasing yield limit (Figure 10). The normal compliance of a two-

sphere combination depends mostly on this radius and, therefore, increases with the increasing yield limit.

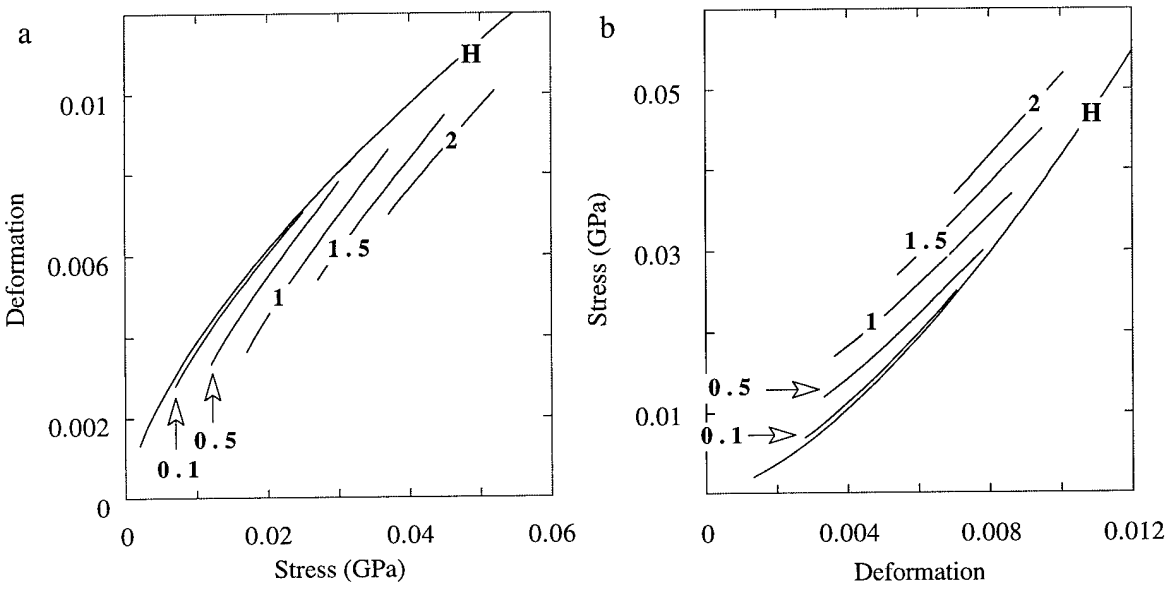

Figure 6. a. Strain-stress curves for random packs of identical glass spheres with plastic cement. a / R = 0.1. The curves are marked with the values of the cement yield limit in GPa. The enveloping curve marked "H" is from the Hertzian solution for the uncemented aggregate. b. The corresponding stress-strain curves.

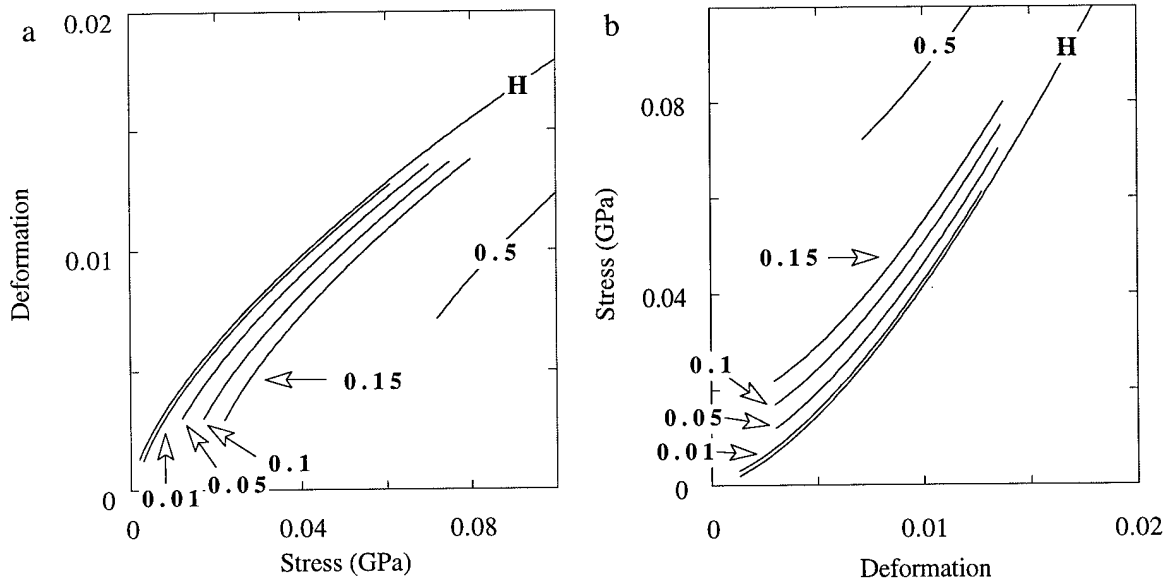

Figure 7. Same as Figure 6, but for a / R = 0.3.

The moduli calculated from stress-strain curves are called "static" moduli, as opposed to "dynamic" moduli which are calculated from the P- and S-wave velocities and density of

a material. We measured the static bulk modulus for two epoxy-cemented glass bead samples. The epoxy saturation of the pore space in the first sample was 0.15, which translates into the a / R value being between 0.24 and 0.48. The epoxy saturation of the second sample was 0.25. Accordingly, the a / R value is between 0.3 and 0.55. Of course, epoxy is not a linear elastic, perfectly plastic material -- it exhibits strong viscoelasticity. The apparent plasticity of epoxy strongly depends on the strain rate. Nevertheless, it is interesting to observe that the static bulk moduli of the epoxy-cemented samples have the same order of magnitude as the theoretical bulk moduli for the pack of uncemented glass beads, and for a cemented pack (Figure 11). This result qualitatively supports our theoretical solution.

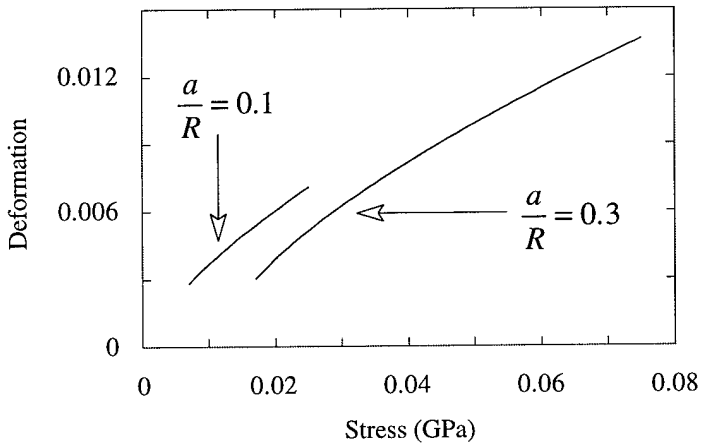

Figure 8. Strain versus stress for random packs of identical glass spheres with plastic cement. The cement yield limit is constant at 0.1 GPa. The amount of cement varies as shown on the graph.

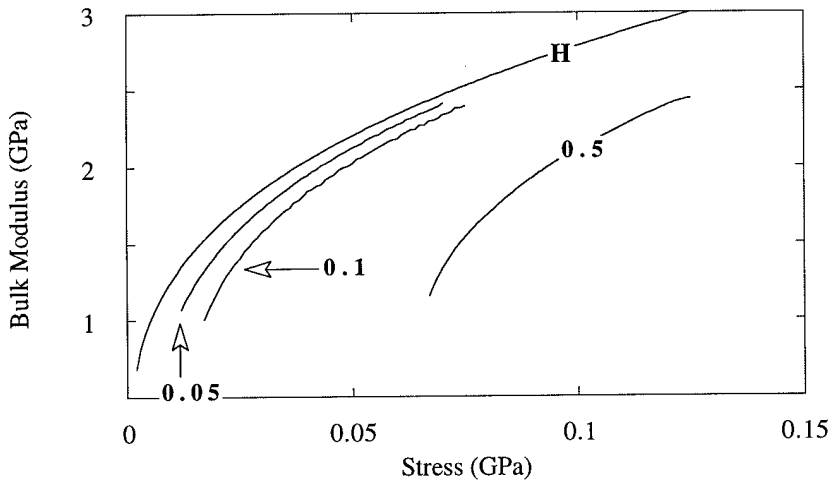

Figure 9. Bulk modulus versus stress for random packs of identical glass spheres with plastic cement for a / R = 0.3 and varying yield limit. The curves are marked with the values of the cement yield limit in GPa. The enveloping curve marked "H" is from the Hertzian solution for the uncemented aggregate.

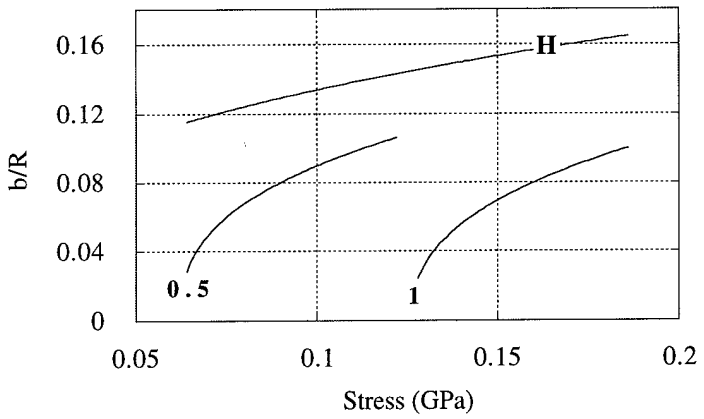

Figure 10. The b / R ratio versus hydrostatic stress for uncemented grains (curve "H") and for cemented grains with a / R = 0.3 and the yield limit 0.5 GPa and 1 GPa (as marked on the curves).

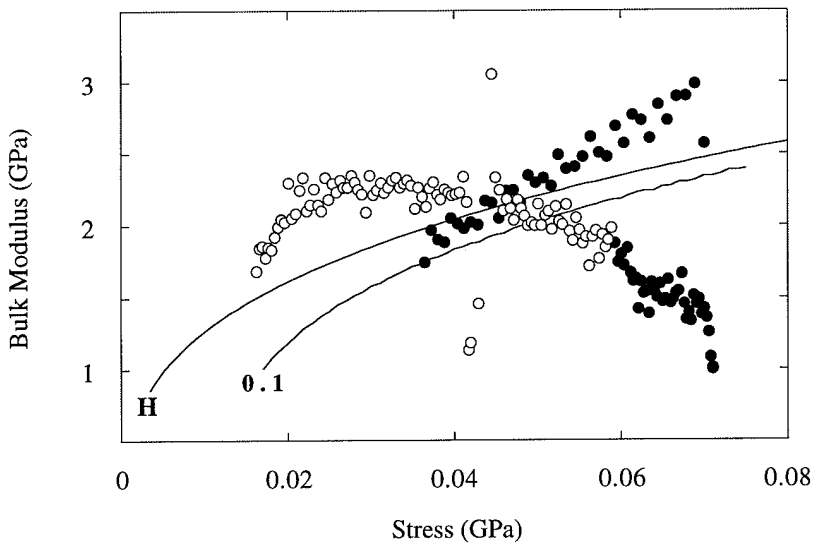

Figure 11. Bulk modulus versus stress for two epoxy-cemented glass bead samples. The epoxy saturation of the pore space is 0.15 (filled symbols) and 0.25 (open symbols). The theoretical curve marked "H" is from the Hertzian solution for the uncemented aggregate. The theoretical curve marked "0.1" is for a cemented aggregate with a / R = 0.3 and the cement yield limit of 0.1 GPa.

INTEGRITY OF GRAINS

The maximum pressure on the sphere surface is at the center of the contact area. It is

$$p_{\max} = \frac{4G(1-\varepsilon)}{\pi(1-\nu)} \frac{b}{R} + \sigma_s \tag{26}$$

for a cemented aggregate and

$$p_{\max} = \frac{4G}{\pi(1-\nu)} \frac{b_H}{R}, \quad b_H = R \sqrt[3]{\frac{3\pi(1-\nu)}{2C(1-\phi)G} P} \tag{27}$$

for the uncemented aggregate.

We calculate p_{max} for the uncemented aggregate as well as for the case where a / b = 0.4, and σ_s = 0.1 GPa. The maximum normal stress between two uncemented spheres may be twice that in the cemented case (Figure 12).

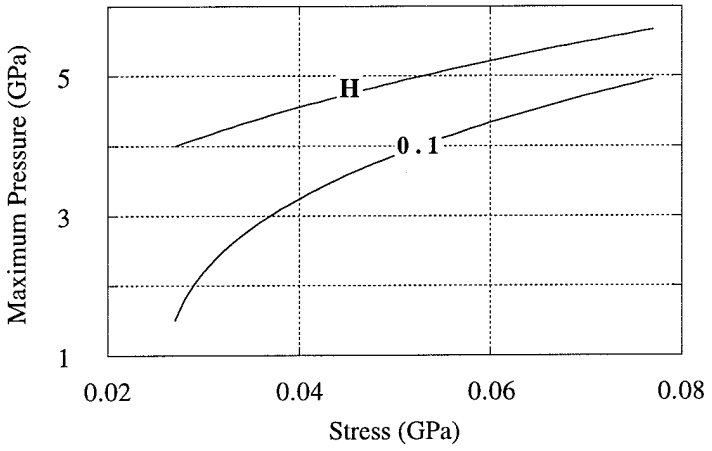

Figure 12. Maximum contact pressure on the sphere surface versus hydrostatic stress for uncemented glass spheres (curve "H") and for cemented spheres (curve "0.1").

This conclusion may explain the results of an experiment where two glass bead samples were hydrostatically compressed [8]. One sample was uncemented, whereas the other was cemented with epoxy. The volume of the epoxy accounted for 10 percent of the pore space volume which translates into the a / R value being between 0.2 and 0.43. The samples were filled with water kept at atmospheric pressure. Porosity versus hydrostatic stress was measured by the volume of expelled fluid.

In the uncemented case, a sharp porosity decrease was observed at about 50 MPa (Figure 13). This decrease is associated with the crushing of grains. The cemented grains did not crush. The photos showed that in the latter case, the grains stayed intact with the failure being localized within the epoxy.

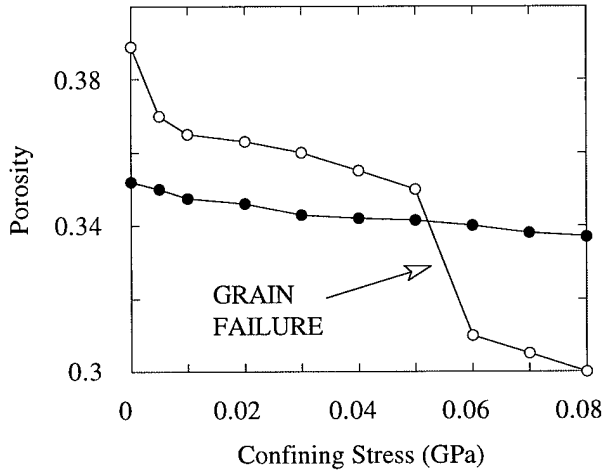

Figure 13. Porosity versus hydrostatic confining stress in two water-saturated glass bead samples. Open symbols are for the uncemented sample, closed symbols are for the cemented one.

CONCLUSION

- Plastic cement has to be squeezed sideways from the contact area between two elastic spheres in order to balance a confining force. A finite direct-contact area between the spheres necessarily has to develop.
- The static bulk modulus of a cemented aggregate with plastic cement is smaller than that of the uncemented one (at a given confining pressure). This modulus decreases with the increasing cement yield limit. The reason is that the higher the yield limit, the smaller the direct contact area between the spheres.
- The maximum contact stress in the cemented aggregate may be much smaller than that in the uncemented one. This effect may contribute to the increased strength of the grains observed in a cemented material.

REFERENCES

1. Dvorkin, J., Mavko, G. and Nur, A., The effect of cementation on the elastic properties of granular material, Mechanics of Materials, **12** (1991), 207-217.
2. Dvorkin, J., Nur, A. and Yin, H., Effective properties of cemented granular material, Mechanics of Materials, **18** (1994), 351-366.
3. Sienkiewicz, F., Shukla, A., Sadd, M., Zhang, Z., and Dvorkin, J., A Combined Experimental and Numerical Scheme for the Determination of Contact Loads Between Cemented Particles, Mechanics of Materials, **22** (1996), 43-50.
4. Dvorkin, J., Large Strains in Cemented Granular Aggregates: Elastic-Plastic Cement, Mechanics of Materials (1995), in press.
5. Yin, H., Acoustic velocity and attenuation of rocks: Isotropy, intrinsic anisotropy, and stress induced anisotropy, Ph.D. thesis, Stanford University (1993).
6. Jacoby, M., Dvorkin, J., and Liu, F., Elasticity of Partially Saturated Frozen Sand, Geophysics, **61** (1996), 288-293.
7. Berge, P.A., Berryman, J.G., and Bonner, B.P., Influence of microstructure on rock elastic properties, Geophysical Research Letters, **20** (1993), 2619-2622.
8. Yin, H., and Dvorkin, J., Strength of cemented grains, Geophysical Research Letters, **21**, (1994), 903-906.
9. Dvorkin, J., and Nur, A., Elasticity of High-Porosity Sandstones: Theory for Two North Sea Datasets, Geophysics (1996), in press.
10. Kachanov, L.M., Foundations of the Theory of Plasticity, North-Holland (1971).
11. Johnson, K.L., Contact Mechanics, Cambridge University Press (1985).
12. Bourbie, T., Coussy, O., and Zinzner, B., Acoustics of Porous Media, Gulf Publishing Company (1987).
13. Gradshteyn, I.S., and Ryzhik, I.M., Table of Integrals, Series, and Products, Academic Press (1980).